NASA TECHNICAL MEMORANDUM

NASA TM X-2446

NASA TM X-2446

HEAT TRANSFER TO FOUR FINENESS-RATIO-1.6 HEXAGONAL PRISMS WITH VARIOUS CORNER RADII AT MACH 6

by James L. Hunt

Langley Research Center

Hampton, Va. 23365

NATIONAL AERONAUTICS AND SPACE ADMINISTRATION • WASHINGTON, D. C. • MARCH 1972

1. Report No.	2. Government Accession No.	3. Recipient's Catalog No.
NASA TM X-2446		

4. Title and Subtitle	5. Report Date
HEAT TRANSFER TO FOUR FINENESS-RATIO-1.6 HEXAGONAL PRISMS WITH VARIOUS CORNER RADII AT MACH 6	March 1972
	6. Performing Organization Code
7. Author(s)	8. Performing Organization Report No.
James L. Hunt	L-7934
	10. Work Unit No.
9. Performing Organization Name and Address	117-07-01-05
NASA Langley Research Center Hampton, Va. 23365	11. Contract or Grant No.
	13. Type of Report and Period Covered
12. Sponsoring Agency Name and Address	Technical Memorandum
National Aeronautics and Space Administration Washington, D.C. 20546	14. Sponsoring Agency Code

15. Supplementary Notes

16. Abstract

An investigation was conducted in the Langley 20-inch Mach 6 tunnel to define the aerodynamic heat transfer to the radioisotope fuel cask (heat source) of the SNAP-19/Pioneer power system. The shape of the SNAP-19/Pioneer heat source is that of a hexagonal prism with flat ends; the fineness ratio, based on maximum (edge to edge) diameter, is 1.61. Phase-change-paint heat-transfer data and schlieren photographs were obtained on four possible $\frac{1}{2}$-scale entry configurations of the SNAP-19/Pioneer heat source. Tests were conducted over a wide range of attitudes and at nominal Reynolds numbers of 0.33×10^6, 0.84×10^6, and 2.2×10^6 based on the length of the unablated configuration.

17. Key Words (Suggested by Author(s))	18. Distribution Statement
Heat transfer SNAP-19 Hexagonal prism Pioneer	Unclassified – Unlimited

19. Security Classif. (of this report)	20. Security Classif. (of this page)	21. No. of Pages	22. Price*
Unclassified	Unclassified	86	$3.00

*For sale by the National Technical Information Service, Springfield, Virginia 22151

HEAT TRANSFER TO FOUR FINENESS-RATIO-1.6 HEXAGONAL PRISMS WITH VARIOUS CORNER RADII AT MACH 6

By James L. Hunt
Langley Research Center

SUMMARY

An investigation was conducted in the Langley 20-inch Mach 6 tunnel to define the aerodynamic heat transfer to the radioisotope fuel cask (heat source) of the SNAP-19/Pioneer power system. The shape of the SNAP-19/Pioneer heat source is that of a hexagonal prism with flat ends; the fineness ratio, based on maximum (edge to edge) diameter, is 1.61. Phase-change-paint heat-transfer data and schlieren photographs were obtained on four possible $\frac{1}{2}$-scale entry configurations of the SNAP-19/Pioneer heat source. Tests were conducted over a wide range of attitudes and at nominal Reynolds numbers of 0.33×10^6, 0.84×10^6, and 2.2×10^6 based on the length of the unablated configurations.

INTRODUCTION

The SNAP-19/Pioneer power system contains a radioisotope heat source. Should an abort occur in the mission in the second or third stages, safety considerations dictate that the nuclear-fuel container must be capable of surviving the reentry intact, even if the rest of the structure fails (refs. 1 and 2).

Calculation of the heat load was complicated by the unusual aerodynamic shape, that is, a hexagonal prism with flat ends, and by the probability of rolling and tumbling during the reentry. Therefore, an experimental study of the heat-transfer patterns was conducted in the Langley 20-inch Mach 6 tunnel using the phase-change paint technique developed at the Langley Research Center (ref. 3). Tests were made on a $\frac{1}{2}$-scale model of the fuel cask over a wide range of attitudes for the original sharp-edged shape and for three round-edged shapes corresponding to possible ablation changes.

The configuration tested, while hardly a normal aerodynamic shape, shows heat-transfer patterns that may be of general interest and may give some insight into the effects to be expected from corners and edges on more conventional shapes.

SYMBOLS

b	width of hexagonal side (fig. 4)
c	specific heat
h	heat-transfer coefficient (H used in computer printout of figs. 8 to 29)
h_s	reference heat-transfer-coefficient stagnation-point value for 15.24-centimeter-radius sphere at test conditions (HS used in computer printout of figs. 8 to 29)
k	thermal conductivity
l	heat-penetration depth
L	length of unablated model
N_{Pr}	Prandtl number
P	pressure
$R_{\infty,L}$	free-stream Reynolds number based on length of unablated model
s	distance along surface of model (fig. 4)
Δs	grid increment (fig. 4)
t	time (T used in computer printout of figs. 8 to 29)
t_d	thermal-interference-diffusion time (eq. (3))
T	temperature
$\bar{T}$	temperature parameter (eq. (2))
u	velocity
α	angle of attack

β heat-transfer parameter (eq. (1))

ϵ roll angle of model with respect to the axis of schlieren system (fig. 6)

λ thermal diffusivity, $k_m/\rho_m c_m$

μ viscosity

ρ density

ϕ roll angle of model with respect to tunnel axes

Subscripts:

a air

aw adiabatic wall conditions

i initial conditions

m model

p constant pressure

pc phase-change coating

s stagnation conditions behind normal shock

t total conditions of free stream

w wall conditions

TEST METHODS AND APPARATUS

Test Technique

Heat-transfer data were obtained by using the phase-change coating technique described in reference 3. This technique employs a thin surface coating of material that undergoes a visible phase change at a known temperature. The times required for the

phase change to occur at various locations on the model are determined from motion pictures taken at a known framing rate. The patterns so obtained represent lines of constant surface temperature.

The value of the heat-transfer coefficient at a given point on these isotherms is obtained from the solution for a semi-infinite slab of the transient one-dimensional heat-conduction equation assuming a step input in the heat-transfer coefficient. The general form of this solution is

$$h = \frac{\beta\sqrt{\rho_m c_m k_m}}{\sqrt{t_{pc}}} \tag{1}$$

where h is the heat-transfer coefficient, $\rho_m c_m k_m$ is the product of the thermophysical properties of the model, and t_{pc} is the time required for a phase change to occur after the model is subjected to the tunnel free-stream conditions. The variable β depends only on the parameter

$$\bar{T} = \frac{T_{pc} - T_i}{T_{aw} - T_i} \tag{2}$$

where T_{pc} is the temperature of the phase-change coating, T_i is the initial temperature of the model, and T_{aw} is the adiabatic-wall temperature. The functional dependence of β on $\bar{T}$ is given in figure 1.

The results obtained from the semi-infinite slab assumption are a good approximation to the solution for actual body geometry when the depth of heat penetration is small compared with pertinent model dimensions. A conservative approximation of the heat-penetration depth (eq. (9) of ref. 3) is given in the notation of the present paper by the following equation:

$$l = \sqrt{\frac{\lambda t_d}{0.2}} \tag{3}$$

Since the general heat-conduction equation is linear, equation (3) can be used to estimate the minimum distance from a protuberance (corresponding to an abrupt change in heating rate or model configuration) where the semi-infinite slab assumption is still valid.

Substitution of t_{pc} (time required for the phase change to occur) of equation (1) for t_d (thermal-interference-diffusion time) in equation (3) gives

$$l = \frac{\beta k}{\sqrt{0.2h}} \tag{4}$$

The value of l from this equation then gives the minimum distance of approach to a surface discontinuity where a semi-infinite slab solution can be used as a valid approximation of the heat conduction. Detailed discussions of the limits of the semi-infinite slab assumption as affected by the heat-penetration depth and model-geometry discontinuities are presented in references 3 and 4, respectively.

Facility

The test program was conducted in the Langley 20-inch Mach 6 tunnel. This facility, which operates with air as the test medium, is the intermittent type and exhausts to the atmosphere through a diffuser augmented by an air ejector. Tests were conducted at nominal stagnation pressures of 0.448×10^6 N/m^2, 1.206×10^6 N/m^2, and 3.21×10^6 N/m^2 with corresponding nominal stagnation temperatures of 461 K, 500 K, and 506 K. These conditions give nominal Reynolds numbers per meter of 3.9×10^6, 10.1×10^6, and 26.6×10^6, respectively. Photographs of the tunnel test section and the test setup utilized are shown in figure 2. A detailed description of the tunnel is given in reference 5.

Models

The four configurations of the SNAP-19/Pioneer heat source tested are as follows:

Unablated configuration	Model 001
Uniformly ablated, random-tumble reentry	Model 003
End ablated, end-on spinning reentry	Model 005
Asymmetrically ablated, side-on stable reentry	Model 007

Dimensional drawings of these four $\frac{1}{2}$-scale configurations are given in figure 3.

The phase-change heat-transfer technique utilizes a grid model for the purpose of locating phase-change patterns. The grid model is photographed in the exact position occupied by the plastic model during tests in order to provide a superposable grid that is used to locate the phase-change patterns on the test model. Sketches of the grid models with designated grids used in identifying phase-change position on test models are presented in figure 4.

Photographs of the four SNAP-19/Pioneer heat-source models tested (cast from an epoxy resin with a silica filler) and of the corresponding grid models with stings and

attitude adapters are shown in figure 5. The square root of the product of the thermophysical properties $\left(\sqrt{\rho_m c_m k_m}\right)$ of these models is essential to the heat-transfer technique utilized. The effective value of this parameter is 1.799×10^3 W/m^{2}sec$^{1/2}$ K. This number was determined by making phase-change heat-transfer tests on a sphere cast from the same batch of material as the models and by using an analytical heat-transfer distribution (ref. 6) in conjunction with a solution of the transient one-dimensional heat-conduction equation (eq. (1)).

Test Conditions

The terminology used and the conditions at which the four configurations of the SNAP-19/Pioneer heat source were tested are as follows:

Terminology

Angle of attack, $\alpha = \begin{cases} 0^\circ \text{ for end-on} \\ 90^\circ \text{ for side-on} \end{cases}$

Roll angle, $\phi = \begin{cases} 0^\circ \text{ for edge leading} \\ 30^\circ \text{ for flat leading} \end{cases}$

Test format

Model 001 (unablated)				Model 003 (uniformly ablated)				Model 005 (end ablated)	Model 007 (asymmetrically ablated)			
α, deg	$\phi = 0^\circ$	$\phi = 15^\circ$	$\phi = 30^\circ$	α, deg	$\phi = 0^\circ$	$\phi = 15^\circ$	$\phi = 30^\circ$	$\alpha = 0^\circ$	α, deg	$\phi = 0^\circ$	$\phi = 15^\circ$	$\phi = 30^\circ$
0			x	0			x		0			
25				25			x		25			
50	x		(x)	50	x		(x)		50			
70				70			(x)		70			x
90	x		x	90	x	x	x		90			x

Heat-transfer tests were conducted on each model at a nominal Reynolds number per meter of 10.1×10^6 for the attitudes designated by the x's in the test format above. Additional tests were also conducted at Reynolds numbers per meter of 3.9×10^6 and 26.6×10^6 for the circled conditions. These Reynolds numbers based on length $\left(R_{\infty,L}\right)$ of the unablated model (model 001) are 0.325×10^6, 0.839×10^6, and 2.19×10^6.

RESULTS

Schlieren Photographs

Schlieren photographs for the four configurations at each test attitude are given in figure 6. The attitude of the model with respect to the tunnel stream is designated in each picture by α and ϕ as defined previously. The roll angle of the model with respect to the schlieren system is denoted by ϵ (definable from the sequences in fig. 6). Two sets of schlieren pictures are presented for each model. The first set, taken with Polaroid and denoted as such, were nearly all made during the phase-change heat-transfer tests. The second set were taken on 75-mm film during tests conducted for schlieren pictures only.

Heat Transfer

Samples of phase-change patterns on each of the configurations at various attitudes are presented in figure 7. These are photographs taken by the time-study camera during the test. The light areas are the unmelted coating and the dark areas are the higher-heating-rate areas in which the phase change has already occurred. The line separating these areas is a line of known temperature, and each successive pattern represents a certain constant heat-transfer coefficient provided the adiabatic wall temperature is constant along a given line. Note the phase-change patterns generated by the vorticities downstream of the windward-leading-edge corners on the unablated configuration (model 001) at $\alpha = 50^{\circ}$, $\phi = 0^{\circ}$ and $\alpha = 50^{\circ}$, $\phi = 30^{\circ}$ (figs. 7(a) and 7(b), respectively).

The results of the phase-change heat-transfer tests on the four SNAP-19 configurations are presented in figures 8 to 29 in terms of nominal heat-transfer-coefficient contours on the models for the test conditions and in the order given in the test format. In these figures, the isotherms (obtained from photographic recordings of phase-change patterns) are superimposed on the camera view of the corresponding grid model. The grid lines can be identified by referring to figure 4. In order to obtain a complete picture of the heat-transfer distribution over the windward surfaces, two views of the models, as seen from the side and top mounted cameras, are given at each test condition. The two cameras were not synchronized, so the contours shown in one view are not necessarily the same as the contours shown in the other.

The values of heat-transfer coefficients given in these figures (figs. 8 to 29) are called nominal values (h_{nom}) because they were obtained (in every case) by assuming that T_{aw} equals the free-stream total temperature T_t. Since T_{aw} is in general not equal to T_t and varies along the isotherms, these nominal values should be corrected before use. A more nearly correct value of the heat-transfer coefficient can be obtained

as follows: First, compute a new value of $\overline{T}$ using the values for T_{pc}, T_i, and T_t in the legend of figures 8 to 29 and the value of T_{aw}/T_t in figure 30 which corresponds to the attitude and/or side of the model on which the nominal contours being corrected appear. The ratios T_{aw}/T_t of figure 30 were calculated by expanding isentropically from the total pressure behind a normal shock to a local Newtonian pressure with a laminar recovery factor of 0.833 (square root of Prandtl number at a wall temperature of 353 K). With the computed value of $\overline{T}$, select the corresponding corrected value of β (β_{corr}) from figure 1. The correction factor for each set of isotherms for a given side is then β_{corr}/β. The correct value of heat-transfer coefficient is

$$h_{corr} = h_{nom} \frac{\beta_{corr}}{\beta}$$

In each of the figures of this sequence (figs. 8 to 29), the contours are numbered in order of decreasing nominal heat-transfer coefficient. The contour numbers are listed in each figure with the corresponding times (T,SEC) at which the contours occurred relative to model injection, with the corresponding nominal heat-transfer coefficient (H,BTU/FT.SQ-SEC-DEG-R; to convert to W/m^2-K, multiply by 2.0428×10^4) calculated for each isotherm in the manner previously described, and with the corresponding nondimensional nominal heat-transfer-coefficient ratio (H/HS). The heat-transfer coefficient h_s is the theoretical value for the stagnation point of a 15.24-centimeter-radius sphere at the same test conditions as the model. The coefficient h_s was calculated from the following expression (ref. 7):

$$h_s = 0.768(c_p)_a(N_{Pr})^{-0.6}(\rho_w\mu_w)^{0.1}(\rho_s\mu_s)^{0.4}\left(\frac{du}{ds}\right)^{0.5}$$

where the velocity gradient du/ds was taken from Newtonian theory.

The semi-infinite slab assumption used to obtain the heat-transfer coefficient from the phase-change isotherm is violated in the vicinity of the prism corners. The minimum distance of approach to these corners (l) where the semi-infinite slab assumption is still valid is given by equation (4). The distance l/b is plotted in figure 31 as a function of h/h_s for the various test conditions and phase-change temperatures encountered in this investigation. How accurate the semi-infinite slab assumption is inside the minimum distance of approach is not known. However, the coefficients which lie inside the minimum distance of approach to a corner may be used as conservative estimates, since any violation of the semi-infinite slab assumption will give a higher calculated heat-transfer coefficient than does actually occur.

The nominal heat-transfer contours suggest that transition may have occurred on both the unablated model 001 (fig. 13) and the uniformly ablated model 003 (fig. 22) for $\alpha = 50^{\circ}$, $\phi = 30^{\circ}$, and at a Reynolds number per meter of 26.5×10^6 $\left(R_{\infty,L} = 2.2 \times 10^6\right)$. This regime is one in which transition is expected on swept cylinders (ref. 8). Of equal interest are the vorticity patterns produced by the sharp corners on the unablated model 001 at $\alpha = 50^{\circ}$ (figs. 9, 11, 12, and 13) and the three-dimensional end effects at $\alpha = 70^{\circ}$ and $\phi = 30^{\circ}$ on the uniformly ablated model 003 (figs. 23 and 24) and the asymmetrically ablated model 007 (fig. 28).

CONCLUDING REMARKS

An increase in heating occurred in the path of vorticity patterns produced by the windward corners on the unablated configuration at an angle of attack of 50°.

Three-dimensional trailing-end effects were prominent at an angle of attack of 70° and an angle of roll of 30° on the uniformly ablated and the asymmetrically ablated configurations.

The nominal heat-transfer contours suggest that transition may have occurred on both the unablated and uniformly ablated SNAP-19/Pioneer heat-source configuration for an angle of attack of 50° and an angle of roll of 30° at a Reynolds number per meter of 26.5×10^6 $\left(R_{\infty,L} = 2.19 \times 10^6\right)$.

Langley Research Center,
National Aeronautics and Space Administration,
Hampton, Va., January 3, 1972.

REFERENCES

1. Kahn, Stewart F.; and Dohner, Clark V.: Reentry Safety of Isotopic Systems. AIAA Paper No. 68-1166, Dec. 1968.

2. Brunner, M. J.; Dohner, C. V.; and Lawit, R. L.: Re-Entry of Radioactive Power Sources. J. Spacecraft Rockets, vol. 5, no. 4, Apr. 1968, pp. 448-453.

3. Jones, Robert A.; and Hunt, James L.: Use of Fusible Temperature Indicators for Obtaining Quantitative Aerodynamic Heat-Transfer Data. NASA TR R-230, 1966.

4. Hunt, James L.; and Jones, Robert A.: Effects of Several Ramp-Fairing, Umbilical, and Pad Configurations on the Aerodynamic Heating to Apollo Command Module at Mach 8. NASA TM X-1640, 1968.

5. Sterrett, James R.; and Emery, James C.: Extension of Boundary-Layer-Separation Criteria to a Mach Number of 6.5 by Utilizing Flat Plates With Forward-Facing Steps. NASA TN D-618, 1960.

6. Lees, Lester: Laminar Heat Transfer Over Blunt-Nosed Bodies at Hypersonic Flight Speeds. Jet Propulsion, vol. 26, no. 4, Apr. 1956, pp. 259-269, 274.

7. Beckwith, Ivan E.; and Cohen, Nathaniel B.: Application of Similar Solutions to Calculation of Laminar Heat Transfer on Bodies With Yaw and Large Pressure Gradient in High-Speed Flow. NASA TN D-625, 1961.

8. Bushnell, Dennis M.: Effects of Shock Impingement and Other Factors on Leading-Edge Heat Transfer. NASA TN D-4543, 1968.

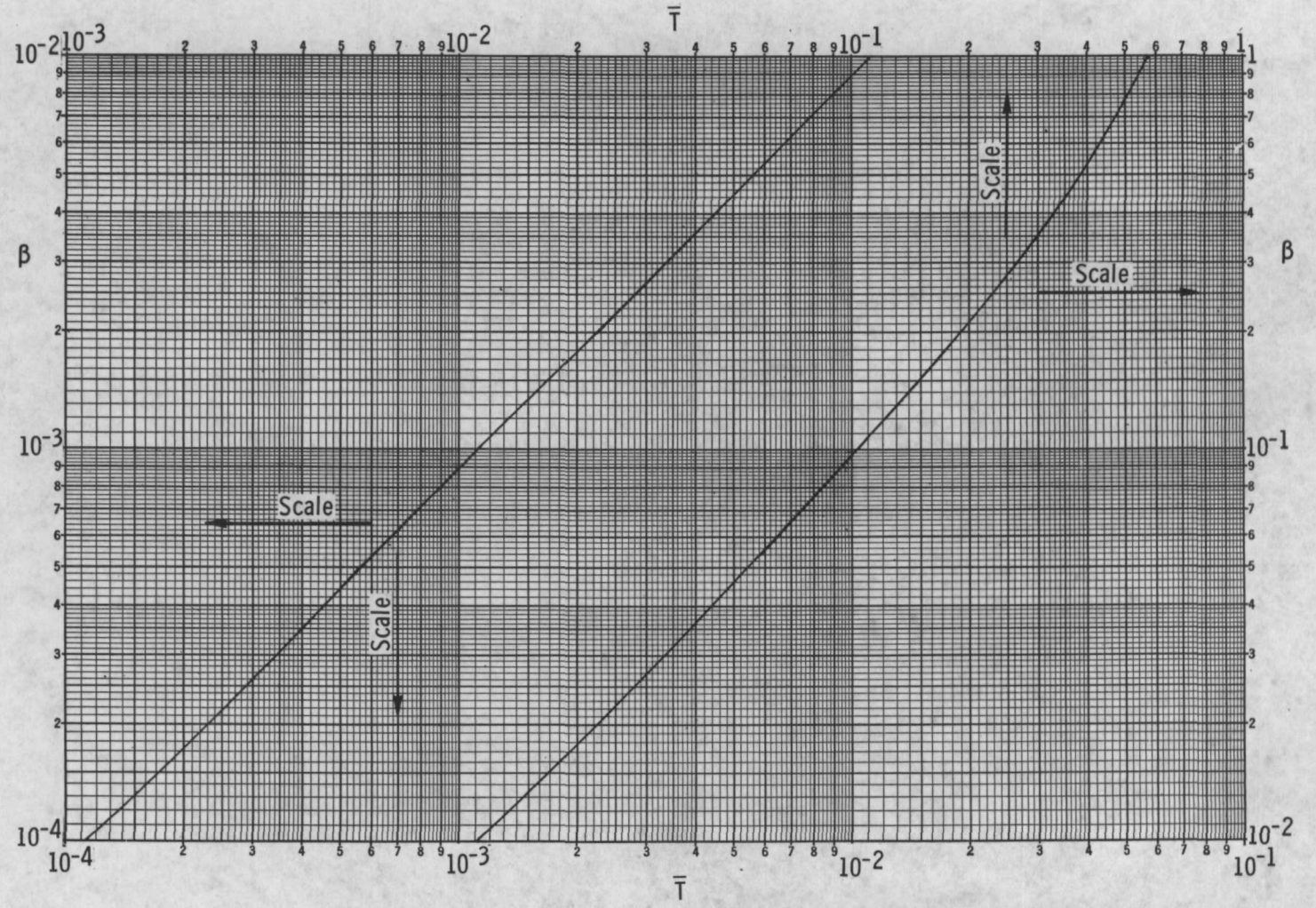

Figure 1.- Solution of one-dimensional heat-conduction equations for a semi-infinite slab assuming step input in heat-transfer coefficients.

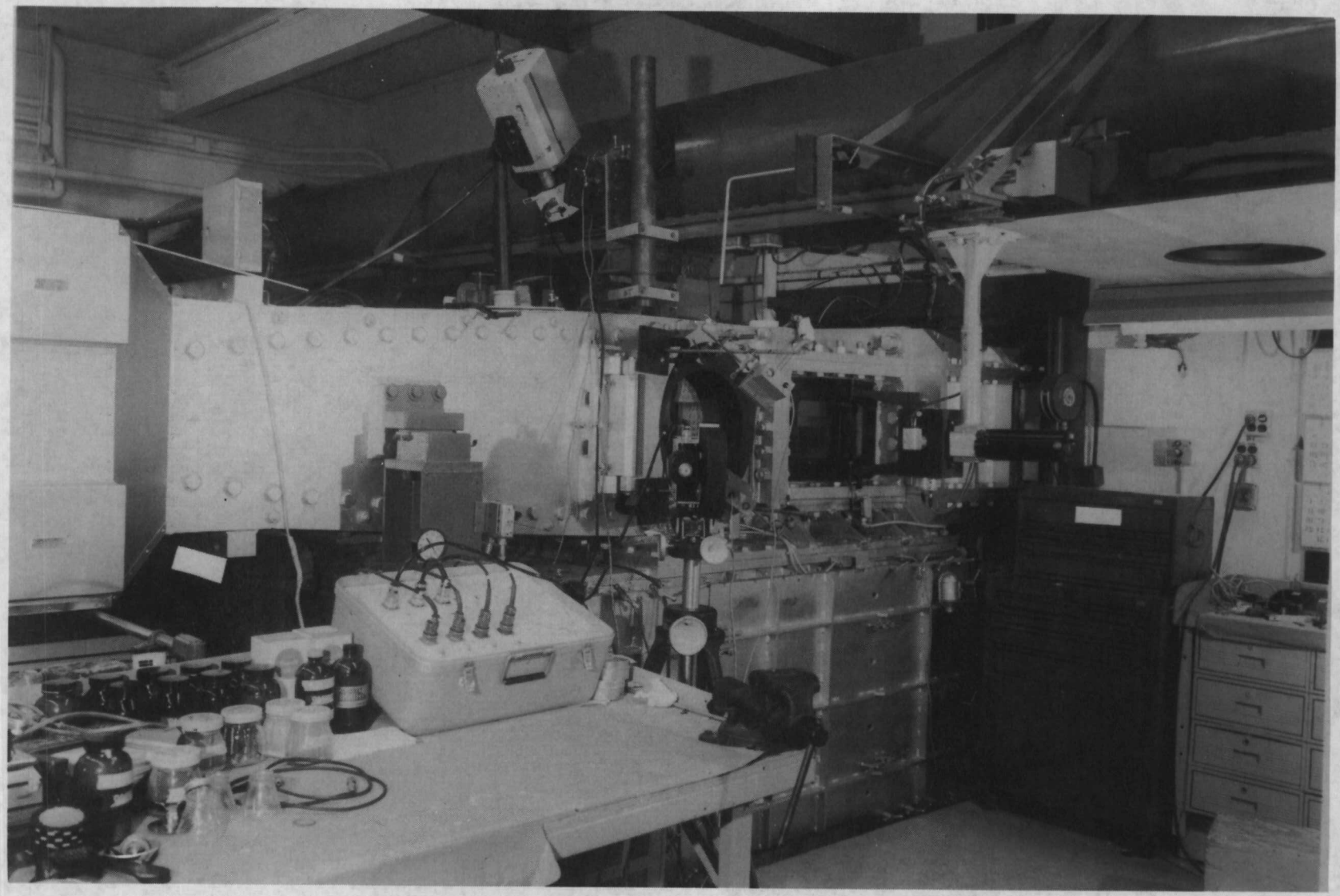

L-70-4399

(a) Top and side mounted cameras.

Figure 2.- Test setup in Langley 20-inch Mach 6 tunnel.

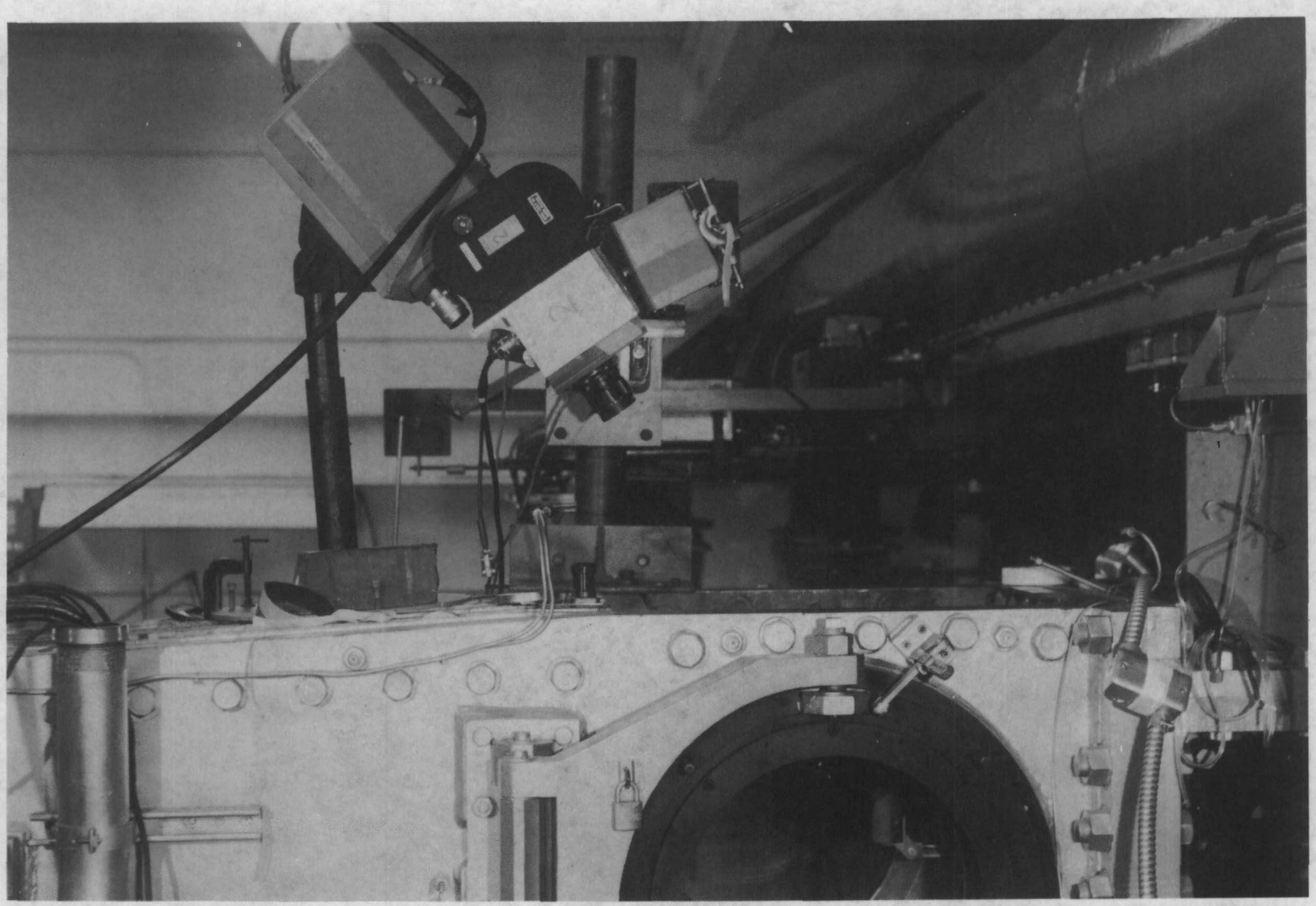

L-70-4400

(b) Camera for recording phase-change patterns and television camera for monitoring tests mounted on top of test section.

Figure 2.- Continued.

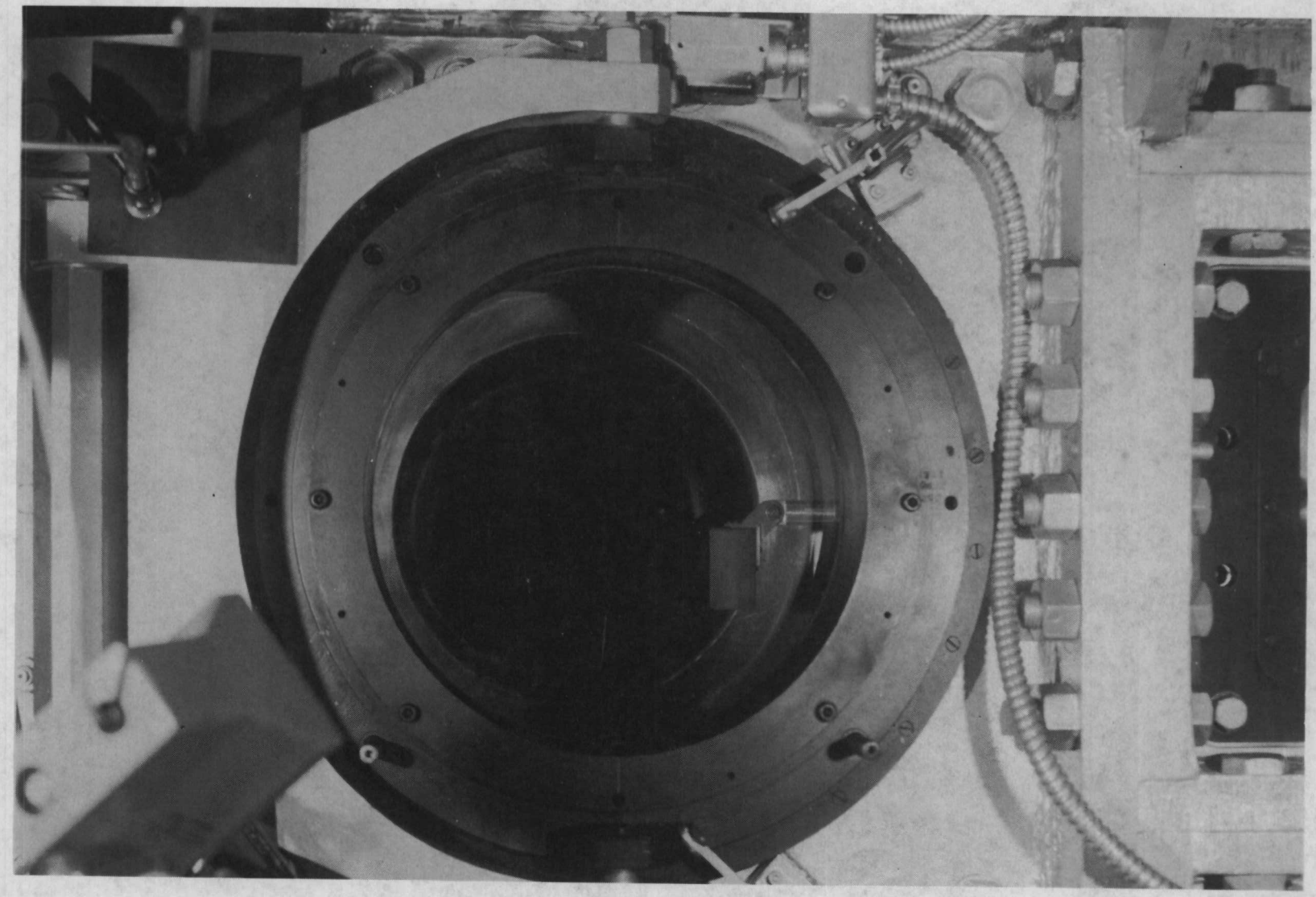

L-70-4401

(c) Model in test section.

Figure 2.- Concluded.

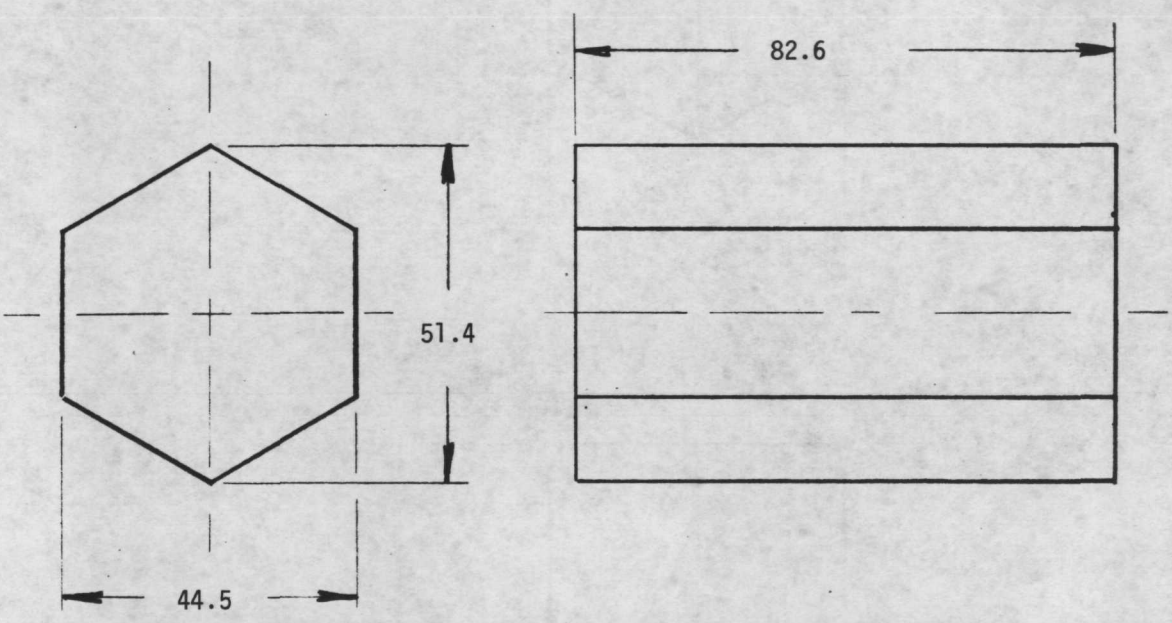

(a) Model 001 (unablated).

Figure 3.- Drawings of $\frac{1}{2}$-scale SNAP-19/Pioneer fuel-cask models.
(All dimensions in mm.)

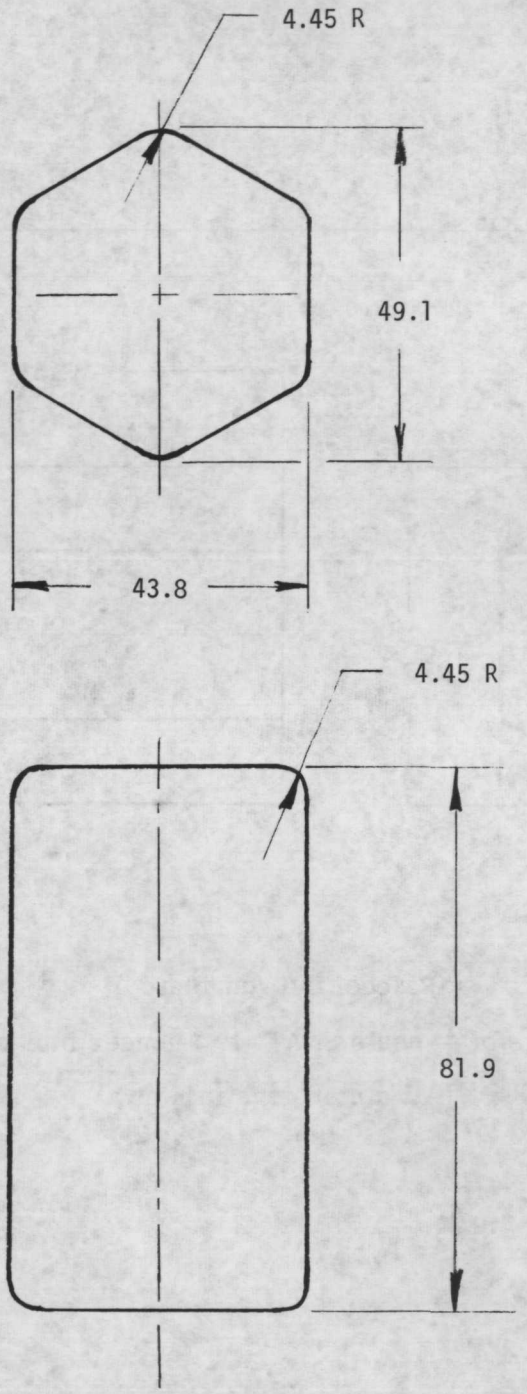

(b) Model 003 (uniformly ablated, random-tumble reentry).

Figure 3.- Continued.

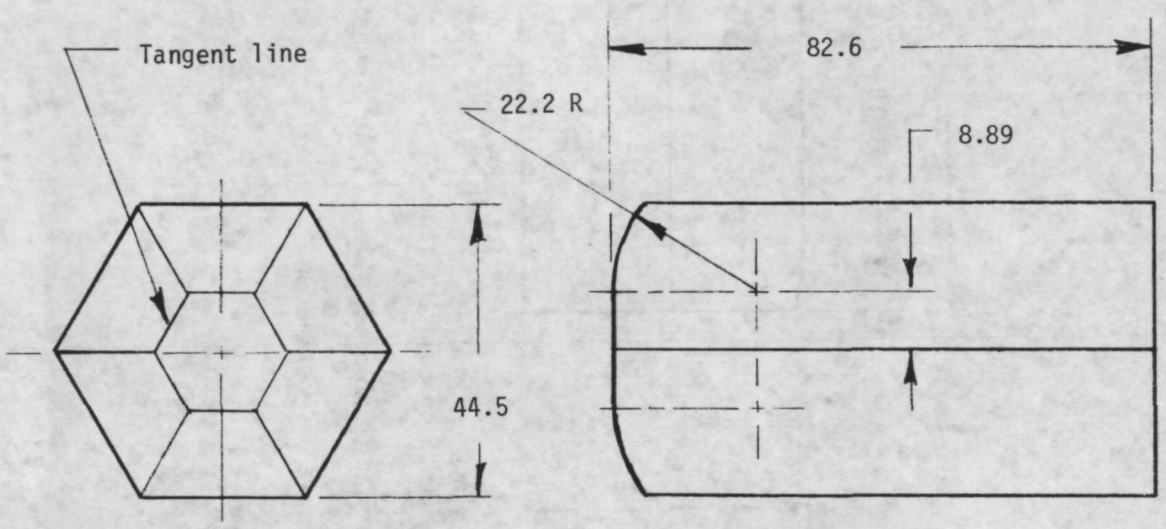

(c) Model 005 (end ablated, end-on spinning reentry).

Figure 3.- Continued.

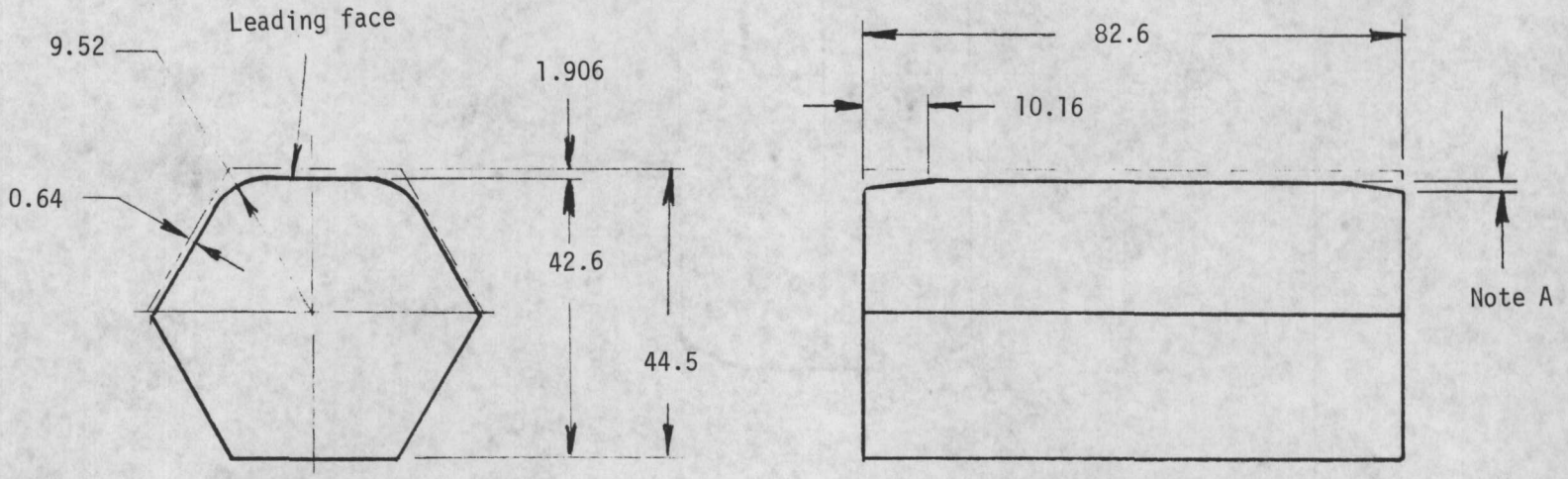

Note A: Taper at ends: 0.5 on leading face
0.25 on adjacent faces.

(d) Model 007 (asymmetrically ablated, side-on stable reentry).

Figure 3.- Concluded.

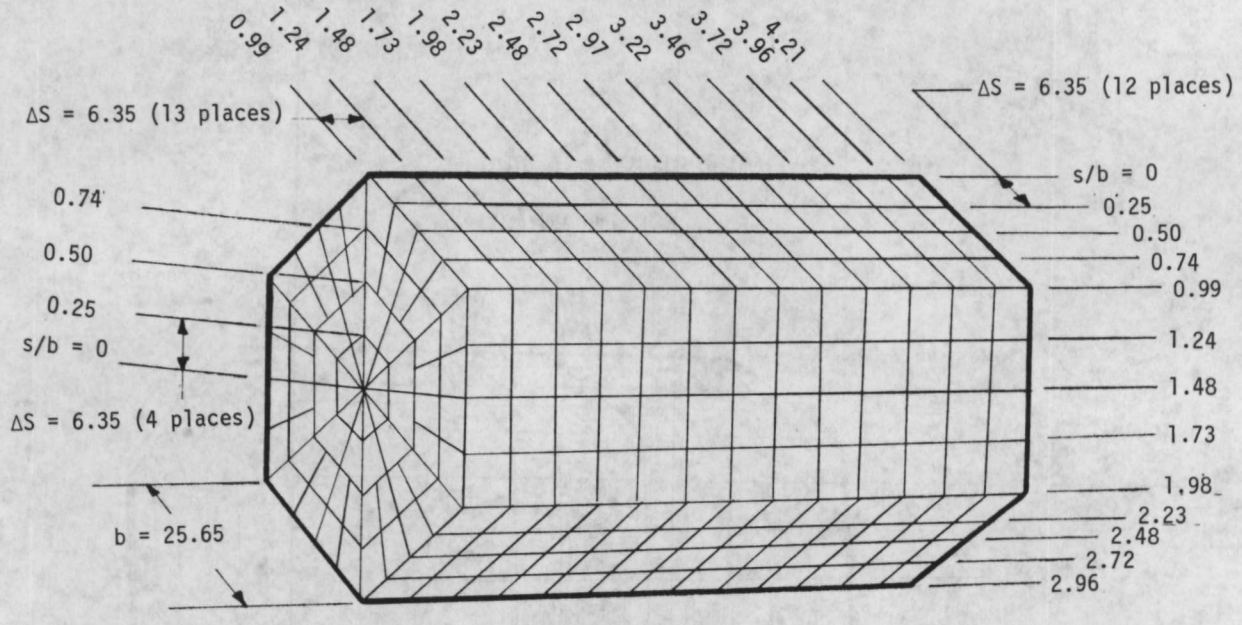

(a) Model 001.

Figure 4.- Grid model with designated grid positions.
(All dimensions in mm.)

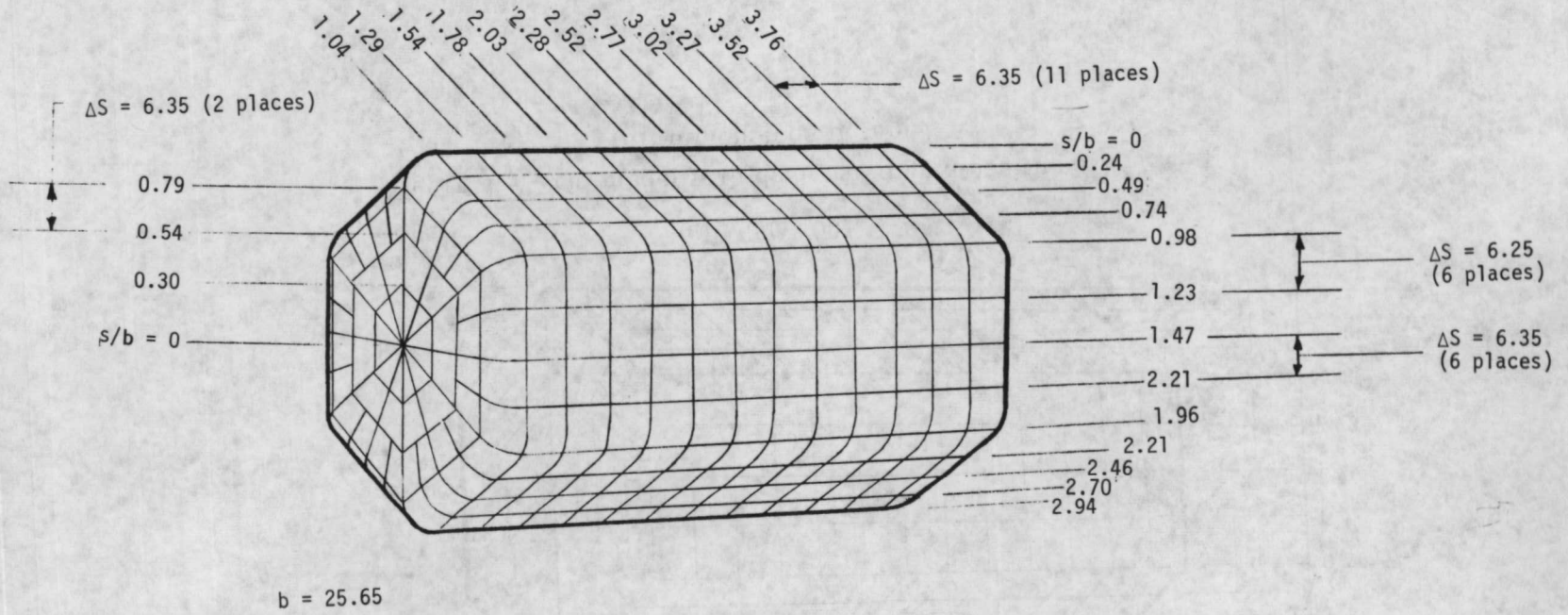

(b) Model 003.

Figure 4.- Continued.

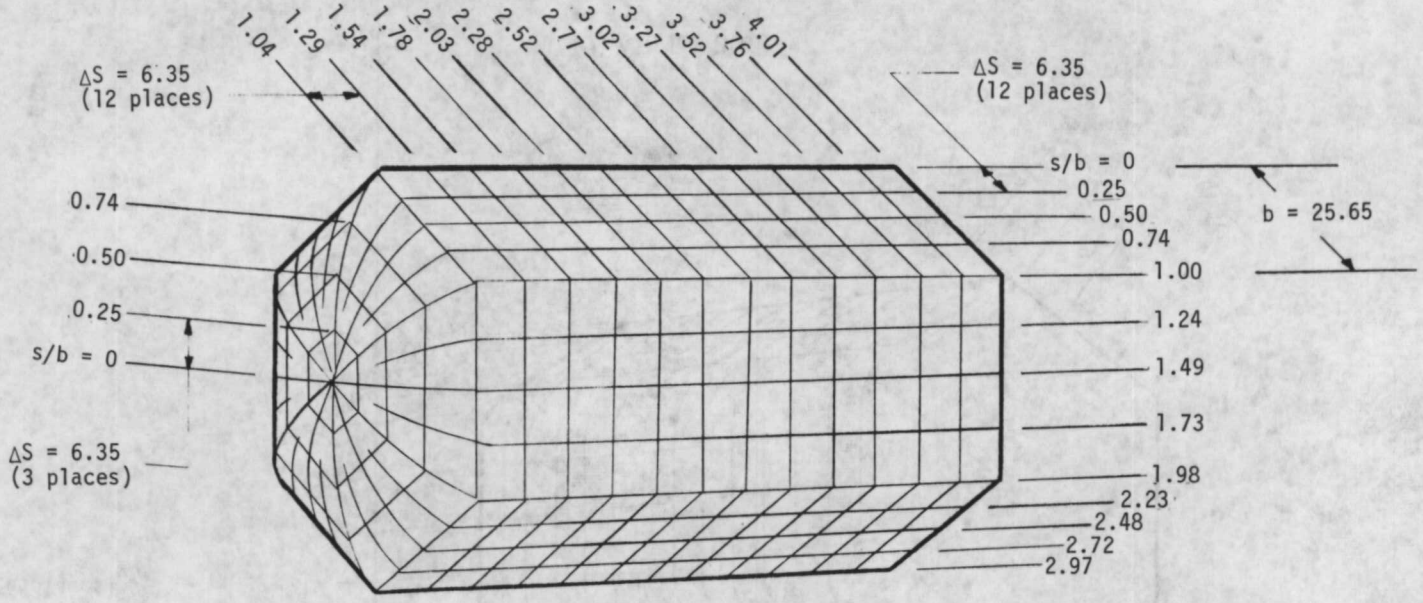

(c) Model 005.

Figure 4.- Continued.

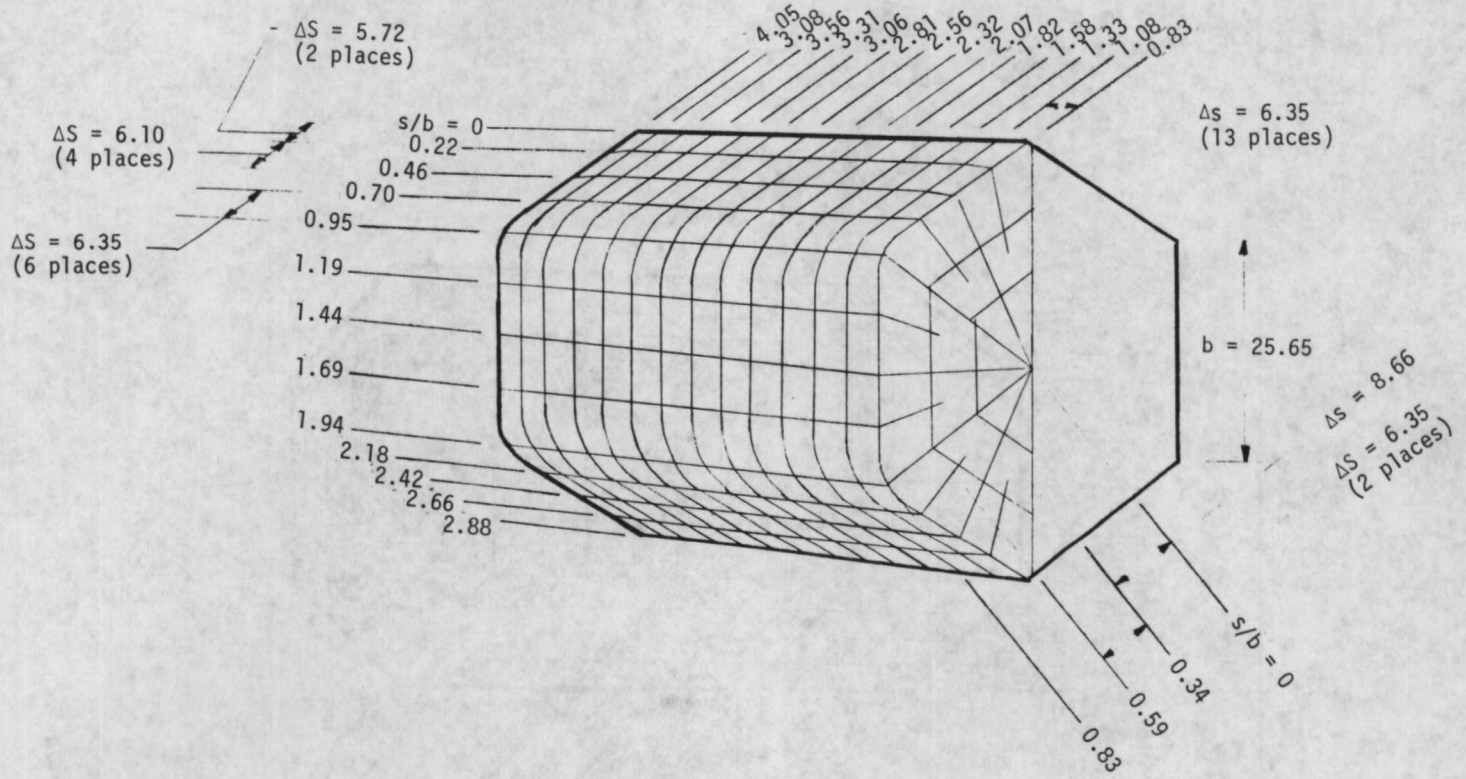

(d) Model 007.

Figure 4.- Concluded.

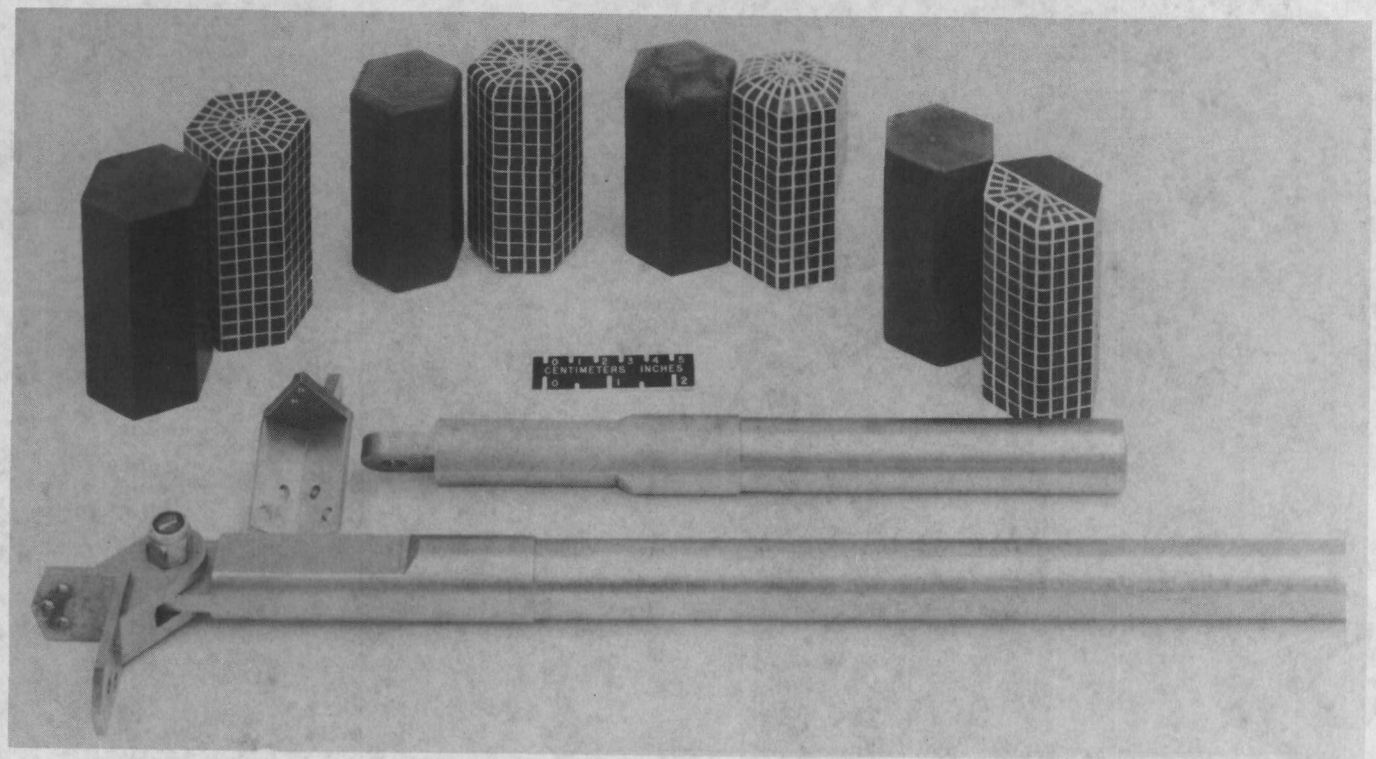

L-70-4650

(a) Heat-source models and corresponding grid models shown with stings and attitude adapters.

Figure 5.- Photographs of $\frac{1}{2}$-scale SNAP-19 models.

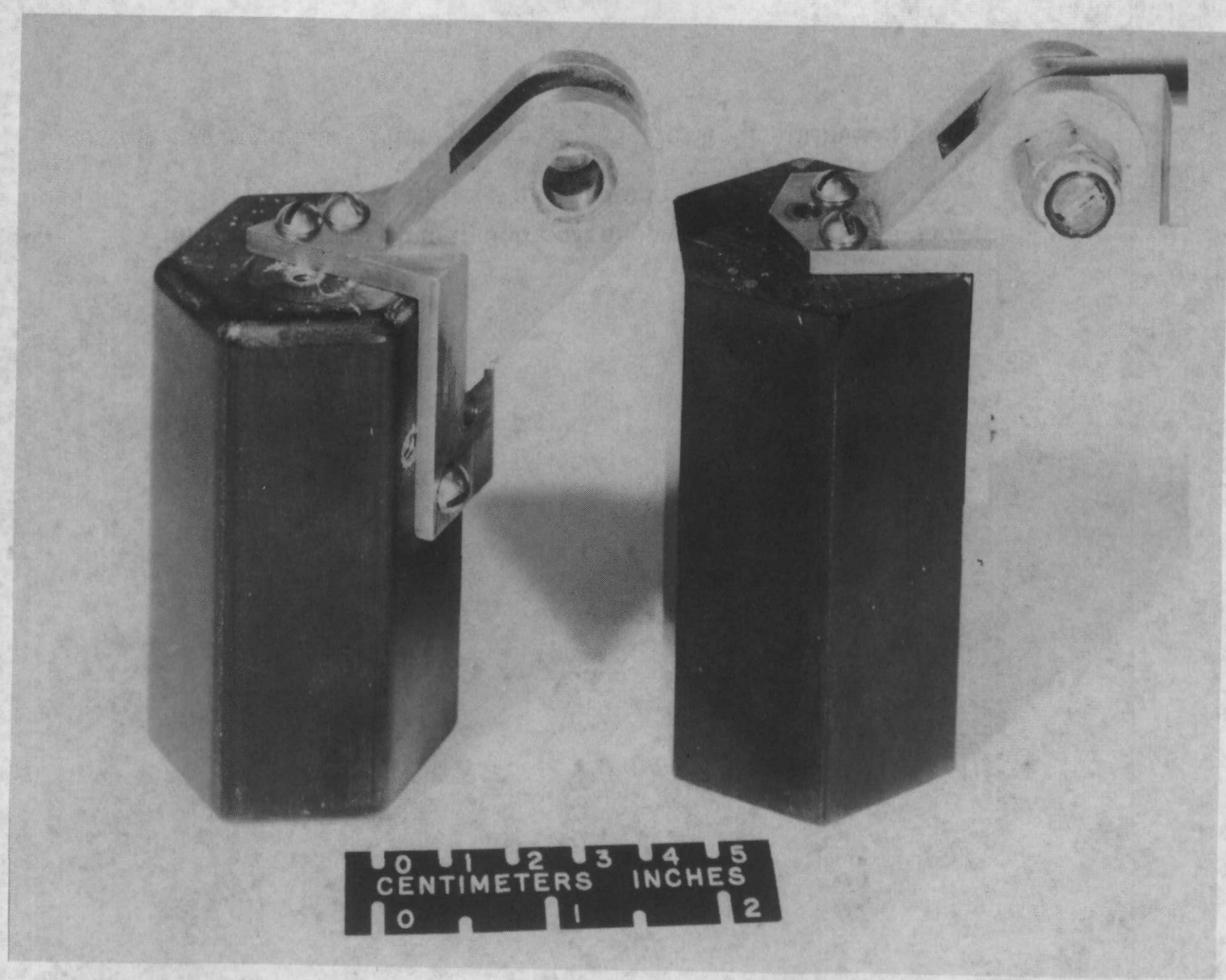

L-70-4651

(b) Attachment positions of attitude adapters for 0^{o} and 30^{o} roll.

Figure 5.- Continued.

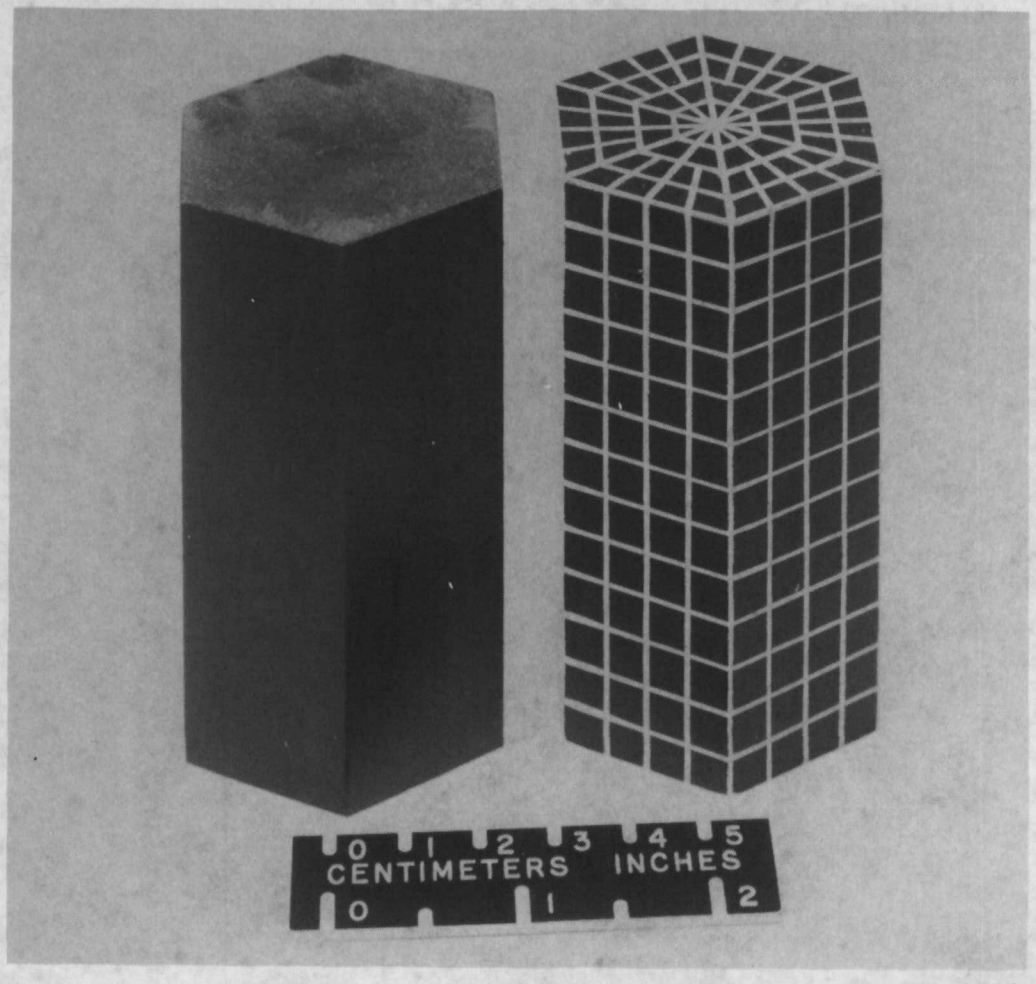

L-70-4654

(c) Unablated model and grid (model 001).

Figure 5.- Continued.

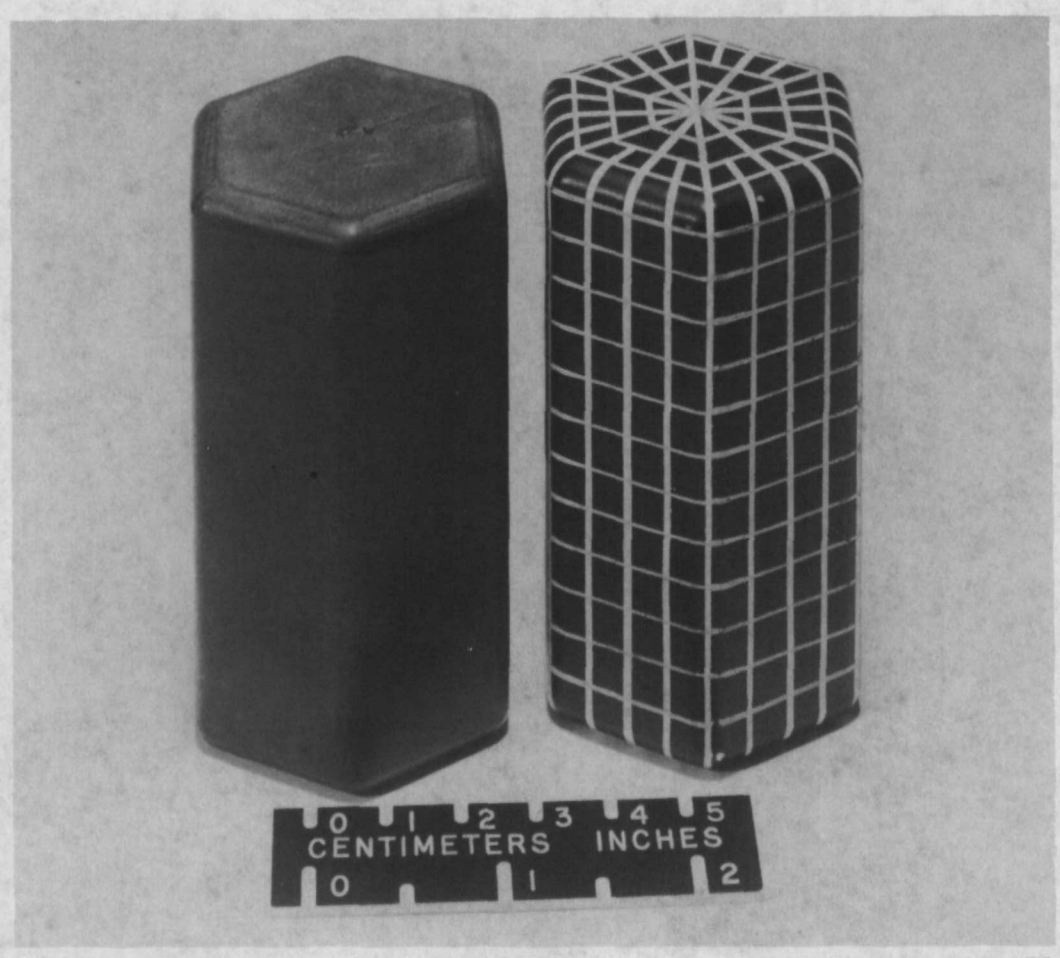

L-70-4653

(d) Uniformly ablated, random-tumble reentry model and grid (model 003).

Figure 5.- Continued.

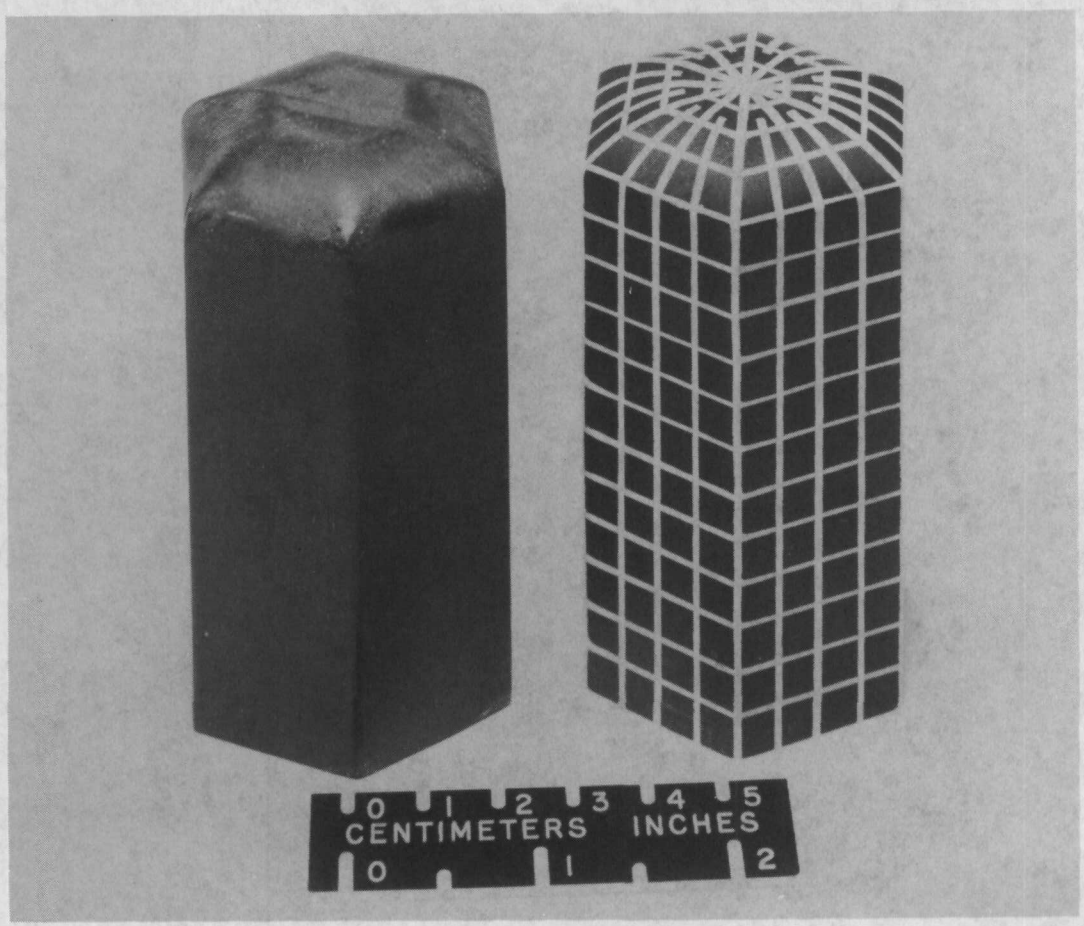

L-70-4655

(e) End ablated, end-on spinning reentry model and grid (model 005).

Figure 5.- Continued.

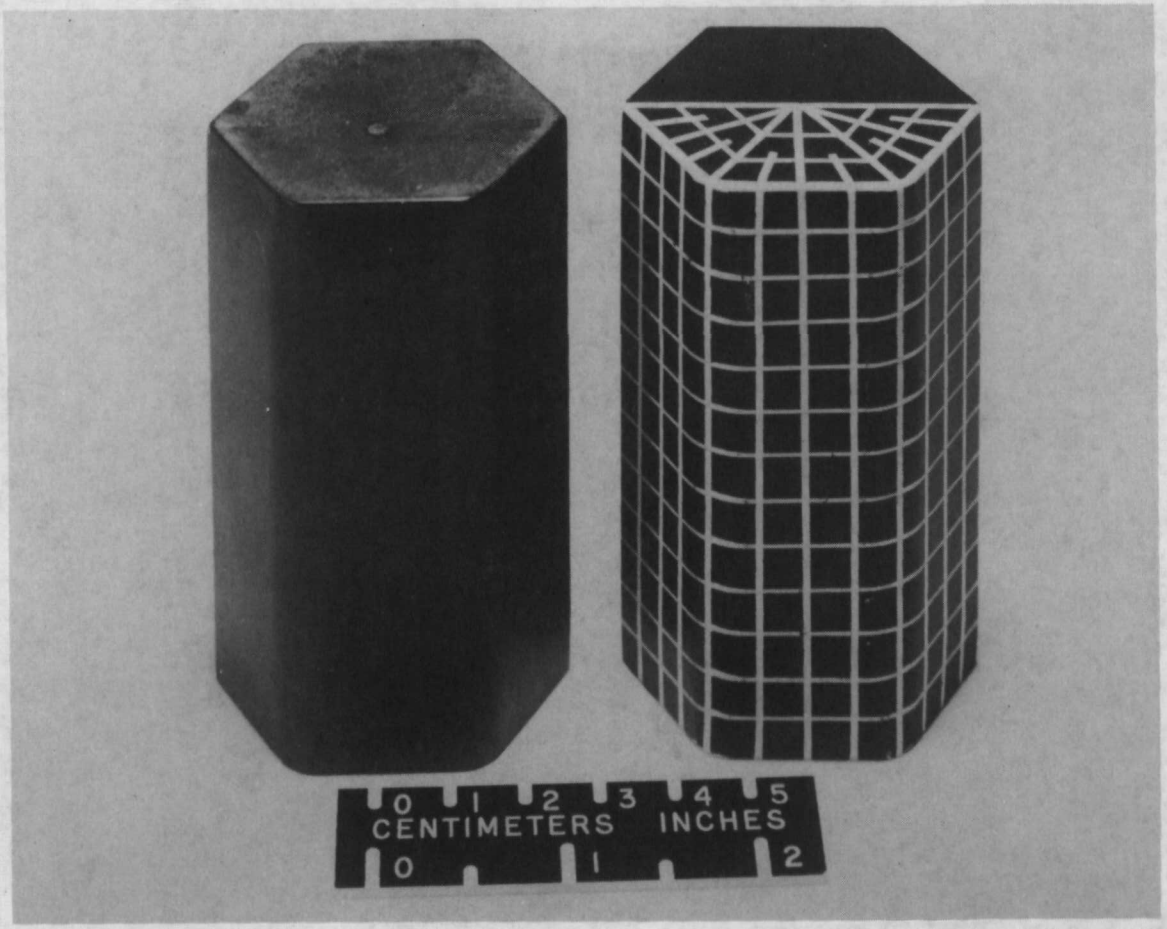

L-70-4652

(f) Asymmetrically ablated, side-on stable reentry model and grid (model 007).

Figure 5.- Concluded.

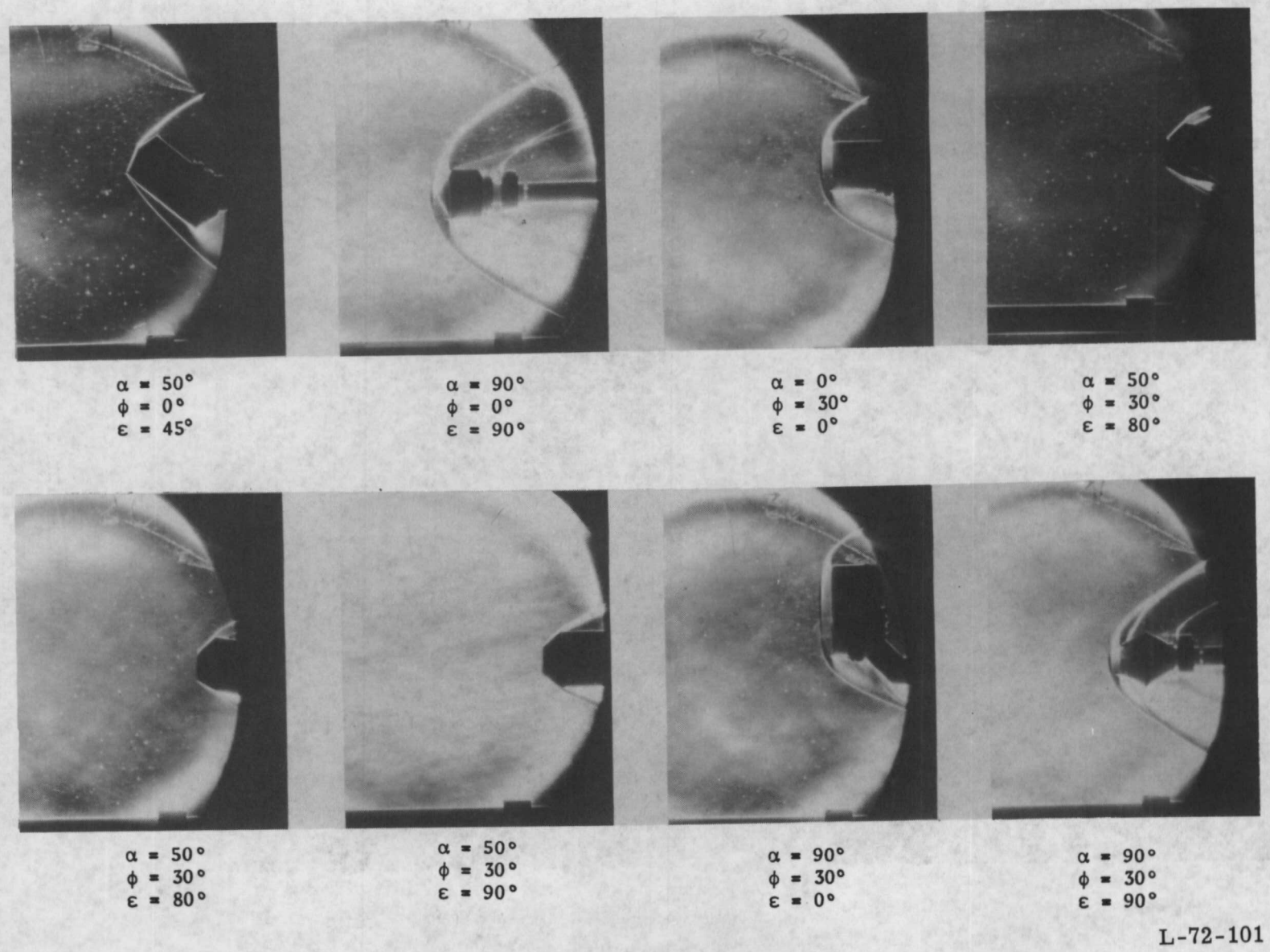

(a) Model 001 taken with Polaroid film.

Figure 6.- Schlieren photographs of $\frac{1}{2}$-scale SNAP-19/Pioneer fuel-cask models at Mach 6.

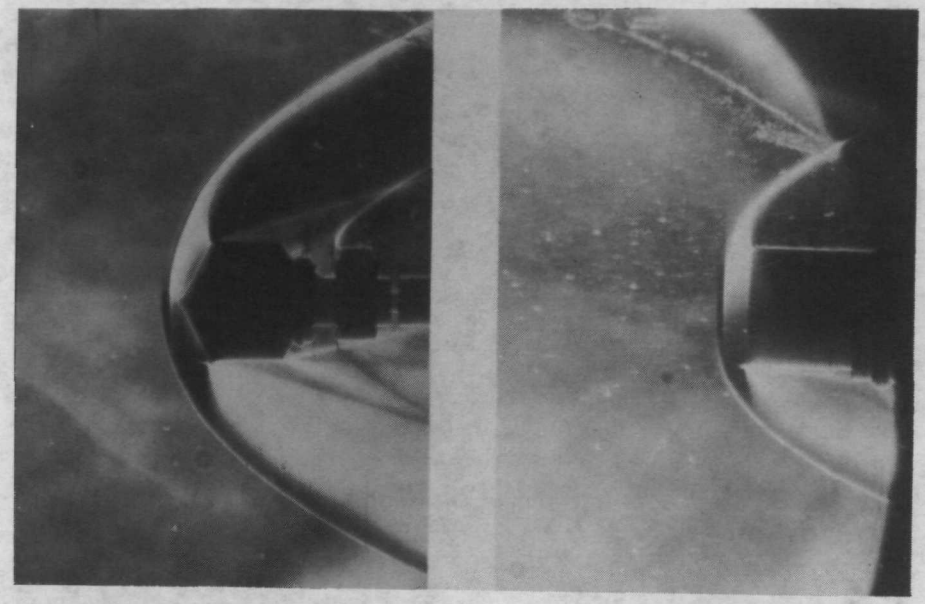

$\alpha = 90°$
$\phi = 0°$
$\varepsilon = 90°$

$\alpha = 0°$
$\phi = 30°$
$\varepsilon = 0°$

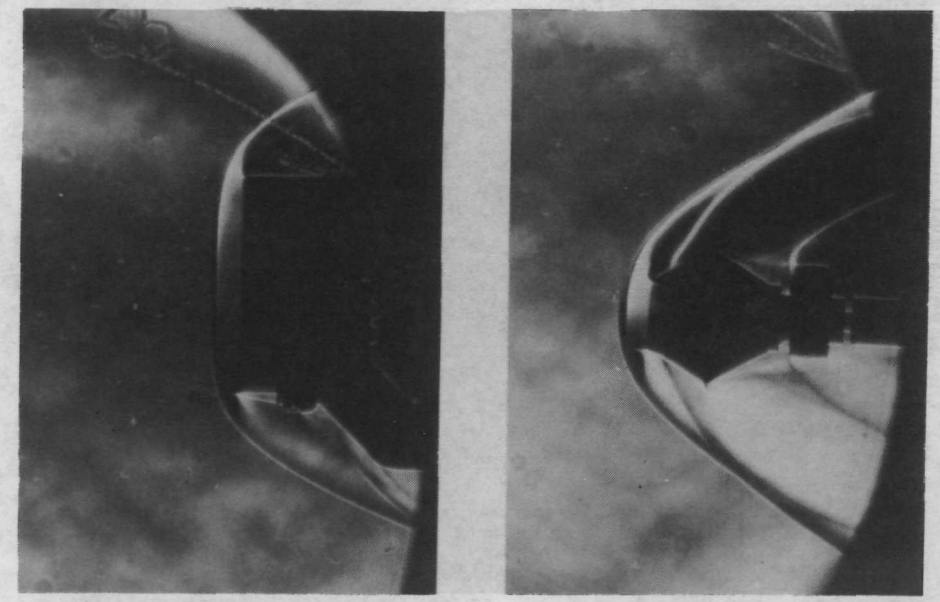

$\alpha = 90°$
$\phi = 30°$
$\varepsilon = 0°$

$\alpha = 90°$
$\phi = 30°$
$\varepsilon = 90°$

L-72-102

(b) Model 001 taken with 75-mm film.

Figure 6.- Continued.

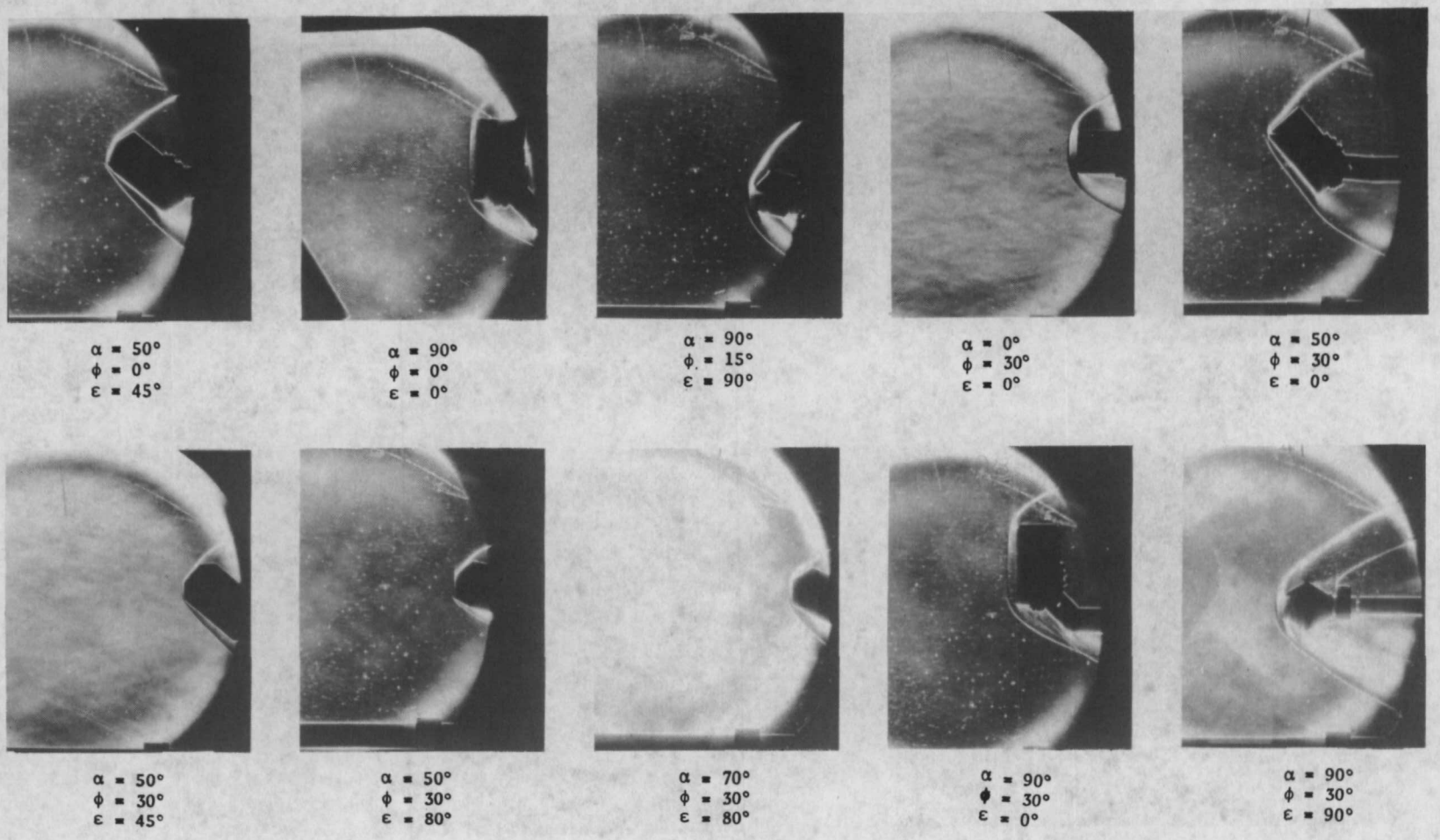

(c) Model 003 taken with Polaroid film.

Figure 6.- Continued.

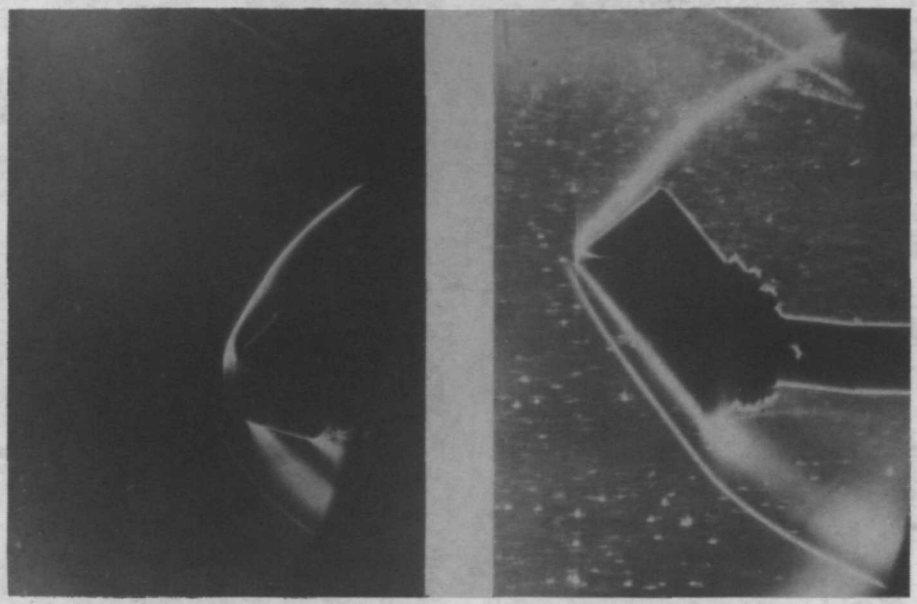

$\alpha = 90°$
$\phi = 15°$
$\varepsilon = 90°$

$\alpha = 50°$
$\phi = 30°$
$\varepsilon = 0°$

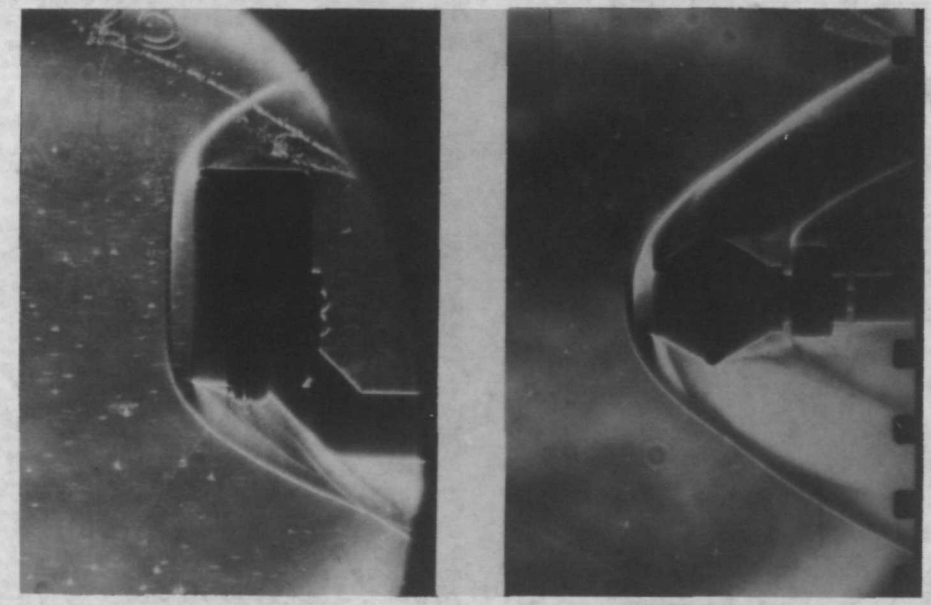

$\alpha = 90°$
$\phi = 30°$
$\varepsilon = 0°$

$\alpha = 90°$
$\phi = 30°$
$\varepsilon = 90°$

L-72-104

(d) Model 003 taken with 75-mm film.

Figure 6.- Continued.

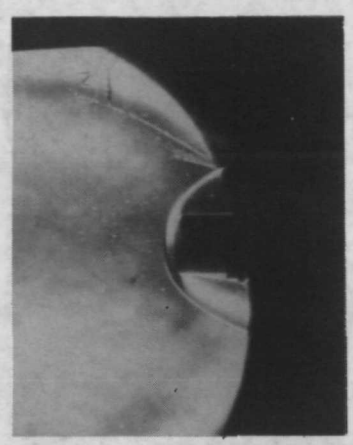

$\alpha = 0°$
$\phi = 30°$
$\varepsilon = 0°$

L-72-105

(e) Model 005 taken with Polaroid film.

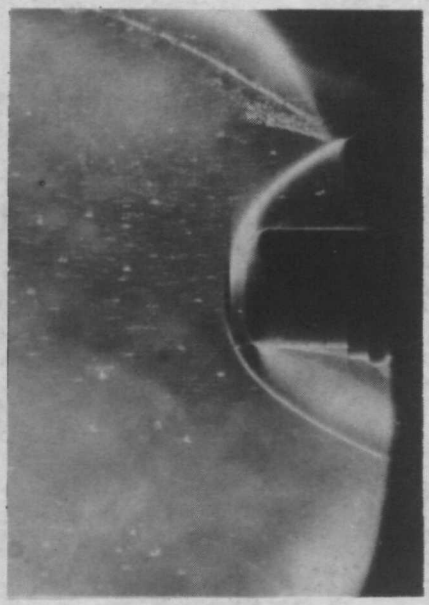

$\alpha = 0°$
$\phi = 30°$
$\varepsilon = 0°$

L-72-106

(f) Model 005 taken with 75-mm film.

Figure 6.- Continued.

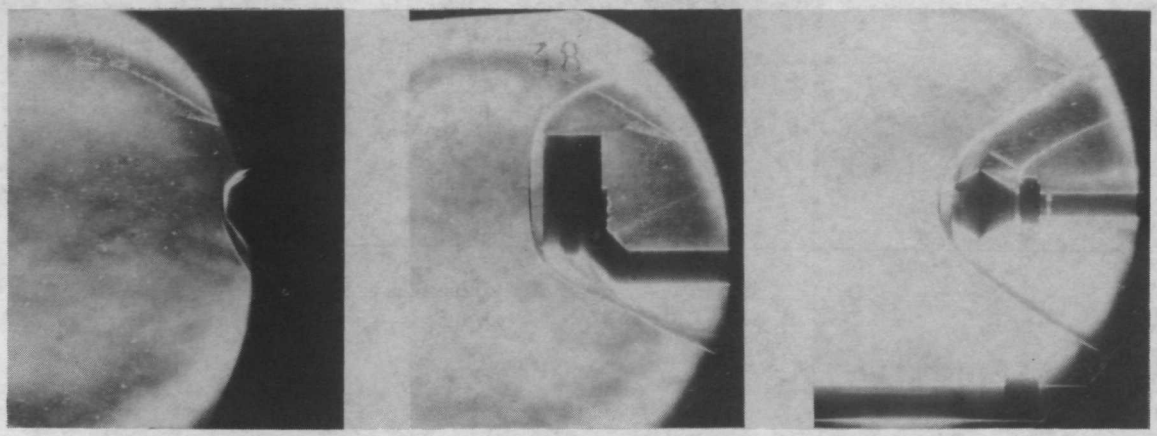

$\alpha = 70°$
$\phi = 30°$
$\varepsilon = 45°$

$\alpha = 90°$
$\phi = 30°$
$\varepsilon = 0°$

$\alpha = 90°$
$\phi = 30°$
$\varepsilon = 90°$

L-72-107

(g) Model 007 taken with Polaroid film.

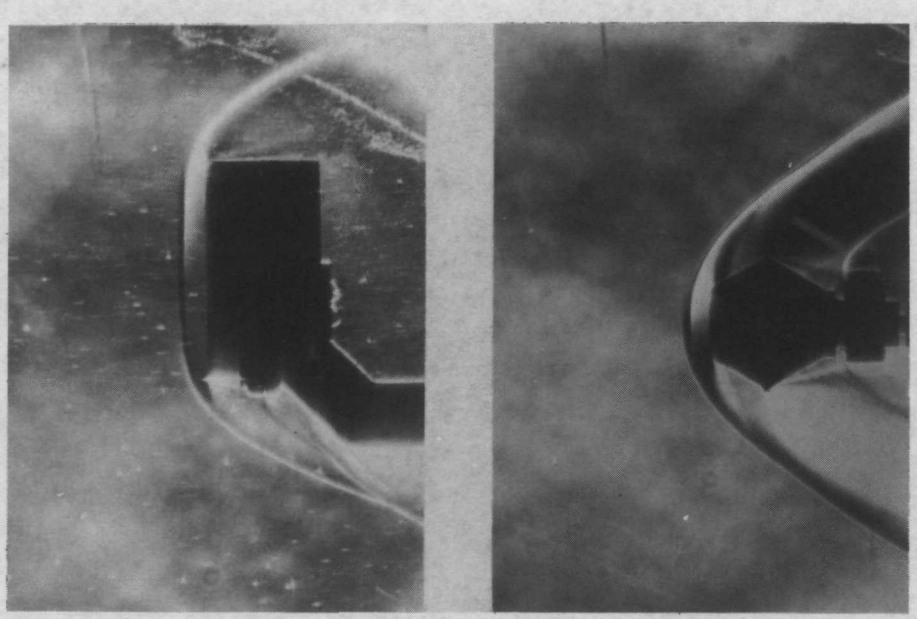

$\alpha = 90°$
$\phi = 30°$
$\varepsilon = 0°$

$\alpha = 90°$
$\phi = 30°$
$\varepsilon = 90°$

L-72-108

(h) Model 007 taken with 75-mm film.

Figure 6.- Concluded.

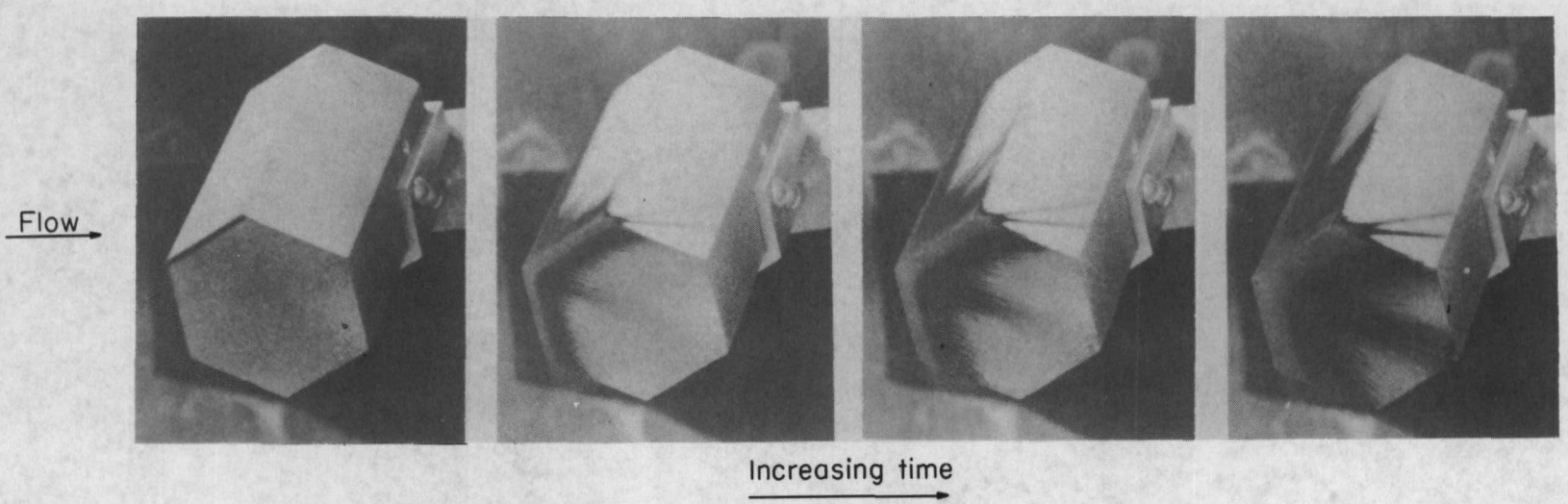

L-72-109

(a) Model 001; $\alpha = 50^{o}$; $\phi = 0^{o}$; $R_{\infty,L} = 0.82 \times 10^{6}$.

Figure 7.- Phase-change patterns on SNAP-19 entry configurations.

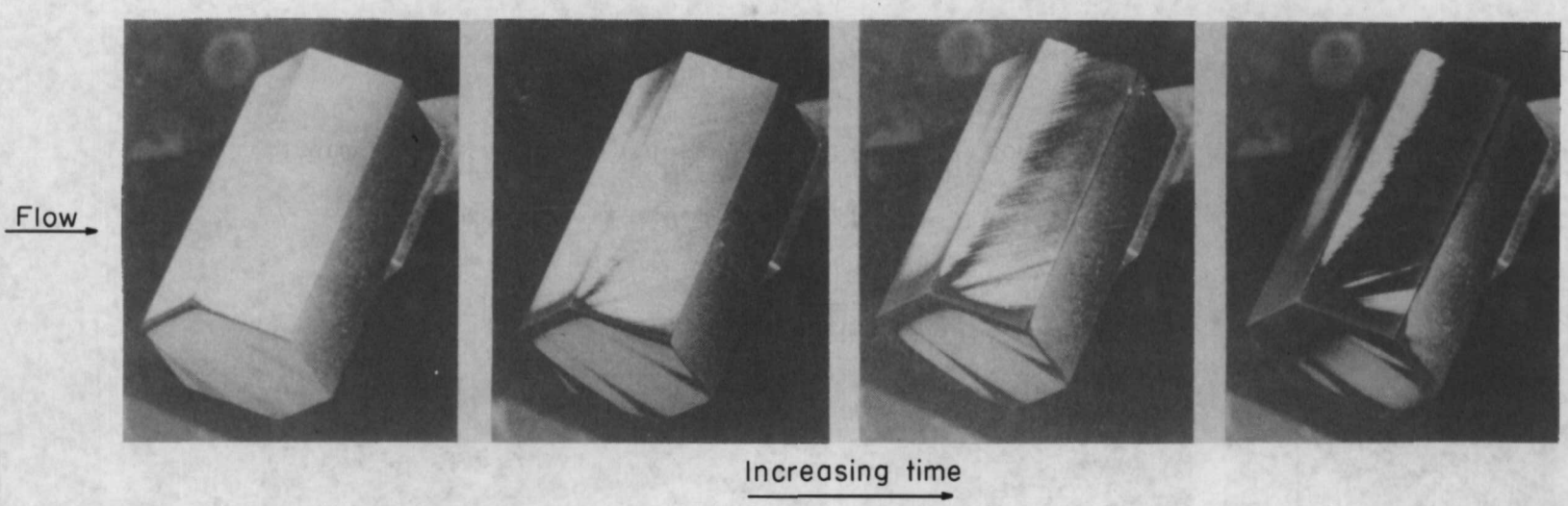

L-72-110

(b) Model 001; $\alpha = 50^{o}$; $\phi = 30^{o}$; $R_{\infty,L} = 2.18 \times 10^{6}$.

Figure 7.- Continued.

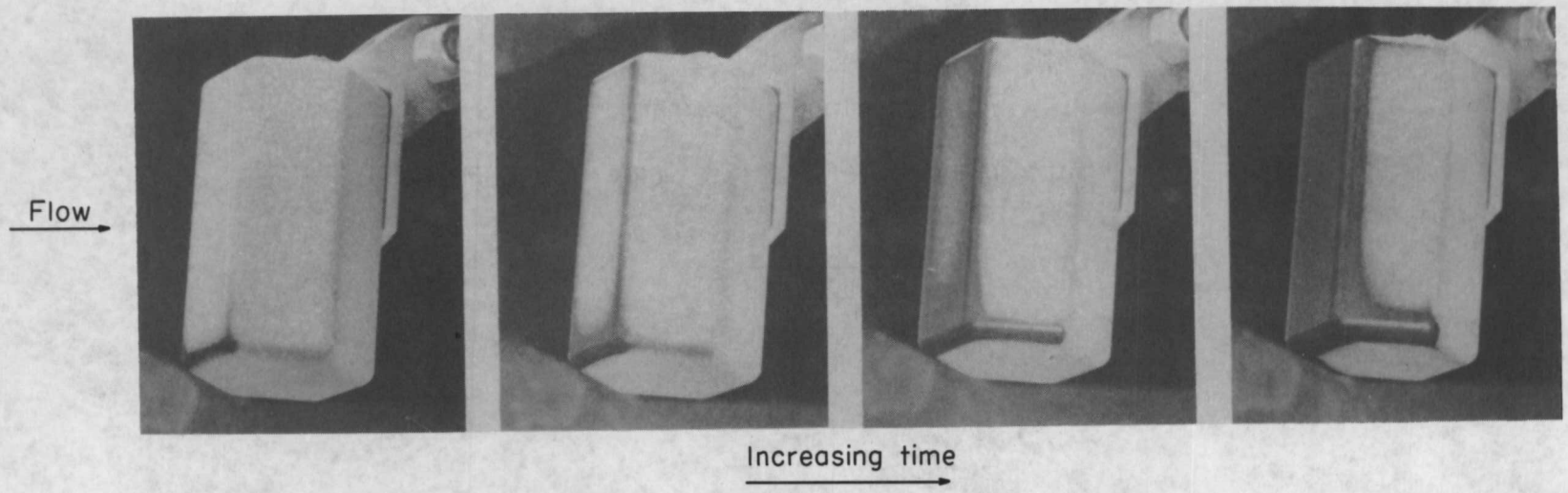

L-72-111

(c) Model 003; $\alpha = 70^{o}$; $\phi = 30^{o}$; $R_{\infty,L} = 2.20 \times 10^{6}$.

Figure 7.- Continued.

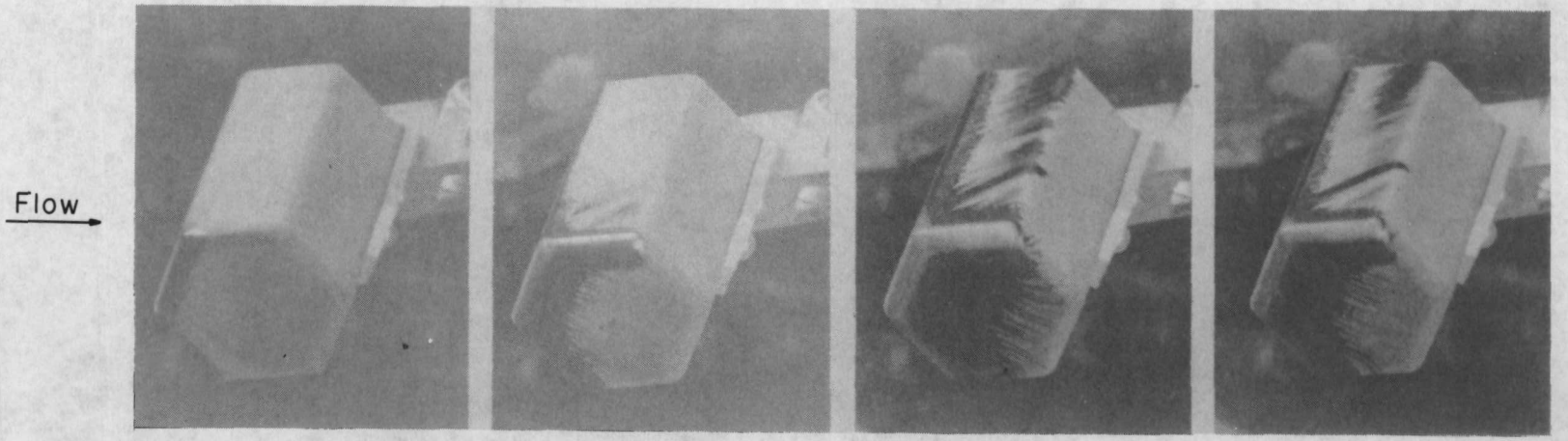

L-72-112

(d) Model 003; $\alpha = 50^{o}$; $\phi = 30^{o}$; $R_{\infty,L} = 2.20 \times 10^{6}$.

Figure 7.- Continued.

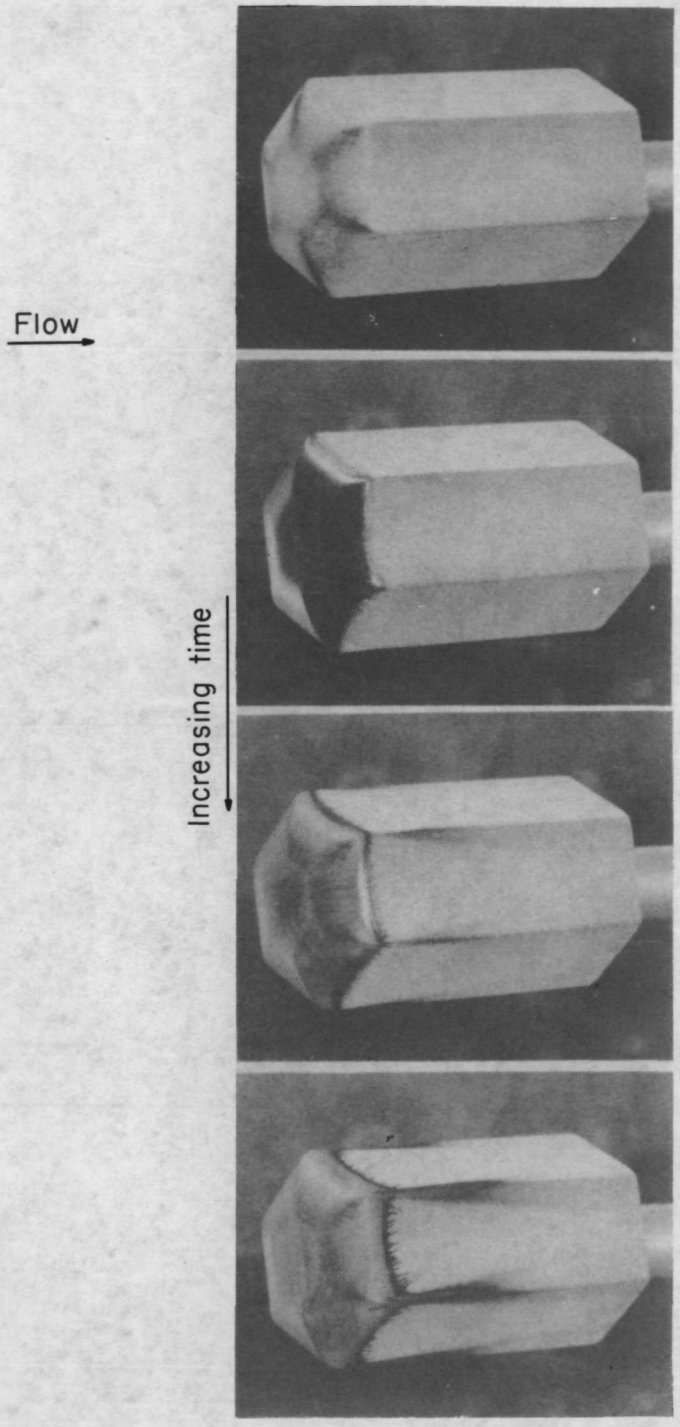

L-72-113

(e) Model 005; $\alpha = 0^{o}$; $R_{\infty,L} = 0.85 \times 10^{6}$.

Figure 7.- Continued.

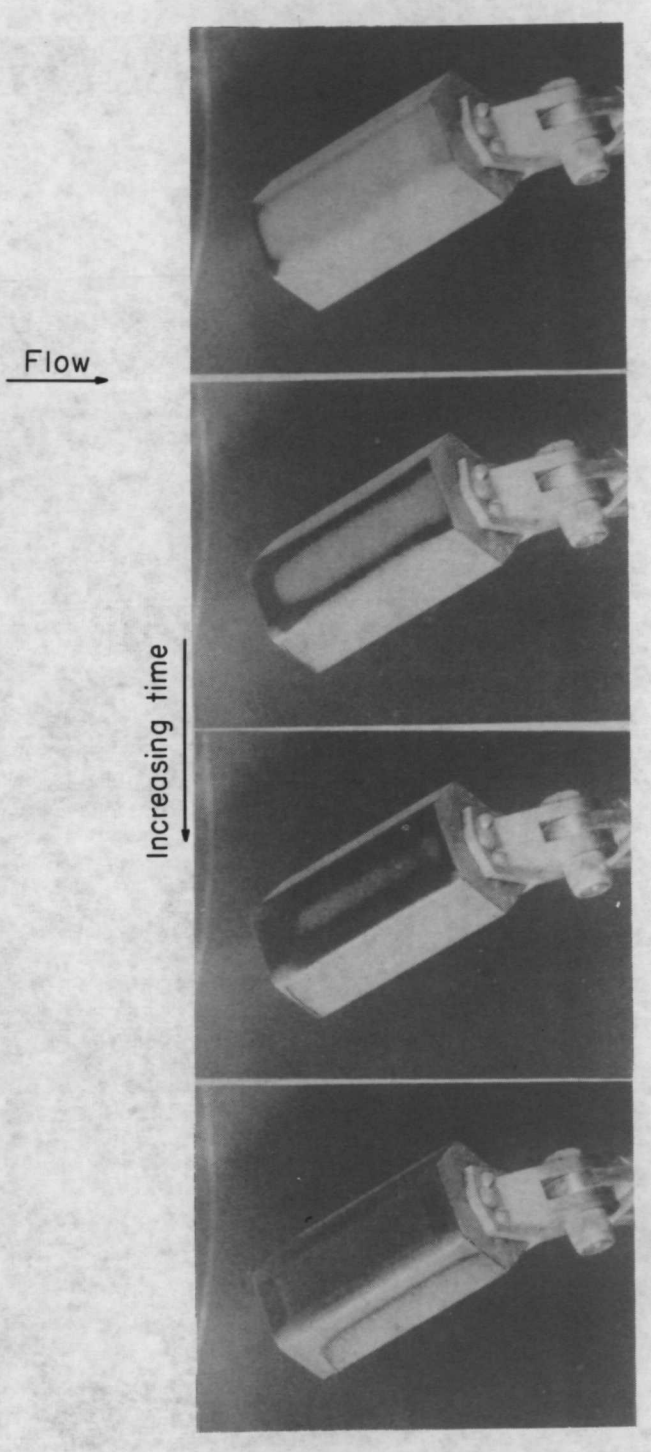

L-72-114

(f) Model 007; $\alpha = 70^{o}$; $\phi = 30^{o}$; $R_{\infty,L} = 0.84 \times 10^{6}$.

Figure 7.- Concluded.

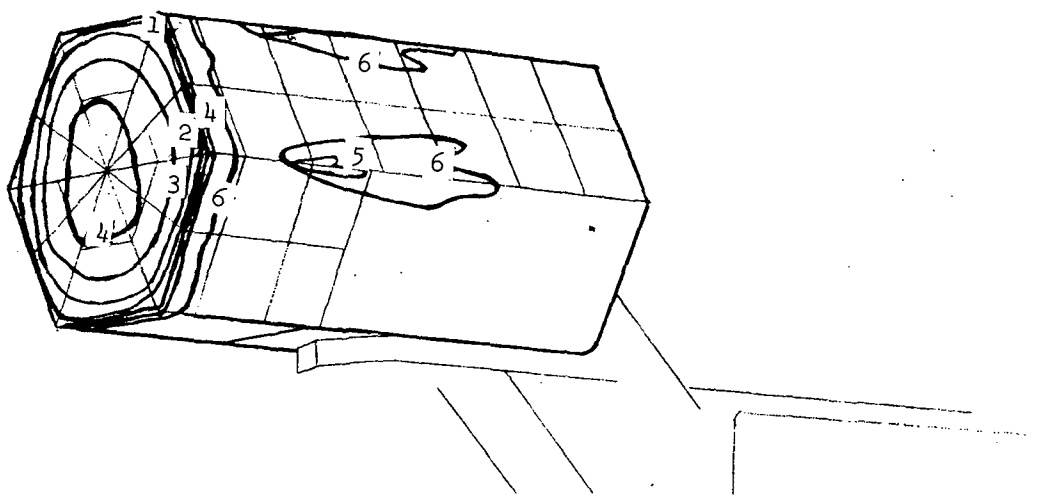

CONTOUR	T, SEC	H, BTU/FT. SQ-SEC-DEG-R	H/HS
1	2.00	1.48203E-02	1.98827E+00
2	3.00	1.21007E-02	1.62342E+00
3	4.00	1.04795E-02	1.40592E+00
4	5.00	9.37315E-03	1.25750E+00
5	10.00	6.62782E-03	8.89183E-01
6	33.50	3.62116E-03	4.85813E-01

(a) Side camera view.

Figure 8.- Nominal heat-transfer-coefficient contours on model 001 for $\alpha = 0^{o}$ and $R_{\infty,L} = 0.83 \times 10^{6}$. $T_{pc} = 353$ K; $T_i = 305$ K; $T_t = 520$ K; $\beta = 0.238$; $P_t = 1.27 \times 10^{6}$ N/m^2.

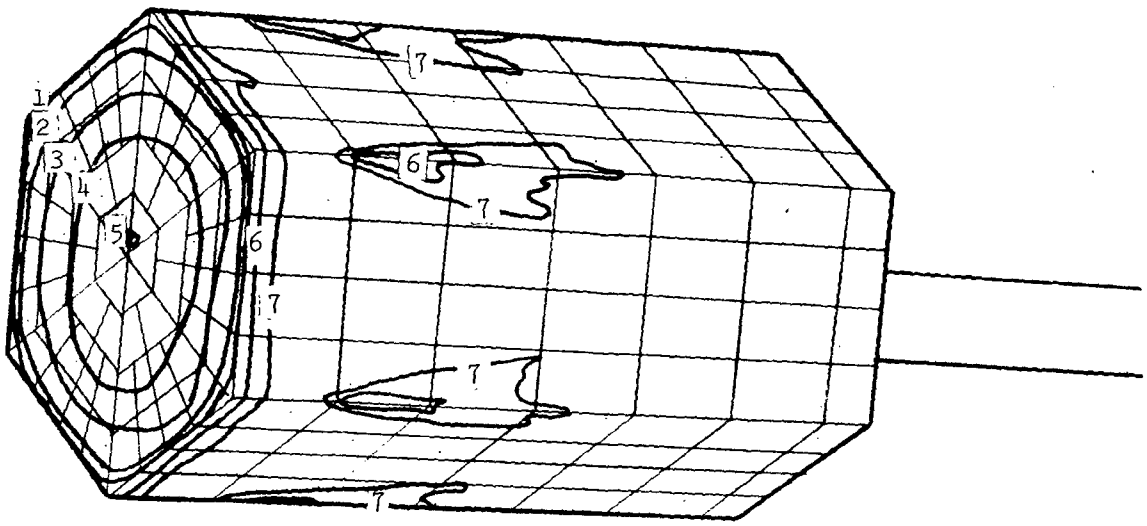

CONTOUR	T,SEC	H,BTU/FT.SQ-SEC-DEG-R	H/HS
1	2.00	1.48203E-02	1.98827E+00
2	2.50	1.32556E-02	1.77837E+00
3	3.50	1.12031E-02	1.50299E+00
4	4.50	9.88017E-03	1.32552E+00
5	6.00	8.55648E-03	1.14793E+00
6	10.00	6.62782E-03	8.89183E-01
7	25.00	4.19180E-03	5.62369E-01

(b) Top camera view.

Figure 8.- Concluded.

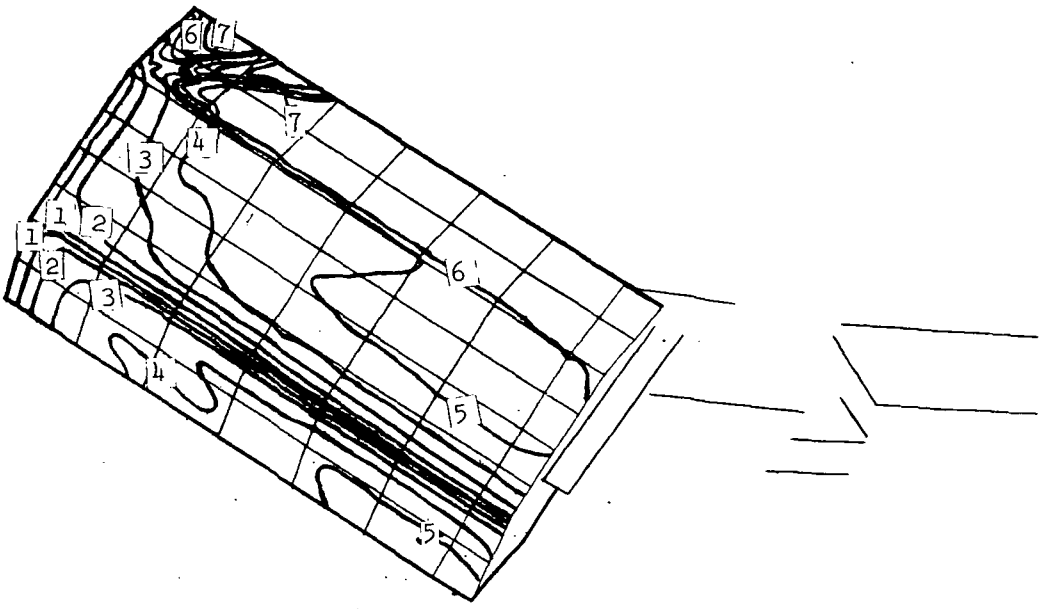

CONTOUR	T, SEC	H, BTU/FT.SQ-SEC-DEG-R	H/HS
1	.50	3.23860E-02	4.43964E+00
2	1.50	1.86981E-02	2.56322E+00
3	3.50	1.22408E-02	1.67802E+00
4	7.50	8.36203E-03	1.14631E+00
5	12.50	6.47720E-03	8.87927E-01
6	17.50	5.47424E-03	7.50435E-01

(a) Side camera view.

Figure 9.- Nominal heat-transfer-coefficient contours on model 001 for $\alpha = 50^{o}$, $\phi = 0^{o}$, and $R_{\infty,L} = 0.82 \times 10^{6}$. $T_{pc} = 353$ K; $T_i = 304$ K; $T_t = 510$ K; $\beta = 0.260$; $P_t = 1.22 \times 10^{6}$ N/m^2.

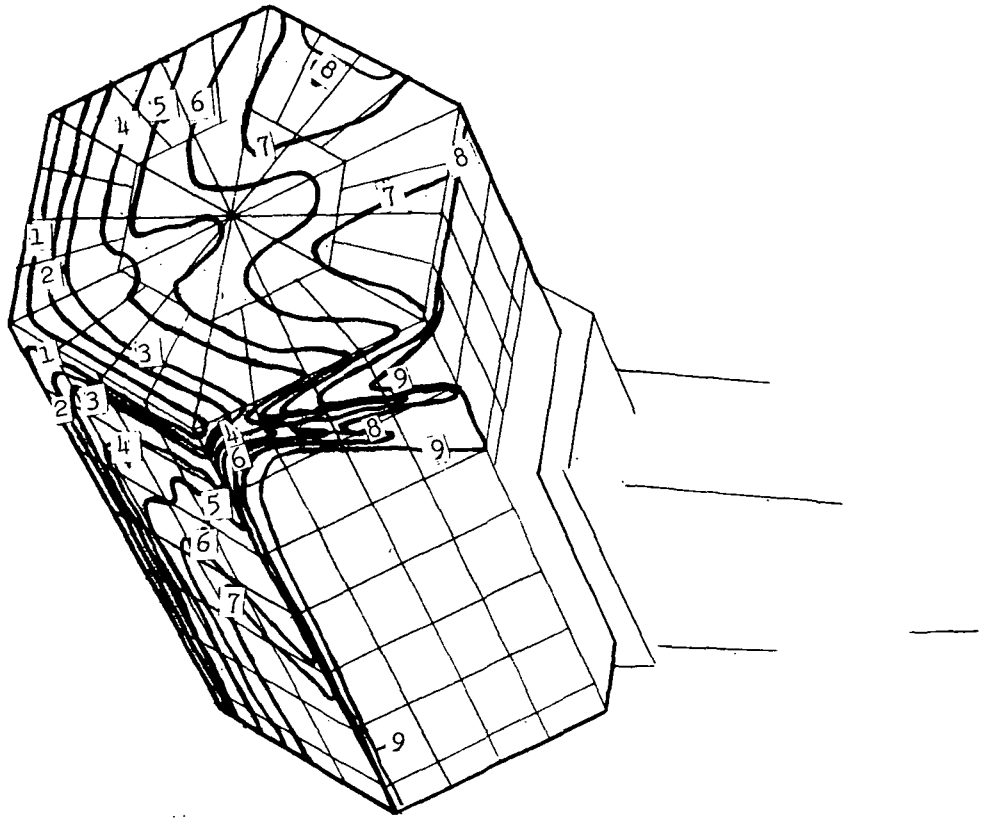

CONTOUR	T,SEC	H,BTU/FT.SQ-SEC-DEG-R	H/HS
1	.50	3.23860E-02	4.43964E+00
2	1.50	1.86981E-02	2.56322E+00
3	2.50	1.44835E-02	1.98547E+00
4	5.00	1.02414E-02	1.40394E+00
5	7.50	8.36203E-03	1.14631E+00
6	10.00	7.24173E-03	9.92733E-01
7	13.50	6.23269E-03	8.54408E-01
8	17.50	5.47424E-03	7.50435E-01
9	30.00	4.18102E-03	5.73154E-01

(b) Top camera view.

Figure 9.- Concluded.

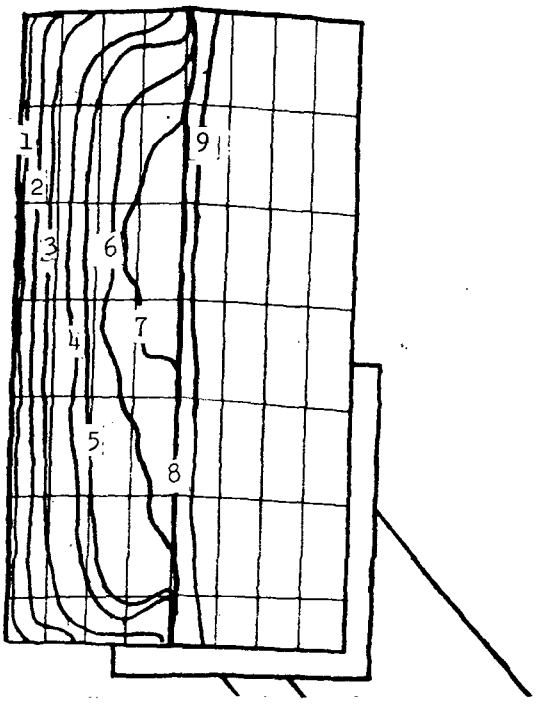

CONTOUR	T, SEC	H, BTU/FT. SQ-SEC-DEG-R	H/HS
1	.50	3.21404E-02	4.31479E+00
2	1.50	1.85563E-02	2.49115E+CC
3	2.5C	1.43736E-02	1.92963E+C0
4	4.00	1.13634E-02	1.52551E+C0
5	4.50	1.07135E-02	1.43826E+C0
6	5.50	9.69070E-03	1.30096E+00
7	6.CC	9.27814E-03	1.24557E+CC
8	6.5C	8.91415E-03	1.19671E+C0
9	30.00	4.14931E-03	5.57C37E-C1

(a) Side camera view.

Figure 10.- Nominal heat-transfer-coefficient contours on model 001 for $\alpha = 90^{o}$, $\phi = 0^{o}$, and $R_{\infty,L} = 0.84 \times 10^{6}$. $T_{pc} = 353$ K; $T_i = 304$ K; $T_t = 517$ K; $\beta = 0.258$; $P_t = 1.27 \times 10^{6}$ N/m^2.

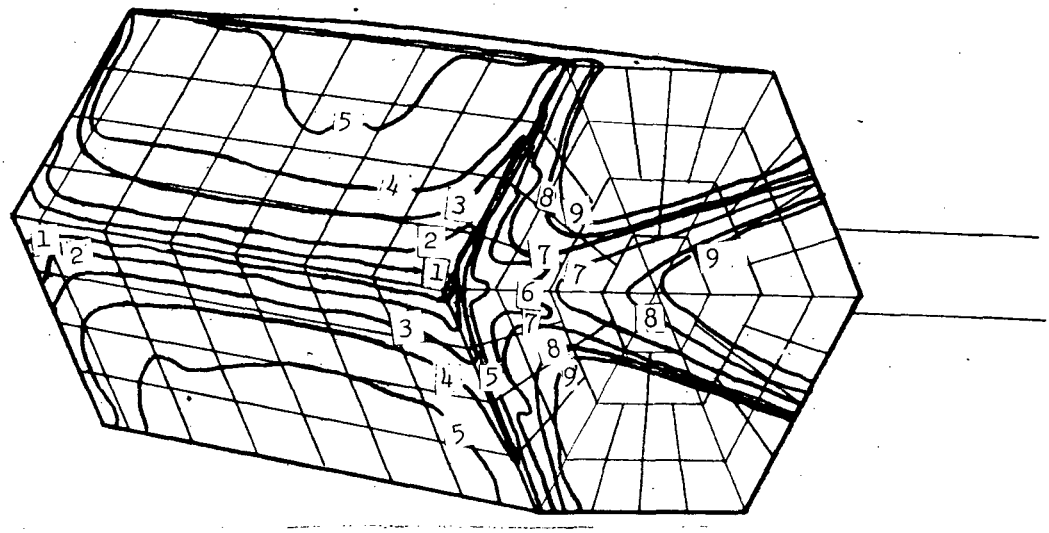

CONTOUR	T, SEC	H, BTU/FT. SQ-SEC-DEG-R	H/HS
1	.80	2.54092E-02	3.41114E+00
2	1.50	1.85563E-02	2.49115E+00
3	2.50	1.43736E-02	1.92963E+00
4	3.50	1.21479E-02	1.63084E+00
5	5.00	1.01637E-02	1.36446E+00
6	11.60	6.67279E-03	8.95810E-01
7	16.70	5.56133E-03	7.46598E-01
8	30.00	4.14931E-03	5.57037E-01
9	38.00	3.68676E-03	4.94941E-01

(b) Top camera view.

Figure 10.- Concluded.

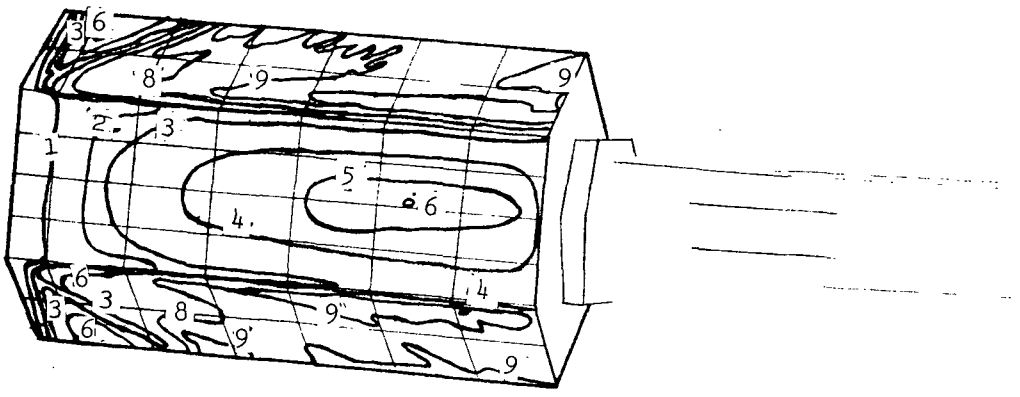

CONTOUR	T, SEC	H, BTU/FT. SQ-SEC-DEG-R	H/HS
1	.50	1.29186E-02	2.90098E+00
2	1.10	8.70974E-03	1.95584E+00
3	1.60	7.22174E-03	1.62170E+00
4	2.50	5.77739E-03	1.29736E+00
5	3.20	5.10654E-03	1.14671E+00
6	3.50	4.88278E-03	1.09647E+00
7	7.50	3.33558E-03	7.49030E-01
8	10.00	2.88869E-03	6.48679E-01
9	15.00	2.35861E-03	5.29644E-01

(a) Side camera view.

Figure 11.- Nominal heat-transfer-coefficient contours on model 001 for $\alpha = 50^{\circ}$, $\phi = 30^{\circ}$, and $R_{\infty,L} = 0.35 \times 10^{6}$. $T_{pc} = 325$ K; $T_i = 307$ K; $T_t = 478$ K; $\beta = 0.104$; $P_t = 0.47 \times 10^{6}$ N/m^2.

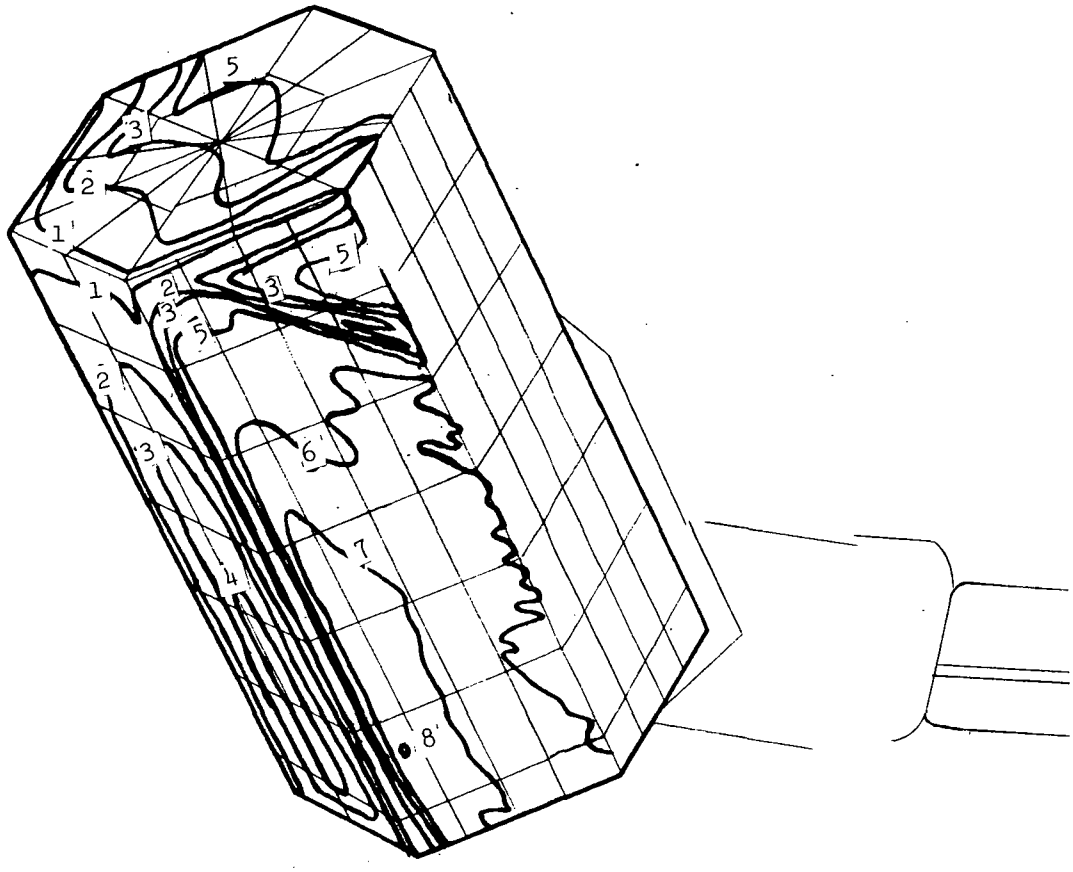

CONTOUR	T,SEC	H,BTU/FT.SQ-SEC-DEG-R	H/HS
1	.40	1.44435E-02	3.24340E+CO
2	1.60	7.22174E-03	1.62170E+CC
3	2.50	5.77739E-03	1.29736E+CO
4	3.10	5.18825E-03	1.165C6E+CO
5	4.60	4.25915E-03	9.56425E-C1
6	11.50	2.69372E-03	6.C4897E-C1
7	17.00	2.21553E-03	4.97514E-C1
8	23.00	1.90475E-03	4.27726E-C1

(b) Top camera view.

Figure 11.- Concluded.

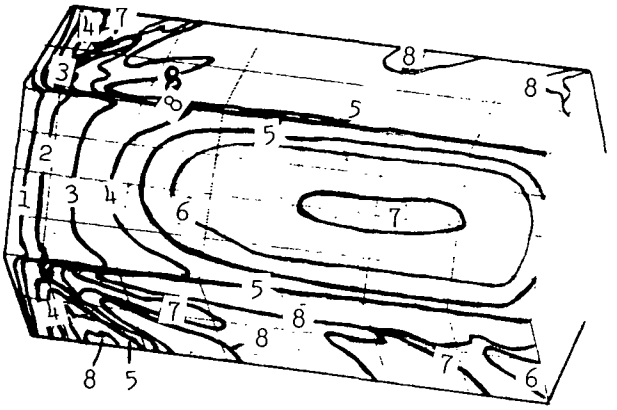

CONTOUR	T, SEC	H, BTU/FT. SQ-SEC-DEG-R	H/HS
1	.60	2.90668E-02	3.98887E+CC
2	1.5C	1.83835E-02	2.5227EE+CC
3	3.5C	1.20348E-02	1.65155E+CC
4	5.50	9.60045E-03	1.31748E+CC
5	6.6C	8.7639?E-03	1.2026?E+CC
6	8.00	7.96C27E-03	1.09240E+CC
7	10.00	7.11988E-03	?.77C69E-C1
8	13.CC	6.24455E-03	8.56?46E-C1

(a) Side camera view.

Figure 12.- Nominal heat-transfer-coefficient contours on model 001 for $\alpha = 50^{\circ}$, $\phi = 30^{\circ}$, and $R_{\infty,L} = 0.83 \times 10^{6}$. $T_{pc} = 353$ K; $T_i = 306$ K; $T_t = 506$ K; $\beta = 0.256$; $P_t = 1.22 \times 10^{6}$ N/m^2.

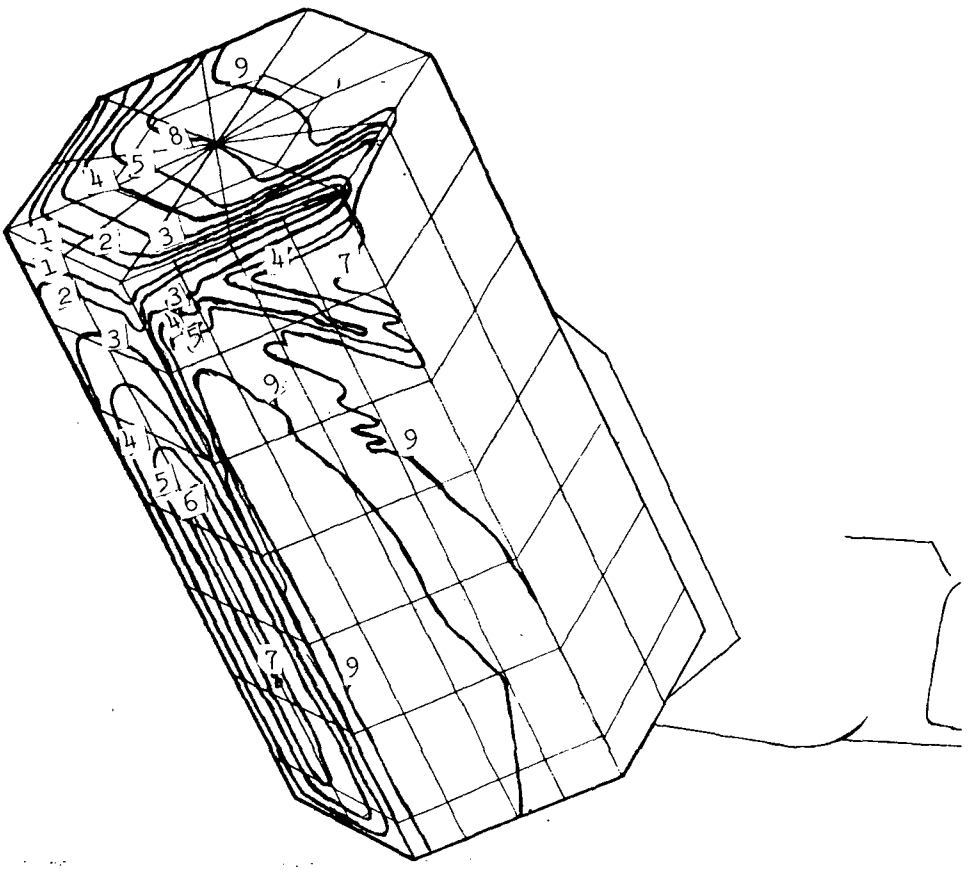

CONTOUR	T, SEC	H, BTU/FT.SQ-SEC-DEG-R	H/HS
1	1.00	2.25150E-02	3.08976E+00
2	2.00	1.59205E-02	2.18479E+00
3	4.00	1.12575E-02	1.54488E+00
4	6.00	9.19173E-03	1.26139E+00
5	8.00	7.96027E-03	1.09240E+00
6	9.50	7.30484E-03	1.00245E+00
7	10.30	7.01543E-03	9.62735E-01
8	11.00	6.78854E-03	9.31599E-01
9	15.00	5.81336E-03	7.97773E-01

(b) Top camera view.

Figure 12.- Concluded.

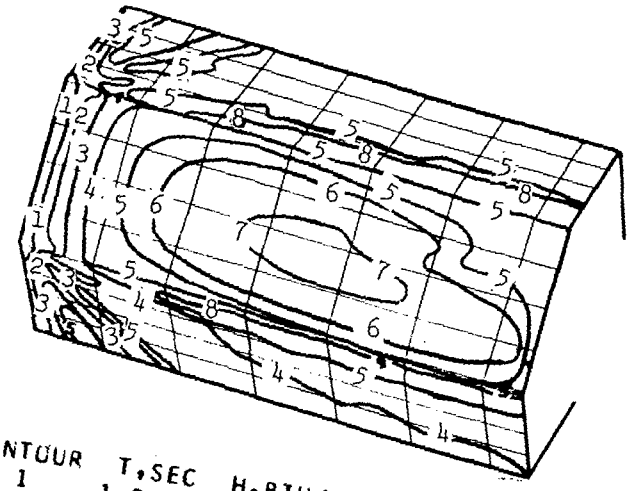

CONTOUR	T, SEC	H, BTU/FT.SQ-SEC-DEG-R	H/HS
1	1.00	5.56934E-02	4.71287E+00
2	2.50	3.52236E-02	2.98068E+00
3	5.00	2.49069E-02	2.10766E+00
4	6.50	2.18448E-02	1.84854E+00
5	10.00	1.76118E-02	1.49034E+00
6	12.50	1.57525E-02	1.33300E+00
7	17.50	1.33133E-02	1.12659E+00
8	20.00	1.24534E-02	1.05383E+00

(a) Side camera view.

Figure 13.- Nominal heat-transfer-coefficient contours on model 001 for $\alpha = 50^{o}$, $\phi = 30^{o}$, and $R_{\infty,L} = 2.18 \times 10^{6}$. $T_{pc} = 394$ K; $T_i = 304$ K; $T_t = 506$ K; $\beta = 0.633$; $P_t = 3.20 \times 10^{6}$ N/m2.

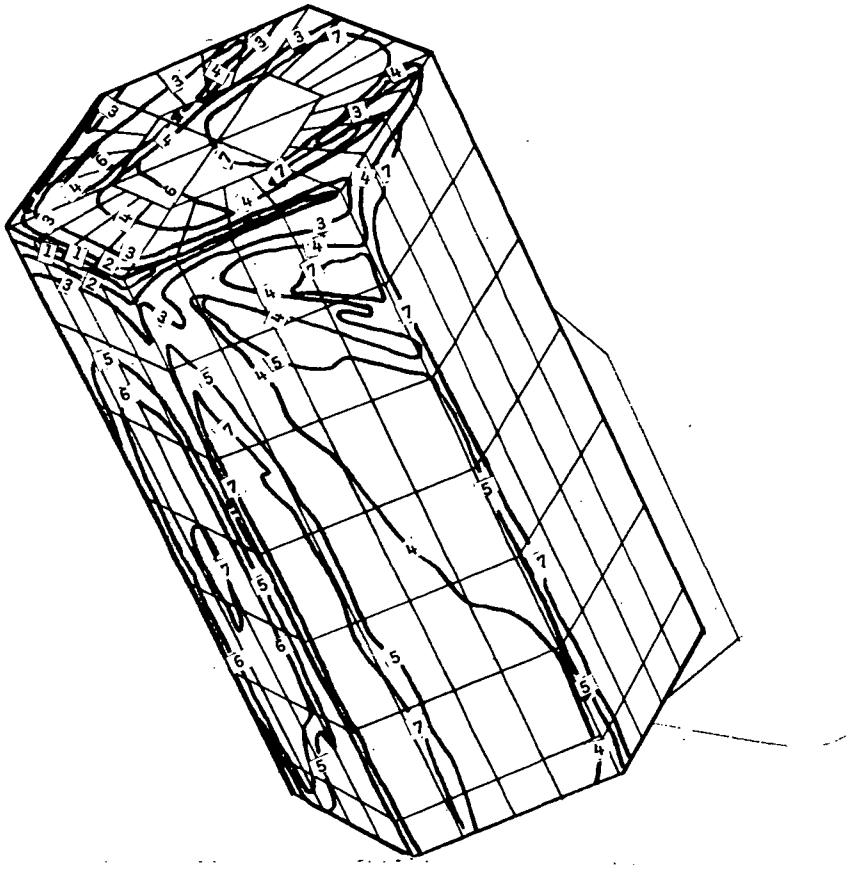

CONTOUR	T,SEC	H,BTU/FT.SQ-SEC-DEG-R	H/HS
1	.50	7.87624E-02	6.66500E+00
2	1.50	4.54735E-02	3.84804E+00
3	3.50	2.97694E-02	2.51913E+00
4	8.00	1.96906E-02	1.66625E+00
5	10.00	1.76118E-02	1.49034E+00
6	12.50	1.57525E-02	1.33300E+00
7	17.50	1.33133E-02	1.12659E+00

(b) Top camera view.

Figure 13.- Concluded.

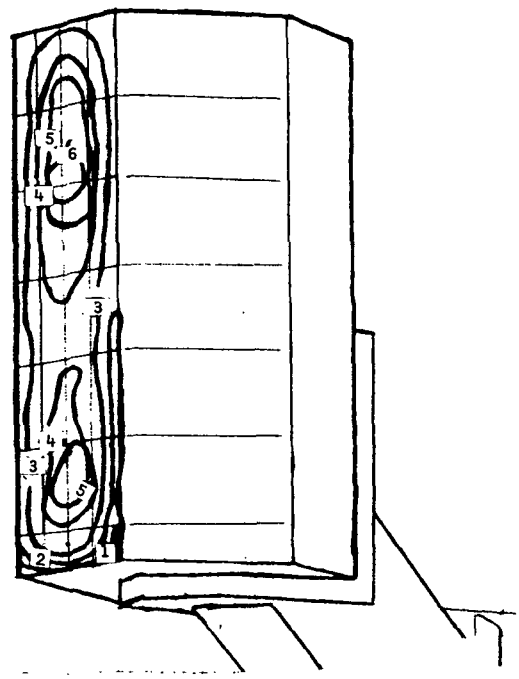

CONTOUR	T, SEC	H, BTU/FT. SQ-SEC-DEG-R	H/HS
1	2.10	2.14958E-02	2.95131E+00
2	3.50	1.66537E-02	2.28608E+00
3	4.50	1.46872E-02	2.01613E+00
4	5.80	1.29369E-02	1.77567E+00
5	6.20	1.25126E-02	1.71763E+00
6	6.80	1.19478E-02	1.64010E+00

(a) Side camera view.

Figure 14.- Nominal heat-transfer-coefficient contours on model 001 for $\alpha = 90^{\circ}$, $\phi = 30^{\circ}$, and $R_{\infty,L} = 0.82 \times 10^{6}$. $T_{pc} = 367$ K; $T_i = 304$ K; $T_t = 511$ K; $\beta = 0.354$; $P_t = 1.22 \times 10^{6}$ N/m^2.

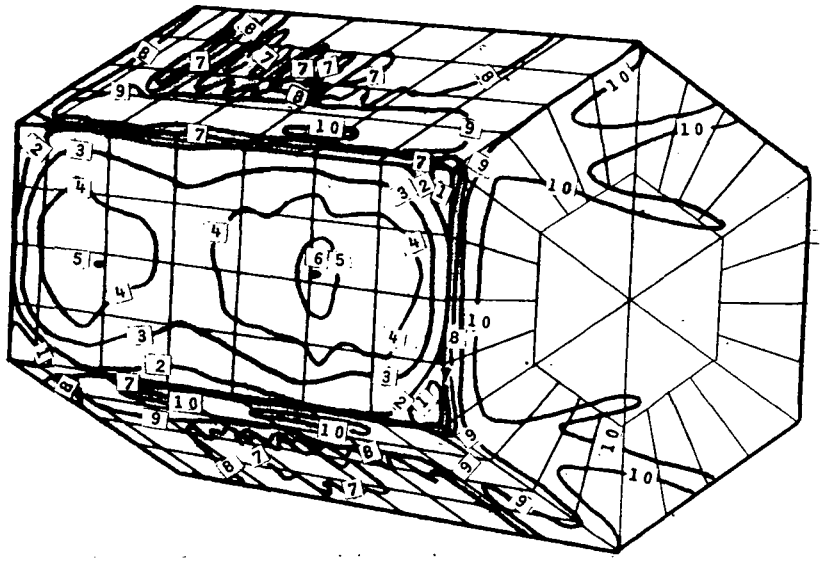

CONTOUR	T, SEC	H, BTU/FT. SQ-SEC-DEG-R	H/HS
1	3.70	1.61973E-02	2.22343E+00
2	4.00	1.55781E-02	2.13843E+00
3	5.00	1.39335E-02	1.91267E+00
4	6.00	1.27194E-02	1.74602E+00
5	7.00	1.17759E-02	1.61650E+00
6	7.60	1.13015E-02	1.55138E+00
7	10.00	9.85244E-03	1.35246E+00
8	15.00	8.04448E-03	1.10428E+00
9	20.00	6.96673E-03	9.56334E-01
10	35.50	5.22913E-03	7.17811E-01

(b) Top camera view.

Figure 14.- Concluded.

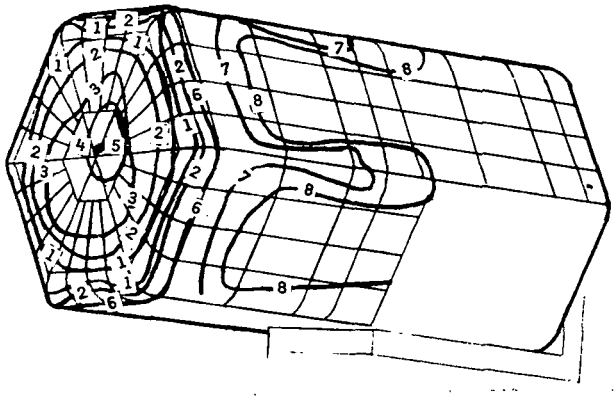

CONTOUR	T, SEC	H, BTU/FT.SQ-SEC-DEG-R	H/HS
1	3.00	1.45270E-02	1.98508E+00
2	4.10	1.24264E-02	1.69804E+00
3	4.90	1.13668E-02	1.55325E+00
4	5.70	1.05390E-02	1.44013E+00
5	6.50	9.86917E-03	1.34860E+00
6	10.60	7.72831E-03	1.05606E+00
7	40.80	3.93919E-03	5.38282E-01
8	63.10	3.16754E-03	4.32838E-01

(a) Side camera view.

Figure 15.- Nominal heat-transfer-coefficient contours on model 003 for $\alpha = 0^{o}$ and $R_{\infty,L} = 0.86 \times 10^{6}$. $T_{pc} = 353$ K; $T_i = 304$ K; $T_t = 500$ K; $\beta = 0.286$; $P_t = 1.24 \times 10^{6}$ N/m^2.

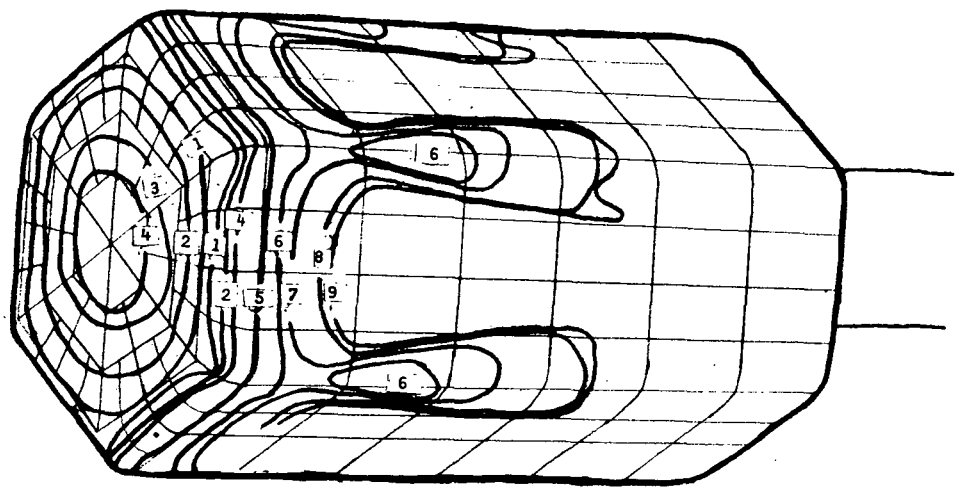

CONTOUR	T,SEC	H,BTU/FT.SQ-SEC-DEG-R	H/HS
1	2.70	1.53128E-02	2.09246E+00
2	3.70	1.30809E-02	1.78747E+00
3	4.70	1.16062E-02	1.58595E+00
4	5.00	1.12526E-02	1.53764E+00
5	14.00	6.72471E-03	9.18916E-01
6	30.80	4.53380E-03	6.19533E-01
7	41.00	3.92957E-03	5.36967E-01
8	59.20	3.27022E-03	4.46867E-01
9	63.10	3.16754E-03	4.32838E-01

(b) Top camera view.

Figure 15.- Concluded.

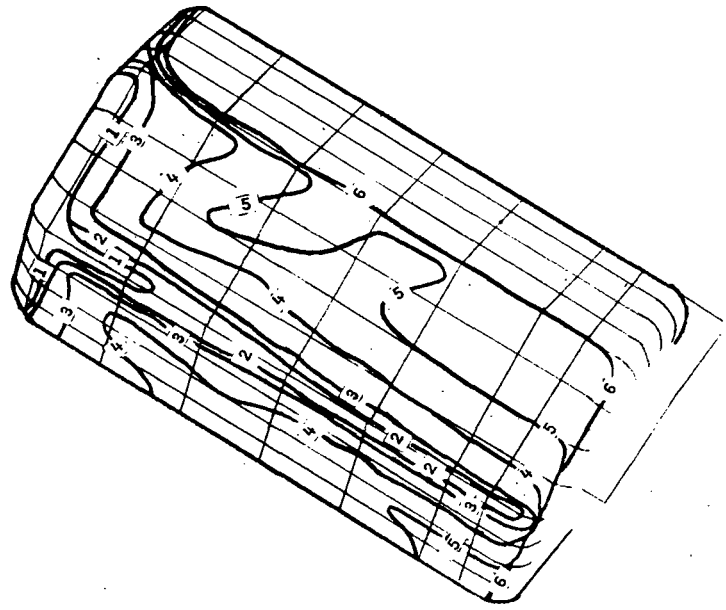

CONTOUR	T, SEC	H, BTU/FT. SQ-SEC-DEG-R	H/HS
1	1.00	2.33832E-02	3.21583E+00
2	2.00	1.65344E-02	2.27393E+00
3	3.50	1.24968E-02	1.71893E+00
4	7.50	8.53834E-03	1.17425E+00
5	11.50	6.89533E-03	9.48295E-01
6	15.00	6.03752E-03	8.30323E-01

(a) Side camera view.

Figure 16.- Nominal heat-transfer-coefficient contours on model 003 for $\alpha = 50^{\circ}$, $\phi = 0^{\circ}$, and $R_{\infty,L} = 0.82 \times 10^{6}$. $T_{pc} = 353$ K; $T_i = 303$ K; $T_t = 508$ K; $\beta = 0.266$; $P_t = 1.22 \times 10^{6}$ N/m^2.

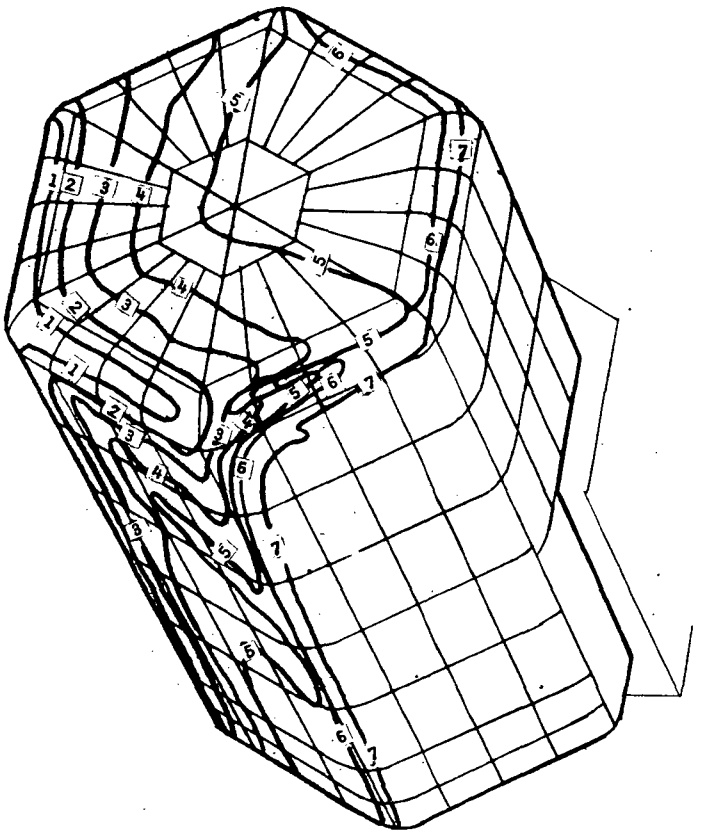

CONTOUR	T, SEC	H, BTU/FT. SQ-SEC-DEG-R	H/HS
1	.60	3.01876E-02	4.15161E+00
2	2.00	1.65344E-02	2.27393E+00
3	4.50	1.10229E-02	1.51596E+00
4	7.50	8.53834E-03	1.17425E+00
5	11.50	6.89533E-03	9.48295E-01
6	15.00	6.03752E-03	8.30323E-01
7	27.50	4.45900E-03	6.13234E-01

(b) Top camera view.

Figure 16.- Concluded.

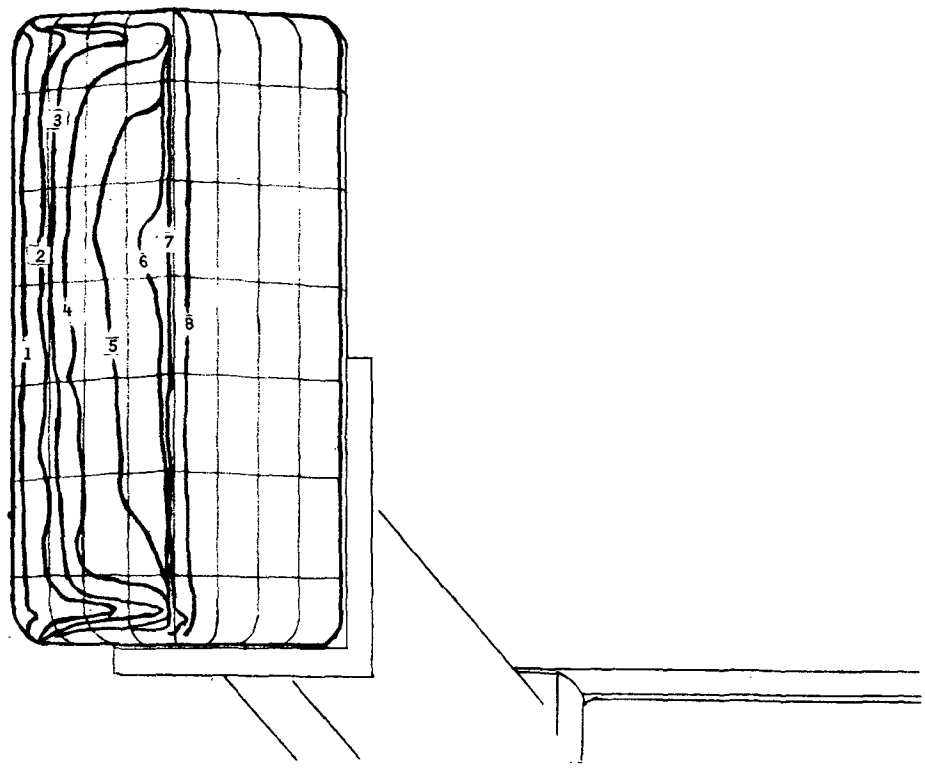

CONTOUR	T, SEC	H, BTU/FT. SQ-SEC-DEG-R	H/HS
1	1.00	2.42936E-02	3.27005E+00
2	2.50	1.53646E-02	2.06816E+00
3	3.50	1.29855E-02	1.74792E+00
4	4.50	1.14521E-02	1.54152E+00
5	6.00	9.91782E-03	1.33499E+00
6	7.00	9.18212E-03	1.23596E+00
7	10.00	7.68231E-03	1.03408E+00
8	20.00	5.43221E-03	7.31206E-01

(a) Side camera view.

Figure 17.- Nominal heat-transfer-coefficient contours on model 003 for $\alpha = 90^{\circ}$, $\phi = 0^{\circ}$, and $R_{\infty,L} = 0.87 \times 10^{6}$. $T_{pc} = 353$ K; $T_i = 302$ K; $T_t = 506$ K; $\beta = 0.276$; $P_t = 1.27 \times 10^{6}$ N/m^2.

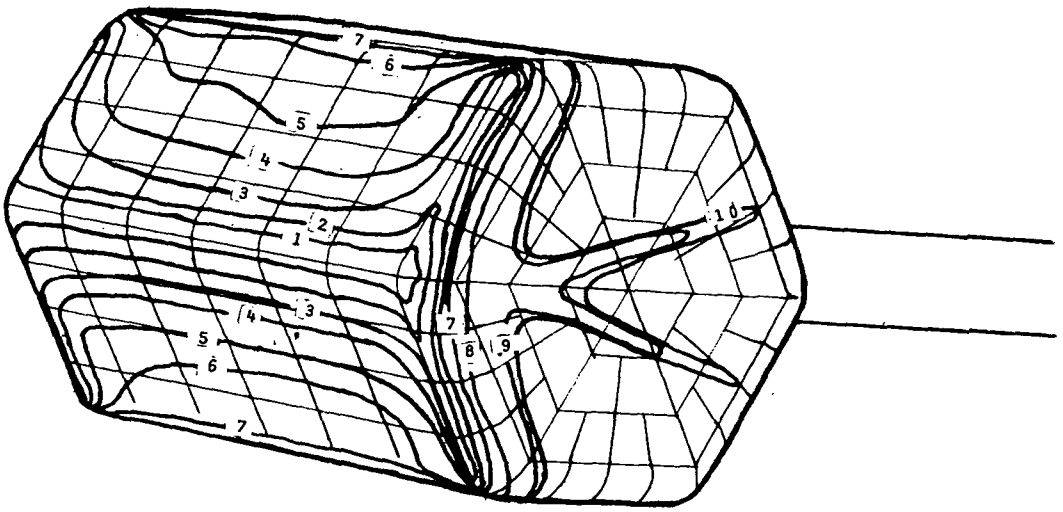

CONTOUR	T,SEC	H,BTU/FT.SQ-SEC-DEG-R	H/HS
1	1.00	2.42936E-02	3.27005E+00
2	2.00	1.71782E-02	2.31228E+00
3	3.00	1.40259E-02	1.88796E+00
4	4.00	1.21468E-02	1.63503E+00
5	5.00	1.08644E-02	1.46241E+00
6	6.00	9.91782E-03	1.33499E+00
7	7.00	9.18212E-03	1.23596E+00
8	10.00	7.68231E-03	1.03408E+00
9	30.00	4.43538E-03	5.97027E-01
10	33.20	4.21621E-03	5.67526E-01

(b) Top camera view.

Figure 17.- Concluded.

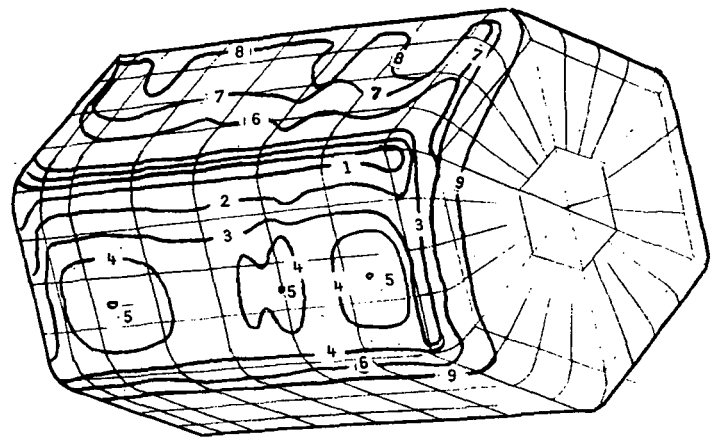

CONTOUR	T, SEC	H, BTU/FT. SQ-SEC-DEG-R	H/HS
1	.80	2.50249E-02	3.38462E+00
2	1.30	1.96312E-02	2.65512E+00
3	2.20	1.50906E-02	2.04100E+00
4	3.00	1.29228E-02	1.74781E+00
5	3.50	1.19642E-02	1.61816E+00
6	5.00	1.00100E-02	1.35385E+00
7	6.00	9.13781E-03	1.23589E+00
8	7.00	8.45996E-03	1.14421E+00
9	20.00	5.00498E-03	6.76924E-01

(a) Side camera view.

Figure 18.- Nominal heat-transfer-coefficient contours on model 003 for $\alpha = 90^{o}$, $\phi = 15^{o}$, and $R_{\infty,L} = 0.85 \times 10^{6}$. $T_{pc} = 353$ K; $T_i = 305$ K; $T_t = 508$ K; $\beta = 0.254$; $P_t = 1.26 \times 10^{6}$ N/m^2.

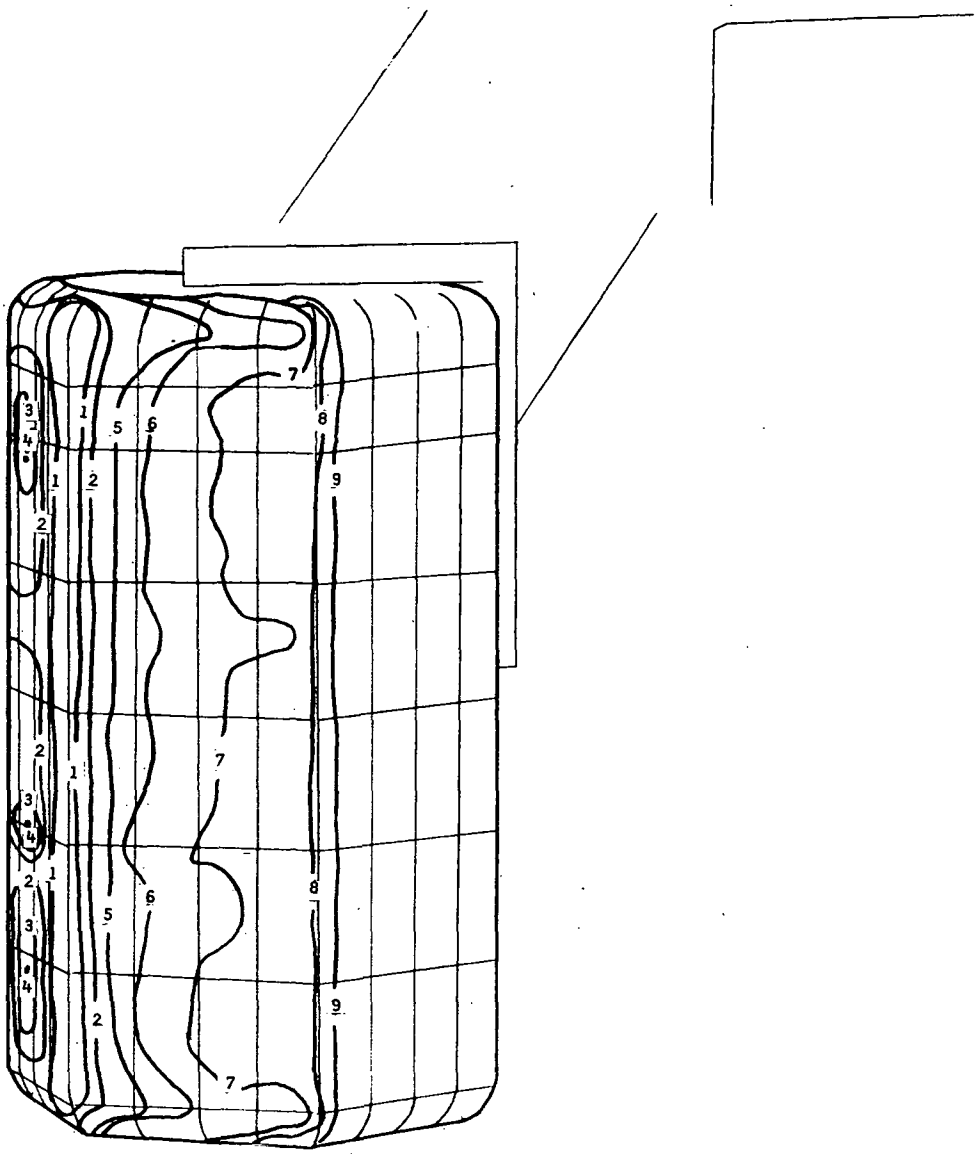

CONTOUR	T, SEC	H, BTU/FT.SQ-SEC-DEG-R	H/HS
1	1.20	2.04328E-02	2.76353E+C0
2	2.00	1.58271E-02	2.14062E+C0
3	2.90	1.31437E-02	1.77769E+0C
4	3.90	1.13341E-02	1.53293E+C0
5	4.00	1.11915E-02	1.51365E+0C
6	5.00	1.001C0E-02	1.35385E+CC
7	6.50	8.77932E-03	1.18740E+C0
8	7.50	8.17310E-03	1.1C541E+C0
9	22.40	4.72926E-03	6.39633E-C1

(b) Top camera view.

Figure 18.- Concluded.

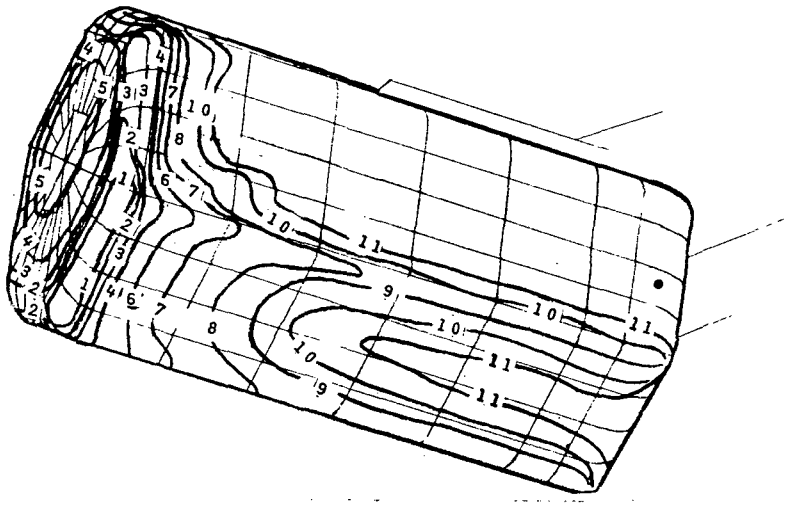

CONTOUR	T, SEC	H, BTU/FT.SQ-SEC-DEG-R	H/HS
1	1.00	2.39631E-02	3.25034E+00
2	2.00	1.69444E-02	2.29834E+00
3	3.00	1.38351E-02	1.87659E+00
4	4.50	1.12963E-02	1.53223E+00
5	6.50	9.39908E-03	1.27489E+00
6	7.50	8.75077E-03	1.18686E+00
7	10.00	7.57778E-03	1.02785E+00
8	15.00	6.18723E-03	8.39235E-01
9	20.00	5.35830E-03	7.26759E-01
10	25.00	4.79261E-03	6.50069E-01
11	30.00	4.37503E-03	5.93429E-01

(a) Side camera view.

Figure 19.- Nominal heat-transfer-coefficient contours on model 003 for $\alpha = 25^{\circ}$, $\phi = 30^{\circ}$, and $R_{\infty,L} = 0.85 \times 10^{6}$. $T_{pc} = 353$ K; $T_i = 304$ K; $T_t = 508$ K; $\beta = 0.272$; $P_t = 1.25 \times 10^{6}$ N/m^2.

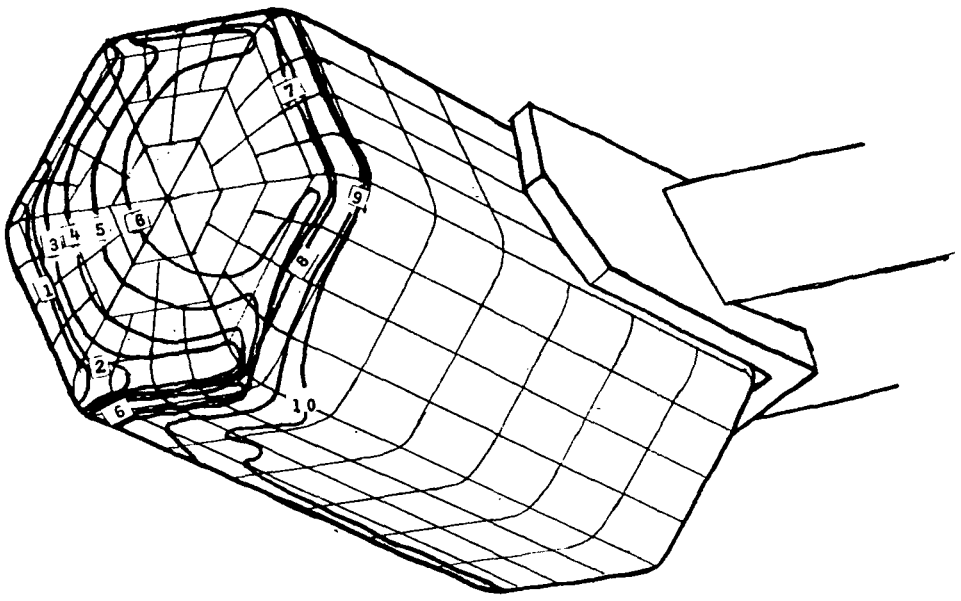

CONTOUR	T, SEC	H, BTU/FT.SQ-SEC-DEG-R	H/HS
1	1.10	2.28479E-02	3.09908E+00
2	1.70	1.83788E-02	2.49290E+00
3	2.20	1.61559E-02	2.19138E+00
4	3.10	1.36101E-02	1.84607E+00
5	4.50	1.12963E-02	1.53223E+00
6	5.40	1.03121E-02	1.39873E+00
7	6.40	9.47223E-03	1.28481E+00
8	7.30	8.86912E-03	1.20301E+00
9	18.70	5.54142E-03	7.51638E-01
10	36.80	3.95019E-03	5.35803E-01

(b) Top camera view.

Figure 19.- Concluded.

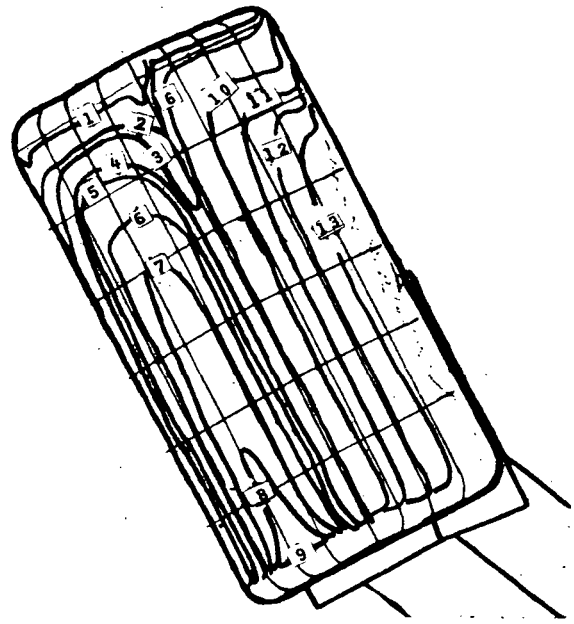

CONTOUR	T, SEC	H, BTU/FT.SQ-SEC-DEG-R	H/HS
1	1.10	1.25364E-02	2.79154E+00
2	2.00	9.29727E-03	2.07026E+00
3	2.50	8.31573E-03	1.85170E+00
4	3.40	7.13068E-03	1.58782E+00
5	3.90	6.65791E-03	1.48255E+00
6	5.00	5.88011E-03	1.30935E+00
7	5.90	5.41308E-03	1.20535E+00
8	6.50	5.15720E-03	1.14838E+00
9	6.70	5.07964E-03	1.13111E+00
10	13.80	3.53941E-03	7.88136E-01
11	20.00	2.94005E-03	6.54675E-01
12	25.00	2.62966E-03	5.85559E-01
13	30.00	2.40054E-03	5.34540E-01

(a) Side camera view.

Figure 20.- Nominal heat-transfer-coefficient contours on model 003 for $\alpha = 50^{\circ}$, $\phi = 30^{\circ}$, $R_{\infty,L} = 0.39 \times 10^{6}$. $T_{pc} = 325$ K; $T_i = 304$ K; $T_t = 455$ K; $\beta = 0.149$; $P_t = 0.48 \times 10^{6}$ N/m^2.

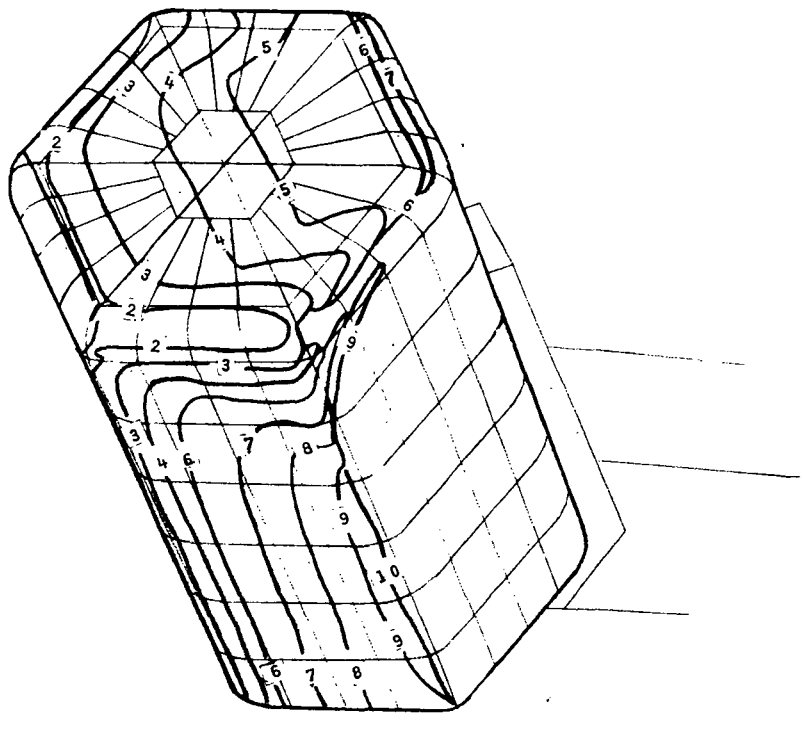

CONTOUR	T, SEC	H, BTU/FT. SQ-SEC-DEG-R	H/HS
1	.50	1.85945E-02	4.14053E+CC
2	1.40	1.11124E-02	2.47444E+CO
3	3.70	6.83549E-03	1.522C9E+CO
4	8.10	4.61985E-03	1.C2872E+CO
5	11.50	3.87723E-03	8.633&0E-C1
6	14.00	3.51404E-03	7.82486E-01
7	22.60	2.76577E-03	6.15666E-01
8	29.10	2.43738E-03	5.42743E-C1
9	33.80	2.26158E-03	5.03596E-01
10	37.30	2.15286E-03	4.79387E-C1

(b) Top camera view.

Figure 20.- Concluded.

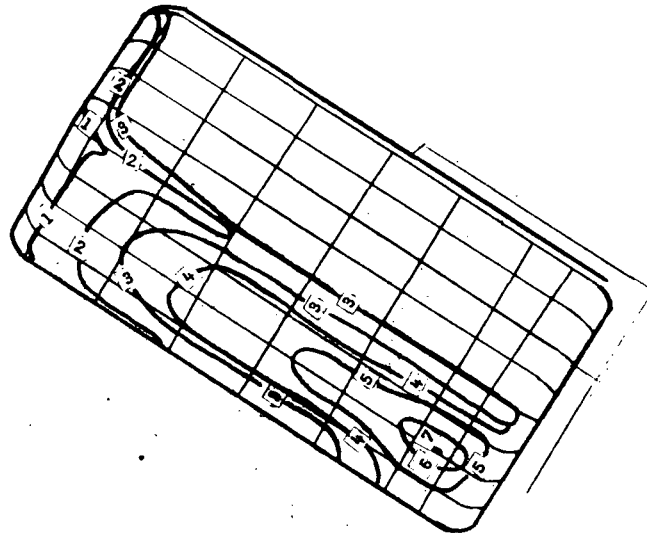

CONTOUR	T, SEC	H, BTU/FT. SQ-SEC-DEG-R	H/H^c
1	.60	2.12650E-02	2.87648E+00
2	1.60	1.30221E-02	1.76148E+00
3	2.40	1.06325E-02	1.43824E+00
4	3.00	9.51000E-03	1.28640E+00
5	3.40	8.93309E-03	1.20836E+00
6	3.80	8.44986E-03	1.14300E+00
7	4.20	8.03742E-03	1.08721E+00

(a) Side camera view.

Figure 21.- Nominal heat-transfer-coefficient contours on model 003 for $\alpha = 50^{o}$, $\phi = 30^{o}$, and $R_{\infty,L} = 0.87 \times 10^{6}$. $T_{pc} = 339$ K; $T_i = 306$ K; $T_t = 502$ K; $\beta = 0.187$; $P_t = 1.27 \times 10^{6}$ N/m^2.

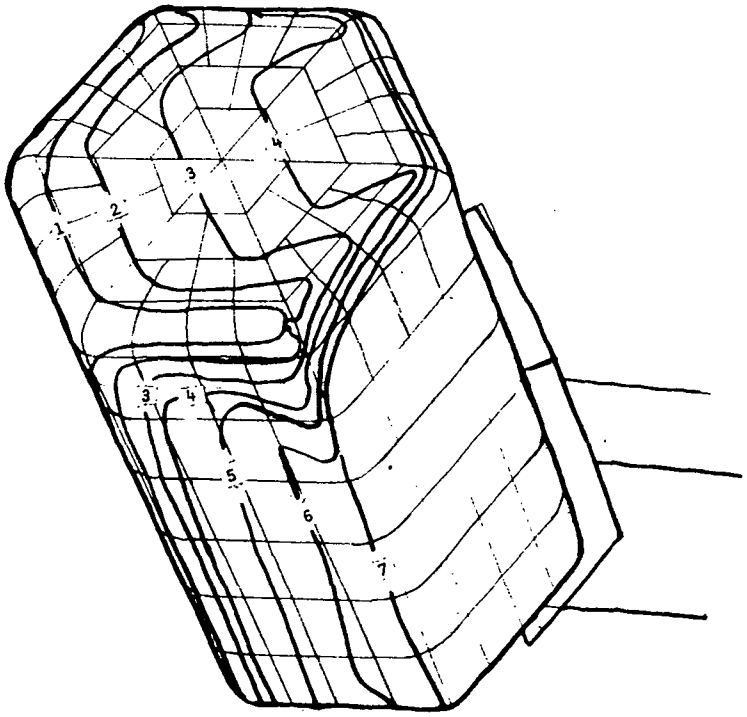

CONTOUR	T, SEC	H, BTU/FT. SQ-SEC-DEG-R	H/HS
1	.80	1.84160E-02	2.49111E+00
2	2.30	1.08612E-02	1.46917E+00
3	4.90	7.44120E-03	1.00656E+00
4	8.20	5.75221E-03	7.78091E-01
5	12.70	4.62210E-03	6.25223E-01
6	18.40	3.84001E-03	5.19431E-01
7	23.70	3.38351E-03	4.57681E-01

(b) Top camera view.

Figure 21.- Concluded.

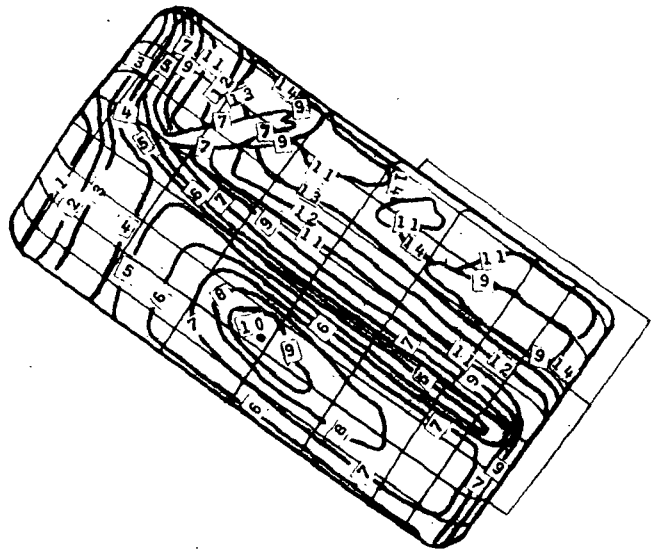

CONTOUR	T, SEC	H, BTU/FT. SQ-SEC-DEG-R	H/HS
1	.50	6.54258E-02	5.54560E+00
2	1.50	3.77736E-02	3.20175E+00
3	2.50	2.92593E-02	2.48007E+00
4	5.00	2.06895E-02	1.75367E+00
5	6.00	1.88868E-02	1.60088E+00
6	7.50	1.68929E-02	1.43187E+00
7	9.00	1.54210E-02	1.30711E+00
8	9.50	1.50097E-02	1.27225E+00
9	10.00	1.46297E-02	1.24003E+00
10	10.70	1.41430E-02	1.19879E+00
11	12.50	1.30852E-02	1.10912E+00
12	20.00	1.03447E-02	8.76836E-01
13	30.00	8.44644E-03	7.15934E-01
14	40.00	7.31483E-03	6.20017E-01

(a) Side camera view.

Figure 22.- Nominal heat-transfer-coefficient contours on model 003 for $\alpha = 50^{\circ}$, $\phi = 30^{\circ}$, and $R_{\infty,L} = 2.20 \times 10^{6}$. $T_{pc} = 380$ K; $T_i = 300$ K; $T_t = 503$ K; $\beta = 0.526$; $P_t = 3.20 \times 10^{6}$ N/m^2.

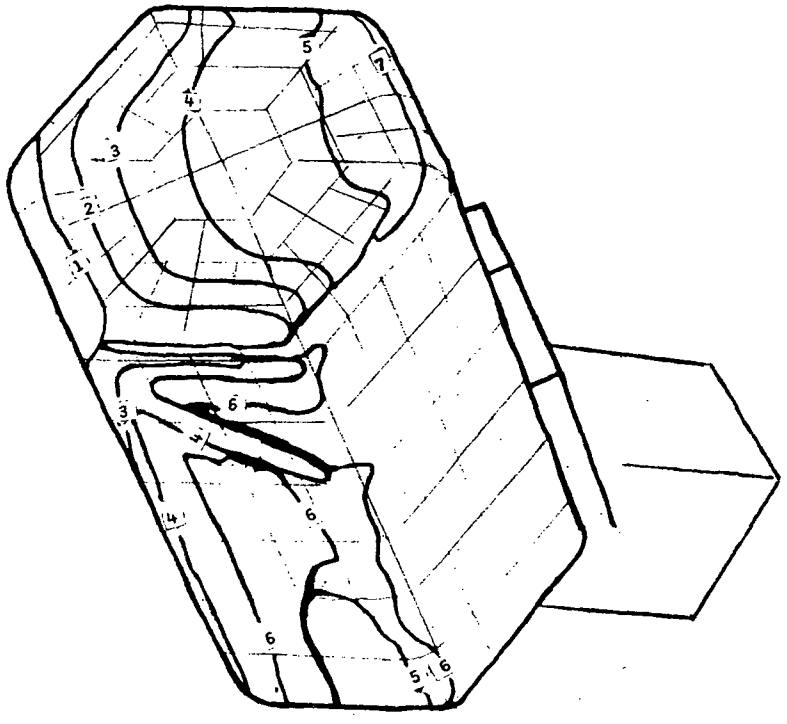

CONTOUR	T,SEC	H,BTU/FT.SQ-SEC-DEG-R	H/HS
1	1.00	4.62630E-02	3.92133E+00
2	2.80	2.76475E-02	2.34344E+00
3	5.80	1.92057E-02	1.62824E+00
4	9.50	1.50057E-02	1.27225E+00
5	11.10	1.38859E-02	1.17699E+00
6	15.80	1.16387E-02	9.86518E-01
7	29.10	8.57606E-03	7.26920E-01

(b) Top camera view.

Figure 22.- Concluded.

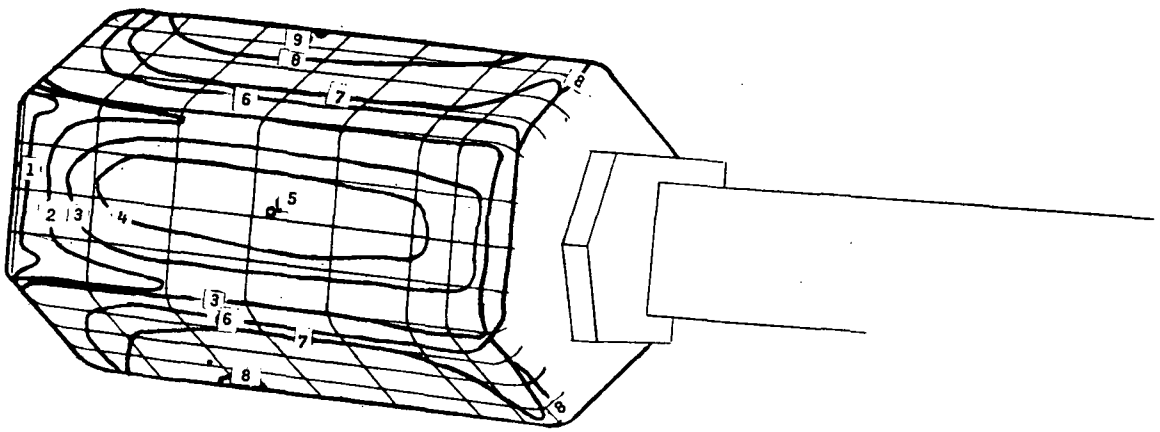

CONTOUR	T, SEC	H, BTU/FT. SQ-SEC-DEG-R	H/HS
1	.20	2.07957E-02	4.78022E+00
2	.60	1.20064E-02	2.75986E+00
3	1.00	9.30010E-03	2.13778E+00
4	1.40	7.86002E-03	1.80675E+00
5	1.70	7.13285E-03	1.63960E+00
6	5.00	4.15913E-03	9.56044E-01
7	7.50	3.39592E-03	7.80606E-01
8	10.00	2.94095E-03	6.76025E-01
9	12.90	2.58936E-03	5.95207E-01

(a) Side camera view.

Figure 23.- Nominal heat-transfer-coefficient contours on model 003 for $\alpha = 70^{\circ}$, $\phi = 30^{\circ}$, and $R_{\infty,L} = 0.34 \times 10^{6}$. $T_{pc} = 325$ K; $T_i = 306$ K; $T_t = 475$ K; $\beta = 0.106$; $P_t = 0.45 \times 10^{6}$ N/m^2.

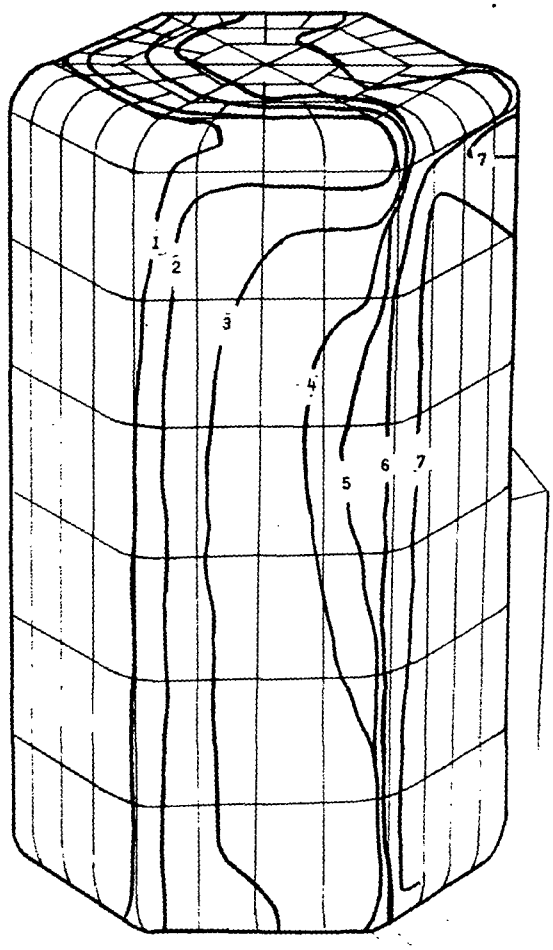

CONTOUR	T, SEC	H, BTU/FT. SQ-SEC-DEG-R	H/HS
1	1.50	7.59350E-03	1.74549E+00
2	3.50	4.97111E-03	1.14269E+00
3	7.50	3.39592E-03	7.80606E-01
4	11.00	2.80409E-03	6.44565E-01
5	12.00	2.68471E-03	6.17124E-01
6	20.00	2.07957E-03	4.78022E-01
7	40.00	1.47048E-03	3.38013E-01

(b) Top camera view.

Figure 23.- Concluded.

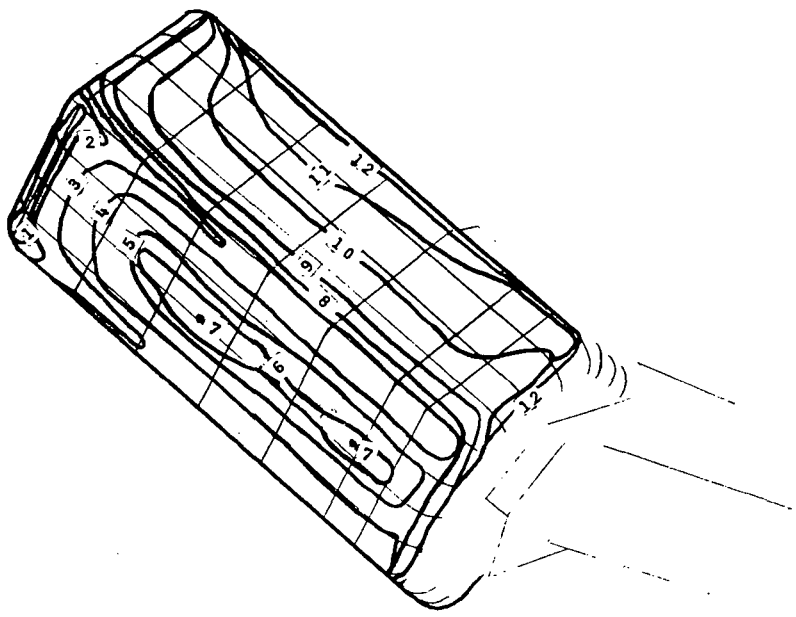

CONTOUR	T, SEC	H, BTU/FT. SQ-SEC-DEG-R	H/HS
1	.50	3.30851E-02	4.52275E+CC
2	1.00	2.33947E-02	3.198C7E+00
3	2.00	1.65425E-02	2.26138E+CC
4	3.00	1.35069E-02	1.84641E+CC
5	3.70	1.21623E-02	1.66260E+00
6	4.00	1.16973E-02	1.59904E+CC
7	4.30	1.12819E-02	1.54225E+CC
8	5.00	1.04624E-02	1.43022E+CC
9	10.00	7.39804E-03	1.01132E+00
10	17.50	5.59239E-03	7.64485E-C1
11	22.50	4.93203E-03	6.74213E-C1
12	30.00	4.27126E-03	5.83885E-C1

(a) Side camera view.

Figure 24.- Nominal heat-transfer-coefficient contours on model 003 for $\alpha = 70^{\circ}$, $\phi = 30^{\circ}$, and $R_{\infty,L} = 0.826 \times 10^{6}$. $T_{pc} = 353$ K; $T_i = 303$ K; $T_t = 510$ K; $\beta = 0.266$; $P_t = 1.23 \times 10^{6}$ N/m^2.

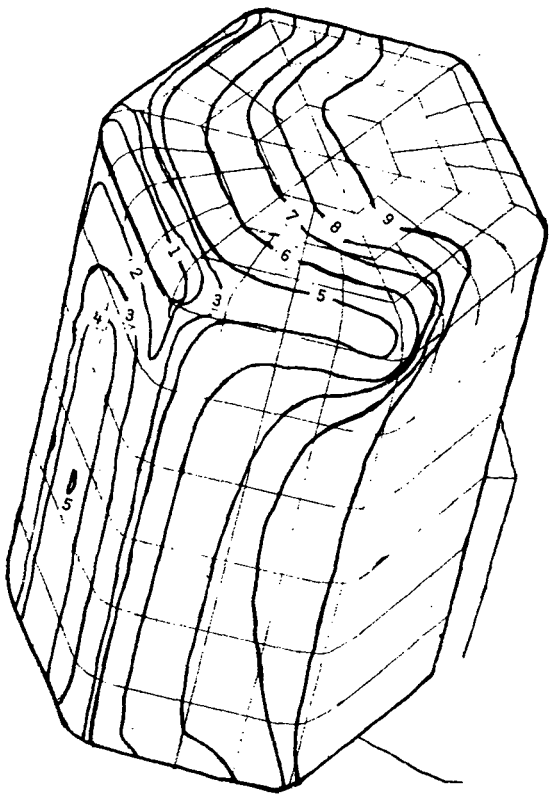

CONTOUR	T, SEC	H, BTU/FT.SQ-SEC-DEG-R	H/HS
1	.80	2.59816E-02	3.55077E+00
2	1.50	1.89743E-02	2.59311E+00
3	2.60	1.44120E-02	1.96961E+00
4	3.20	1.29908E-02	1.77538E+00
5	4.30	1.12067E-02	1.53156E+00
6	11.30	6.91309E-03	9.44774E-01
7	11.00	7.00672E-03	9.57571E-01
8	20.50	5.13257E-03	7.01439E-01
9	29.70	4.26416E-03	5.82759E-01

(b) Top camera view.

Figure 24.- Concluded.

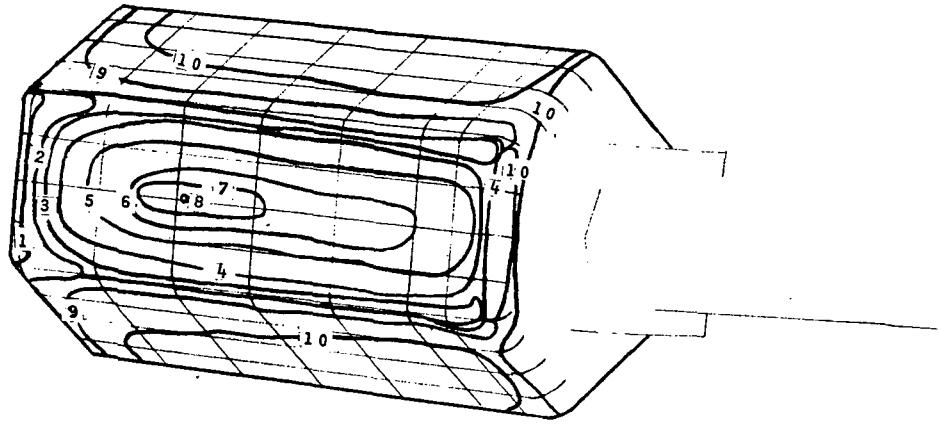

CONTOUR	T, SEC	H, BTU/FT.SQ-SEC-DEG-R	H/HS
1	1.50	4.52188E-02	3.80607E+00
2	3.00	3.19745E-02	2.69129E+00
3	4.00	2.76907E-02	2.33073E+00
4	5.00	2.47673E-02	2.08467E+00
5	7.00	2.09322E-02	1.76187E+00
6	8.50	1.89957E-02	1.59887E+00
7	9.00	1.84605E-02	1.55382E+00
8	9.30	1.81603E-02	1.52855E+00
9	10.00	1.75132E-02	1.47408E+00
10	22.50	1.16754E-02	9.82722E-01

(a) Side camera view.

Figure 25.- Nominal heat-transfer-coefficient contours on model 003 for $\alpha = 70^{o}$, $\phi = 30^{o}$, and $R_{\infty,L} = 2.20 \times 10^{6}$. $T_{pc} = 395$ K; $T_i = 305$ K; $T_t = 506$ K; $\beta = 0.629$; $P_t = 3.21 \times 10^{6}$ N/m^2.

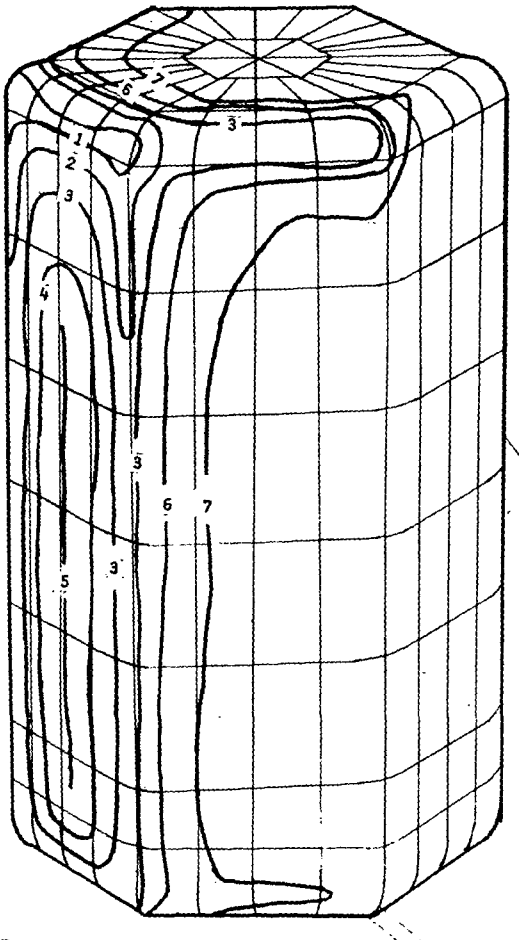

CONTOUR	T, SEC	H, BTU/FT. SQ-SEC-DEG-R	H/HS
1	1.50	4.52188E-02	3.80607E+CC
2	3.00	3.19745E-02	2.69129E+CO
3	5.0C	2.47673E-02	2.08467E+CO
4	7.00	2.09322E-02	1.76187E+CC
5	8.50	1.89957E-02	1.59887E+CO
6	10.00	1.75132E-02	1.47408E+CC
7	20.CC	1.23837E-02	1.04233E+CO

(b) Top camera view.

Figure 25.- Concluded.

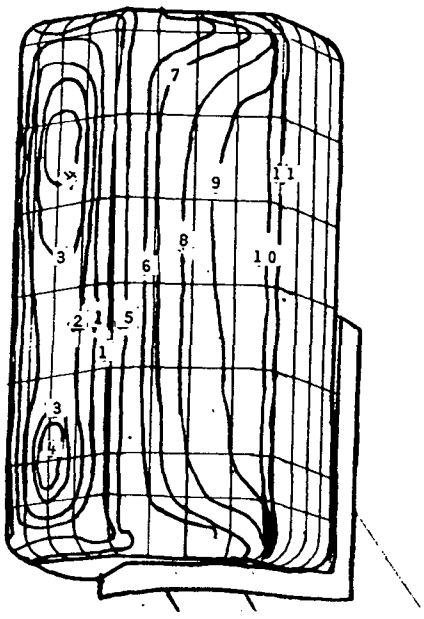

CONTOUR	T, SEC	H, BTU/FT.SQ-SEC-DEG-R	H/HS
1	1.50	1.91372E-02	2.55741E+00
2	2.00	1.65733E-02	2.24942E+00
3	2.50	1.48236E-02	2.01195E+00
4	2.80	1.40070E-02	1.90111E+00
5	5.00	1.04819E-02	1.42266E+00
6	10.00	7.41180E-03	1.00597E+00
7	12.50	6.62932E-03	8.99770E-01
8	15.00	6.05171E-03	8.21374E-01
9	17.50	5.60280E-03	7.60444E-01
10	20.00	5.24054E-03	7.11331E-01
11	36.00	3.90636E-03	5.30195E-01

(a) Side camera view.

Figure 26.- Nominal heat-transfer-coefficient contours on model 003 for $\alpha = 90^{\circ}$, $\phi = 30^{\circ}$, and $R_{\infty,L} = 0.82 \times 10^{6}$. $T_{pc} = 353$ K; $T_i = 301$ K; $T_t = 517$ K; $\beta = 0.266$; $P_t = 1.25 \times 10^{6}$ N/m^2.

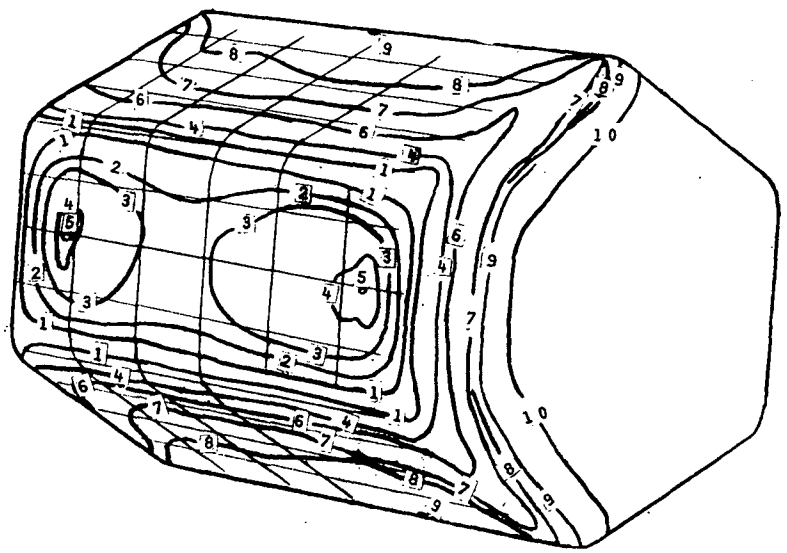

CONTOUR	T, SEC	H, BTU/FT. SQ-SEC-DEG-R	H/HS
1	1.20	2.13960E-02	2.90400E+00
2	1.70	1.79763E-02	2.43984E+00
3	2.00	1.65733E-02	2.24942E+00
4	2.50	1.48236E-02	2.01195E+00
5	3.00	1.35320E-02	1.83665E+00
6	7.50	8.55841E-03	1.16160E+00
7	12.50	6.62932E-03	8.99770E-01
8	15.00	6.05171E-03	8.21374E-01
9	19.30	5.33513E-03	7.24115E-01
10	36.30	3.89019E-03	5.27999E-01

(b) Top camera view.

Figure 26.- Concluded.

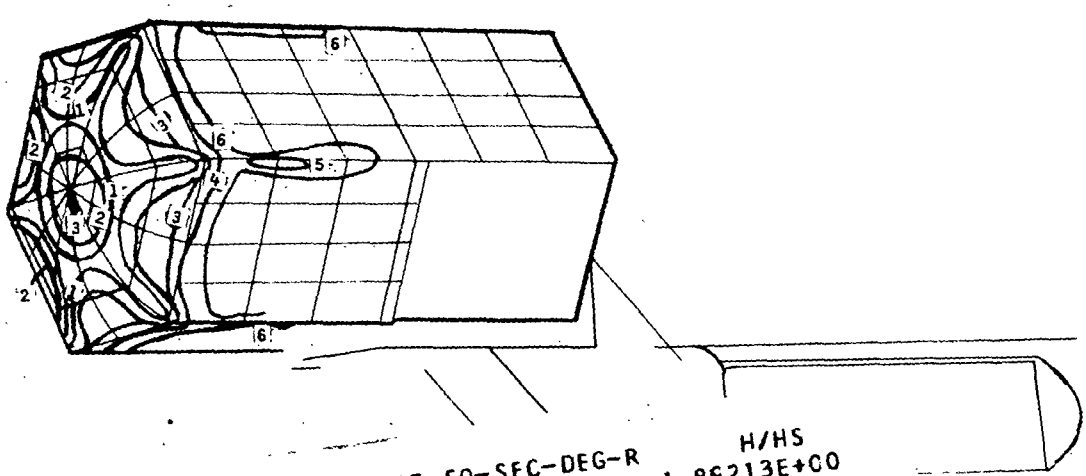

CONTOUR	T, SEC	H, BTU/FT.SQ-SEC-DEG-R	H/HS
1	2.50	1.40756E-02	1.85213E+00
2	3.50	1.18960E-02	1.55514E+00
3	4.50	1.04913E-02	1.41031E+00
4	7.50	8.12654E-03	1.09242E+00
5	10.00	7.03779E-03	5.46065E-01
6	25.00	4.45109E-03	5.98344E-01

(a) Side camera view.

Figure 27.- Nominal heat-transfer-coefficient contours on model 005 for $\alpha = 0^o$, $\phi = 0^o$, and $R_{\infty,L} = 0.85 \times 10^6$. $T_{pc} = 353$ K; $T_i = 305$ K; $T_t = 511$ K; $\beta = 0.253$; $P_t = 1.27 \times 10^6$ N/m^2.

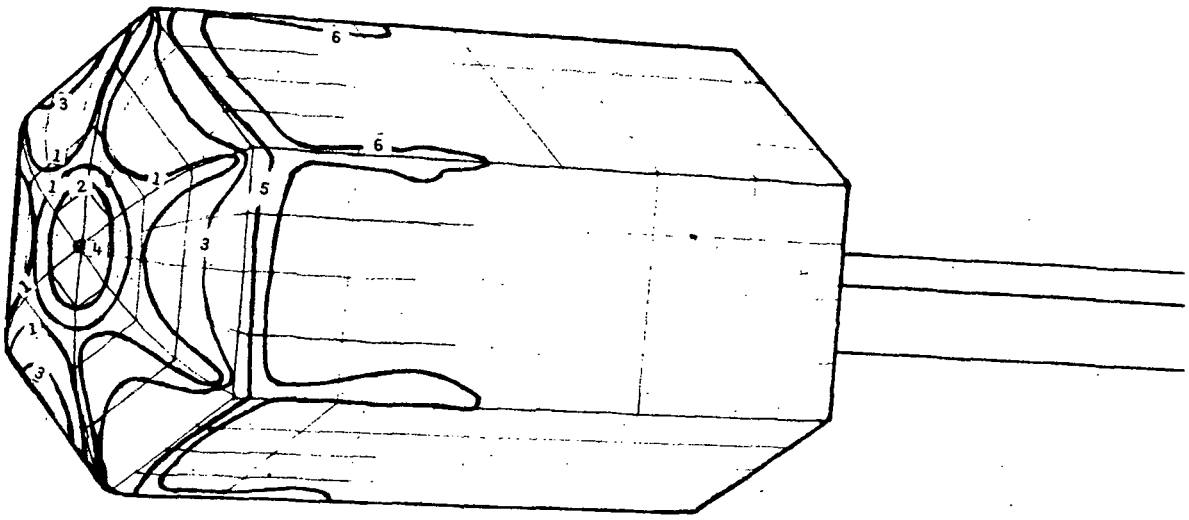

CONTOUR	T, SEC	H, BTU/FT. SQ-SEC-DEG-R	H/HS
1	2.10	1.53577E-02	2.06448E+00
2	3.30	1.22512E-02	1.64689E+00
3	3.50	1.18960E-02	1.59914E+00
4	5.00	9.95294E-03	1.33794E+00
5	7.50	8.12654E-03	1.09242E+00
6	20.00	4.97647E-03	6.68969E-01

(b) Top camera view.

Figure 27.- Concluded.

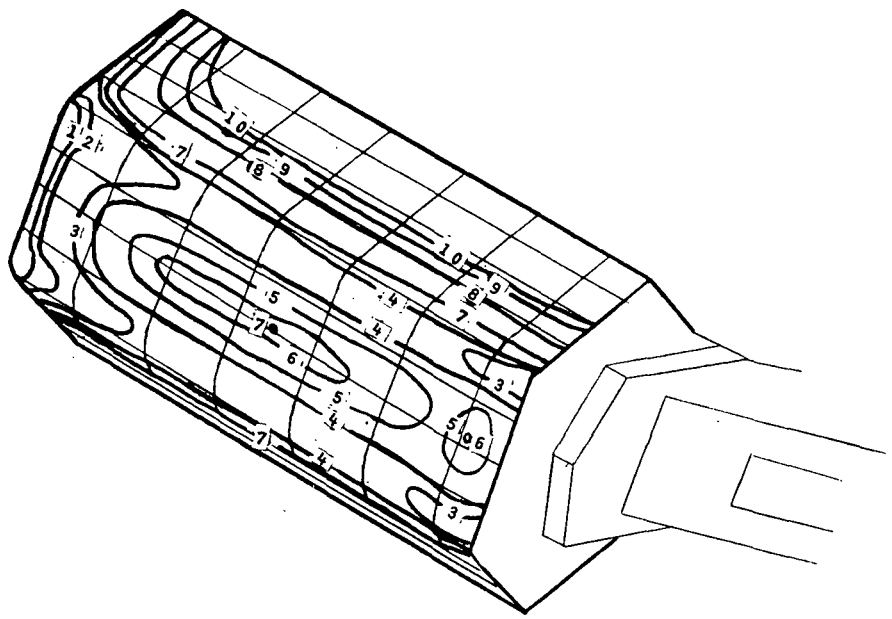

CONTOUR	T,SEC	H,BTU/FT.SQ-SEC-DEG-R	H/HS
1	1.50	2.69801E-02	3.72304E+00
2	2.50	2.08987E-02	2.88286E+00
3	5.00	1.47776E-02	2.03920E+00
4	6.50	1.29608E-02	1.78849E+00
5	8.50	1.13339E-02	1.56399E+00
6	9.50	1.07208E-02	1.47939E+00
7	10.00	1.04493E-02	1.44193E+00
8	20.00	7.38880E-03	1.01960E+00
9	30.00	6.03293E-03	8.32498E-01
10	34.00	5.66695E-03	7.81996E-01

(a) Side camera view.

Figure 28.- Nominal heat-transfer-coefficient contours on model 007 for $\alpha = 70^{o}$, $\phi = 30^{o}$, and $R_{\infty,L} = 0.84 \times 10^{6}$. $T_{pc} = 366$ K; $T_i = 305$ K; $T_t = 501$ K; $\beta = 0.375$; $P_t = 1.22 \times 10^{6}$ N/m^2.

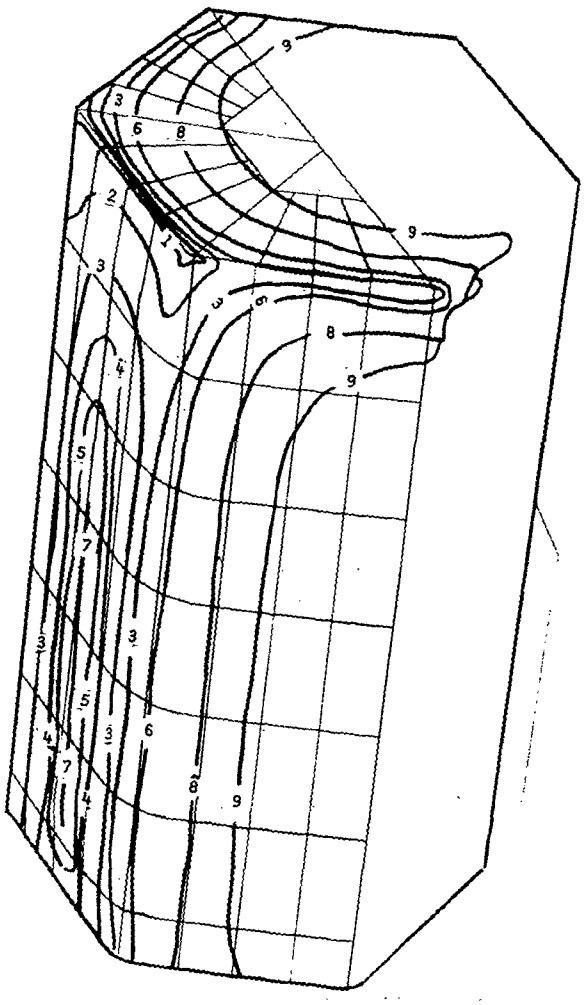

CONTOUR	T, SEC	H, BTU/FT. SQ-SEC-DEG-R	H/HS
1	1.00	3.30437E-02	4.55978E+00
2	2.50	2.08987E-02	2.88386E+00
3	5.00	1.47776E-02	2.03920E+00
4	7.50	1.20659E-02	1.66500E+00
5	8.50	1.13339E-02	1.56399E+00
6	9.00	1.10146E-02	1.51993E+00
7	9.20	1.08942E-02	1.50331E+00
8	20.00	7.38880E-03	1.01960E+00
9	34.40	5.63390E-03	7.77436E-01

(b) Top camera view.

Figure 28.- Concluded.

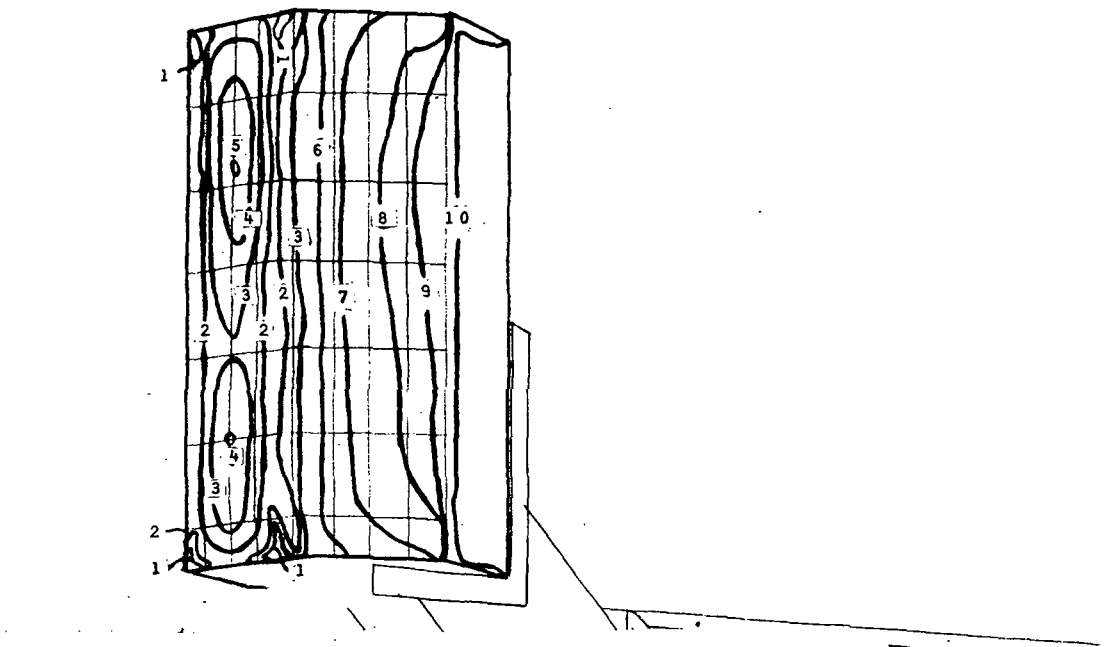

CONTOUR	T, SEC	H, BTU/FT. SQ-SEC-DEG-R	H/HS
1	2.00	2.15639E-02	2.89259E+00
2	3.00	1.76069E-02	2.36212E+00
3	4.00	1.52480E-02	2.04566E+00
4	5.00	1.36382E-02	1.82969E+00
5	5.70	1.27734E-02	1.71366E+00
6	10.00	9.64368E-03	1.29379E+00
7	20.00	6.81911E-03	9.14845E-01
8	30.00	5.56778E-03	7.46968E-01
9	40.00	4.82184E-03	6.46693E-01
10	54.90	4.11582E-03	5.52174E-01

(a) Side camera view.

Figure 29.- Nominal heat-transfer-coefficient contours on model 007 for $\alpha = 90^{\circ}$, $\phi = 30^{\circ}$, and $R_{\infty,L} = 0.84 \times 10^{6}$. $T_{pc} = 366$ K; $T_i = 305$ K; $T_t = 514$ K; $\beta = 0.347$; $P_t = 1.27 \times 10^{6}$ N/m^2.

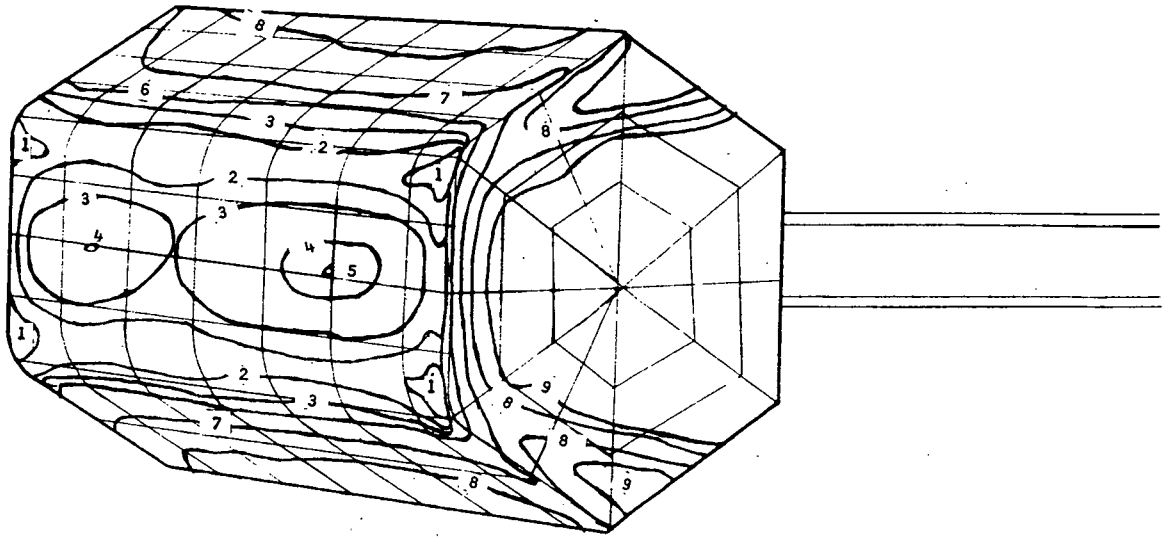

CONTOUR	T, SEC	H, BTU/FT. SQ-SEC-DEG-R	H/HS
1	2.40	1.96851E-02	2.64C93E+C0
2	3.50	1.630C8E-02	2.18690E+C0
3	4.50	1.43760E-02	1.92866E+C0
4	5.50	1.30035E-02	1.74454E+C0
5	6.20	1.22475E-02	1.64311E+00
6	10.00	9.64368E-03	1.29379E+00
7	20.00	6.81911E-03	9.14845E-01
8	30.00	5.56778E-03	7.46968E-C1
9	45.CC	4.546C8E-03	6.09897E-01

(b) Top camera view.

Figure 29.- Concluded.

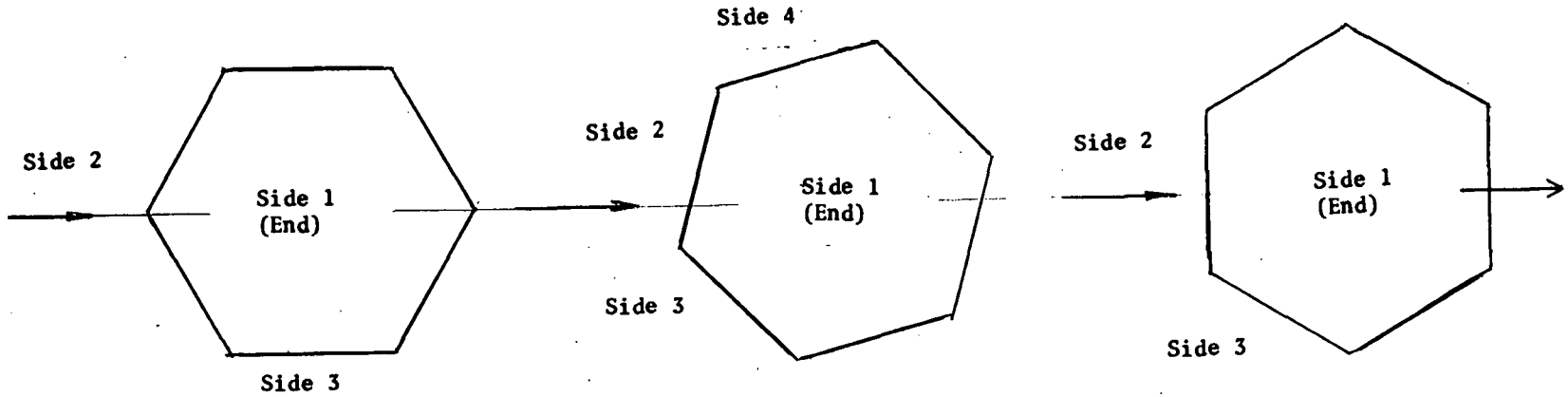

α	Side 1	2	3
0	1.000	0.889	0.889
25	.991	.935	.889
50	.964	.967	.889
70	.929	.982	.889
90	.889	.994	.889

(a) $\phi = 0^{o}$.

α = 90° only

Side	T_{aw}/T_t
1	0.889
2	0.996
3	0.970
4	0.920

(b) $\phi = 15^{o}$.

α	Side 1	2	3
0	1.000	0.889	0.889
25	.991	.938	.900
50	.964	.976	.937
70	.929	.994	.944
90	.889	1.000	.946

(c) $\phi = 30^{o}$.

Figure 30.- Adiabatic wall-to-total temperature ratio for the windward sides of the SNAP-19 heat-source configuration.

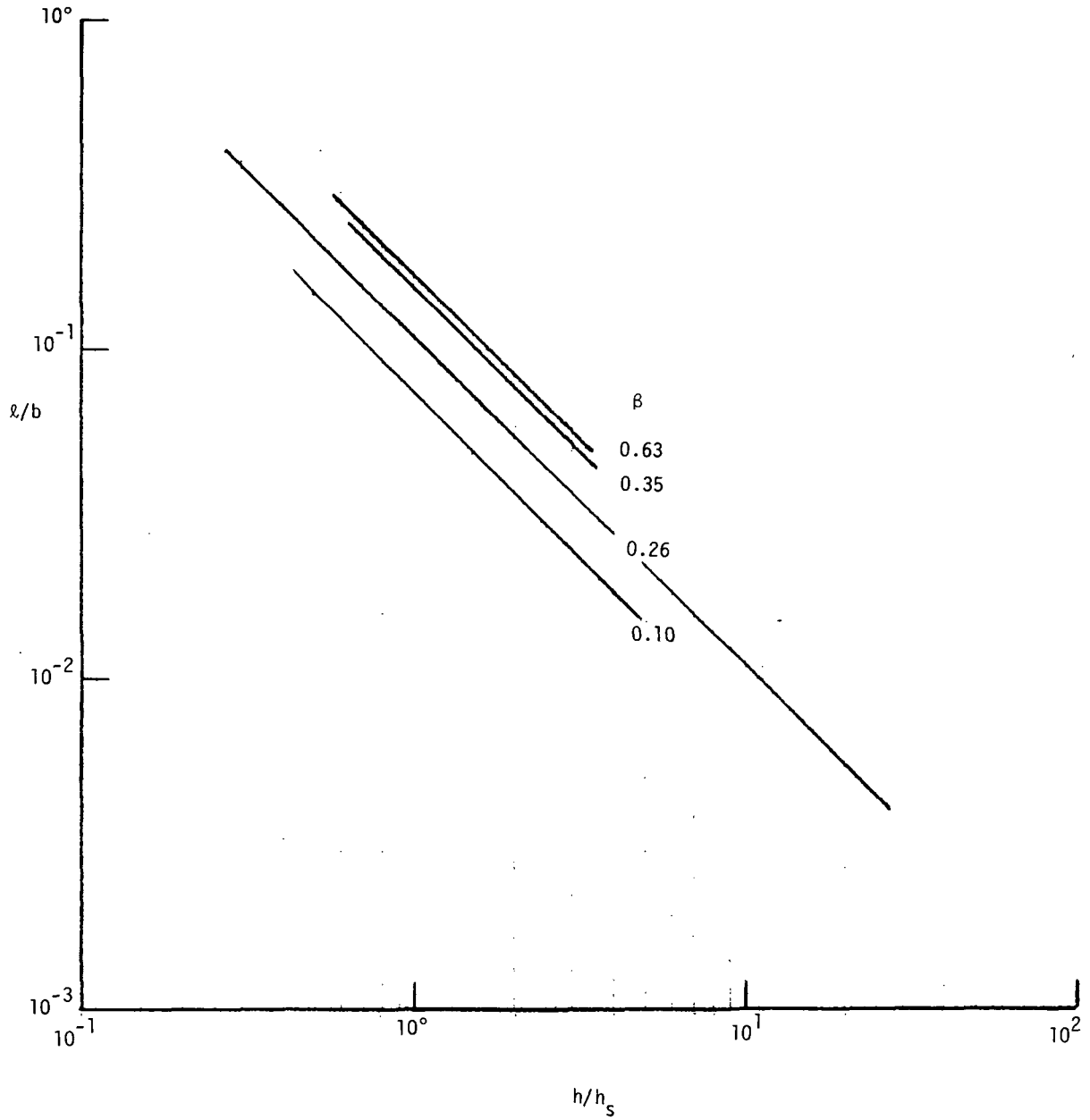

Figure 31.- Minimum distance of approach to a corner for which the semi-infinite slab assumption is not violated.

NASA-Langley, 1972 —— 33 L-7934

"The aeronautical and space activities of the United States shall be conducted so as to contribute . . . to the expansion of human knowledge of phenomena in the atmosphere and space. The Administration shall provide for the widest practicable and appropriate dissemination of information concerning its activities and the results thereof."

—NATIONAL AERONAUTICS AND SPACE ACT OF 1958

NASA SCIENTIFIC AND TECHNICAL PUBLICATIONS

TECHNICAL REPORTS: Scientific and technical information considered important, complete, and a lasting contribution to existing knowledge.

TECHNICAL NOTES: Information less broad in scope but nevertheless of importance as a contribution to existing knowledge.

TECHNICAL MEMORANDUMS: Information receiving limited distribution because of preliminary data, security classification, or other reasons.

CONTRACTOR REPORTS: Scientific and technical information generated under a NASA contract or grant and considered an important contribution to existing knowledge.

TECHNICAL TRANSLATIONS: Information published in a foreign language considered to merit NASA distribution in English.

SPECIAL PUBLICATIONS: Information derived from or of value to NASA activities. Publications include conference proceedings, monographs, data compilations, handbooks, sourcebooks, and special bibliographies.

TECHNOLOGY UTILIZATION PUBLICATIONS: Information on technology used by NASA that may be of particular interest in commercial and other non-aerospace applications. Publications include Tech Briefs, Technology Utilization Reports and Technology Surveys.

Details on the availability of these publications may be obtained from:

SCIENTIFIC AND TECHNICAL INFORMATION OFFICE

NATIONAL AERONAUTICS AND SPACE ADMINISTRATION

Washington, D.C. 20546